GEOTECHNICAL CENTRIFUGE MODELLING OF THE BEHAVIOUR OF A COMPRESSIBLE CLAY HORIZON UNDERLYING A REINFORCED SAND FOUNDATION

by

Brendon Ronald Jones

10436121

UNIVERSITEIT VAN PRETORIA
UNIVERSITY OF PRETORIA
YUNIBESITHI YA PRETORIA

Department of Geology

Faculty of Natural and Agricultural Sciences

University of Pretoria

Submitted in accordance with the requirements for the degree of Master of Science

February 2014

Study Supervisor: Prof J. Louis Van Rooy

Co-Supervisor: Prof S.W. Jacobsz

The financial assistance of the National Research Foundation (NRF) towards this research is hereby acknowledged. Opinions expressed and conclusions arrived at, are those of the author, and are not necessarily to be attributed to the NRF.

This study was undertaken in the Department of Geology, Faculty of Natural and Agricultural Sciences, University of Pretoria, under the supervision of Prof J. Louis Van Rooy and Prof S.W. Jacobsz.

The dissertation represents original work by the author and has not otherwise been submitted in any form for any degree or diploma to any tertiary institution. Where use has been made of the work of others, it is duly acknowledged in the text.

Brendon Ronald Jones
10436121

Date:_____

ABSTRACT

Basal reinforcement, where high tensile geogrids are employed beneath structures, is becoming an increasingly accepted construction technique along the eastern coast of southern Africa. The presence of compressible, soft, thin and shallow clay horizons usually associated with complex estuarine or lagoonal deposits are a major consideration when using basal reinforcement as a founding technique. Basal reinforcement involves the use of high tensile strength geogrids beneath a structure to form a reinforced sand foundation. Deformation behaviour under loading is an important component of stability analysis of earth structures. If reinforcement is used, the mechanisms become altered. Geotechnical centrifuge modelling is a unique physical modelling technique, as it allows replication of *in situ* stresses, which is most important because soil behaviour is a function of stress. This is achieved by placing the model at the end of the centrifuge arm, and subjecting it to an increased gravitational field, which creates the correct stress distribution in the model. Centrifuge modelling provides an appropriate technique to observe the behaviour of compressible, soft, thin and shallow clay horizons when basal reinforcement is utilized. An appropriate centrifuge model was constructed and compared the behaviour of the clay horizon under unreinforced and reinforced conditions. Reinforcement configurations were adjusted to observe the influence of additional geogrid layers, and extension of the width of the reinforcement. It was found that deformation behaviour is distinctly different between unreinforced and reinforced tests. Vertical deformation in the unreinforced test localised to the region directly beneath the platform, with little lateral disturbance to the clay horizon beyond the platform edge. As such, the sand directly beneath the platform acts as a deeper rigid platform. The deformation behaviour of the clay horizon changes with the inclusion of reinforcement. When reinforcement is included a wider portion of clay is deformed. The lateral width of this deformation zone is controlled by the width of the reinforcement, as the applied load is spread. A 'wide-slab' effect is evident with an increase in the geogrid width, as the tensioned membrane-effect is mobilised to increase the capacity of the reinforced foundation sand. This results in a wider portion of the clay deforming. Addition of geogrid reinforcement to the sand foundation under a wide platform load enhances deformation of the clay, but has the advantage of an increased load-bearing capacity of the system. Furthermore, the addition of multiple layers of reinforcement contributes to this increase in load-bearing capacity. Additionally, increasing the installation width of the reinforcement contributes to an increased vertical load-bearing capacity. However, this resultant increase is only mobilised after a certain amount of vertical displacement. This is likely due to the reinforcement requiring a certain amount of vertical displacement to mobilise tension in order to support the applied load. The behaviour of a thin compressible clay horizon changes with the inclusion of reinforcement under a wide platform load. The deformation behaviour of the clay is increased by additional layers of reinforcement as well as an increase in the width of the reinforcement. However, the increase in deformation comes at the benefit of an increased vertical load-bearing capacity of the reinforced foundation sand.

CONTENTS

LIST OF FIGURES

LIST OF TABLES

CHAPTER 1 INTRODUCTION

1.1 Background

Harbours along the eastern coastline of southern Africa have been established on river estuaries where several rivers give rise to an interlinked lagoonal system, comprising complex unconsolidated deposits of sands, silts and clays. These sediments are typically characterised by extremely compressible soft materials, with poor geotechnical properties. The poor geotechnical nature of these deposits has lead to limitations on the type of foundation treatment that can be applied to various engineering structures. Accordingly, specialised foundation designs and construction techniques are required when constructing on these unfavourable materials. Initial development for structures constructed on these deposits primarily involved the construction of costly piling solutions. However, with the recent advancement of geosynthetics, it has been possible to provide an alternative to traditional piling techniques using basal reinforcement, whereby suitable high tensile strength geogrids are employed to form a reinforced sand foundation. Moore *et al* (2012), and Zannonni *et al* (2012) have presented case studies where basal reinforcement techniques have been used. The basal reinforcement utilized in both studies was specifically for warehouse structures whereby large platform loads developed as a result of product stockpiling. The major concern on site for both of the studies was the presence of compressible, soft, thin, shallow, clay horizons below the foundation footprint.

Understanding failure mechanisms are an important component of stability analysis of earth structures. It is therefore essential to have a thorough understanding of how the subsoils beneath a structure will behave, upon foundation loading. If reinforcement is used, the mechanisms become altered, and choosing the right mechanism for stability analysis may not always be straightforward (Michalowski and Shi, 2003). Physical modelling is an intrinsic component to understanding and defining the behaviour of the ground profile under a specific loading condition. Both large-scale and small-scale studies assist geotechnical professionals in foundation design, to maximise the stability of a structure. Physical modelling provides a means to replicate a situation, which may be comparable to the behaviour in a prototype situation. Geotechnical centrifuge modelling has developed into an important physical modelling tool in the geotechnical profession, over the last few decades, due to its ability to replicate and investigate many types of problems. The use of a geotechnical centrifuge within the realm of physical model has become popular because it allows reproduction of the similar stress levels in a small-scale model as in a full-scale prototype, which is useful for analysing complex soil-structure interaction problems.

In order to enhance the design of basal reinforcement, specifically for sites underlain by unconsolidated estuarine deposits, it is important to understand the deformation behaviour of compressible, soft clay horizons, which are relatively thin, and usually occur at a shallow depth below ground level. In a qualitative sense, the study of this specific behavioural component will contribute

to the further improvement, success and popularity of utilising basal reinforcement techniques as a founding option, for structures associated with complex estuarine or lagoonal deposits.

1.2 Aim of research

The aim of this research project is to qualitatively define the behaviour of compressible, soft, thin, shallow clay horizons, under a reinforced sand foundation, loaded by a wide platform.

1.3 Objectives

The scope of work for this dissertation is outlined by the following objectives:

i. Produce an appropriate geotechnical centrifuge model to test the model under unreinforced and reinforced conditions,
ii. Vary the reinforcement configuration by increasing the number of reinforcing layers, and the width of the reinforcement,
iii. Qualitatively examine the deformation behaviour under a loaded platform for each test,
iv. Identify the difference in the behaviour of deformation between unreinforced, single and double reinforcement layers,
v. Identify the difference in deformation behaviour between a shorter geogrid width, and a wider geogrid width with relevance to founding width,
vi. Investigate the change in load bearing capacity and observe the response in pore water pressure for each test.

1.4 Methodology

1.4.1 Literature review

A review of the literature related to the research was carried out. This review covered the aspects of geotechnical centrifuge modelling, including; the principal laws, soil reinforcement, and previous work conducted on soil reinforcement in literature. Specific emphasis was placed on the scaling of geogrids.

1.4.2 Geotechnical centrifuge modelling

The aim of the research was investigated using geotechnical centrifuge modelling. Centrifuge modelling enables the study and analysis of design problems by using geotechnical materials. The fundamental issue with modelling geotechnical problems is the necessity of reproducing the soil behaviour both in terms of strength and stiffness. One major reason for this is that *in situ* stresses change with depth and it is well known that soil behaviour is a function of stress level and stress history. Geotechnical centrifuge modelling is an ideal tool available in the profession to replicate this important feature.

1.4.3 Analyses

By reviewing the data obtained from the centrifuge model tests, conclusions are made to satisfy the intended scope of work. The difference in behaviour between the unreinforced scenario, and the reinforced scenario are defined. Analyses of the influence of changing the number of reinforcement layers, and length of reinforcement relative to the foundation width, are examined. The findings from the centrifuge modelling are compared against a numerical model.

1.5 Dissertation structure

Chapter 1 – Introduction

The background to the research is explained and the aims and objectives are stated. The approach and methodology adopted are also stated.

Chapter 2 – Geotechnical centrifuge modelling

The principals of geotechnical centrifuge modelling are explained, and the geotechnical centrifuge housed in the Department of Civil Engineering at the University of Pretoria, is introduced.

Chapter 3 – Literature review

A literature review serves as a research basis to a dissertation. A perusal of literature was conducted to gain knowledge on previous studies with regard to geotechnical centrifuge modelling. Particular emphasis was placed on understanding the techniques previously used for the modelling of sand, clay, and the scaling of geogrid properties. The concept of soil reinforcement is also presented together with previous research conducted on geogrid reinforced sand foundation.

Chapter 4 – Numerical Analyses

In order to provide a comparison to the centrifuge model, a simple qualitative numerical model is set-up. The purpose of the numerical model is to provide details of what would be produced from common used tools in the geotechnical industry, when these structures are designed upon these thin, shallow, soft, and compressible clay horizons. This will provide a relevant set of results to compare with the findings gained from the centrifuge model tests.

Chapter 5 – Centrifuge model

The methodology followed for each centrifuge test was outlined. This included the model conceptualisation phase, through to design, and preparation and selection of materials. The process followed for the model construction is stated, together with any problems experienced.

Chapter 6 – Centrifuge model results

Data gathered from the centrifuge tests is presented. Visuals from the centrifuge tests are introduced, to present the mechanisms of deformation and the applied load and subsequent stresses, displacement, and pore pressure data are charted.

Chapter 7 – Analyses and discussion

The data from the centrifuge tests conducted are compared. The deformation behaviour between unreinforced and reinforced scenarios is investigated, whilst the influence on increasing the length of the reinforcement as well as the number of reinforcement layers is also compared. Load - displacement data for each test is studied to deduce the impact of reinforcement on the load bearing capacity of the system. Pore water pressures aid in the understanding of the materials under load and the pore pressure results gained from the tests are explored to enhance the understanding of the behaviour of the clay.

Chapter 8 – Conclusion

The research is concluded by providing a set of closing remarks, which satisfy the original objectives of the study. These final comments intend answering the original rationale of the research.

CHAPTER 2 GEOTECHNICAL CENTRIFUGE MODELLING

2.1 Introduction

Physical modelling is concerned with replicating an event comparable to what may exist in the prototype. The two events should be similar and that similarity needs to be related by appropriate scaling laws. The geotechnical centrifuge is an important piece of equipment available to the geotechnical profession as it enables the study and analysis of design problems by using geotechnical materials, in the centrifuge model. The following chapter outlines the fundamental principles surrounding geotechnical centrifuge modelling, as well as introducing the geotechnical centrifuge housed at the Department of Civil Engineering, University of Pretoria.

2.2 Principles of geotechnical centrifuge modelling

The fundamental issue with modelling geotechnical problems is the necessity of reproducing the soil behaviour both in terms of strength and stiffness. The field of geotechnics covers a wide range of soil behaviour relevant to a particular problem. One major reason for this is that *in situ* stresses change with depth and it is well known that soil behaviour is a function of stress level and stress history. It is therefore obvious that in a successful physical model these features will be important to replicate (Taylor, 1995). Centrifuge modelling is unique in that the most complex numerical soil mechanics models are only mathematical approximations of reality, while the use of physical modelling negates the need for complex constitutive models to be selected (Jacobsz, 2011). Unlike constitutive models, no assumptions need to be made and an actual physical event can be observed, at model scale (Jacobsz, 2013b).

Geotechnical centrifuge modelling is a useful tool available in the profession to replicate *in situ* stresses. Soil models placed at the end of a centrifuge arm can be accelerated so that they are subjected to an inertial radial acceleration field which, as far as the model is concerned, seems like a gravitational acceleration field but many times stronger than acceleration due to gravity (Taylor, 1995). The soil placed in the container has a free unstressed upper surface and within the soil body the magnitude of stress increases with depth at a rate related to the soil density and the strength of the acceleration field (Taylor, 1995). Centrifuge modelling allows the increase of self weight by the increase of gravitational acceleration, which is equal to the reduction of the model scale, as well as the reduction of time for model tests as the scale is reduced (Schofield, 1988).

2.2.1 Scaling laws

If the model is subjected to a similar stress history ensuring that the packing of the soil particles is replicated, then for the centrifuge model subjected to an inertial acceleration field of N times Earth's gravity, the vertical stress at depth h_m will be identical to that in the corresponding prototype at depth h_p, such that (Taylor, 1995):

$$h_p = Nh_m \tag{2.1}$$

This is the basic scaling law of centrifuge modelling for linear dimensions. Fundamentally, this law enables a stress similarity to be achieved at homologous points by accelerating a model of scale N to N times Earth's gravitation field, as illustrated in Figure 2.1 (Taylor, 1995). If an acceleration of N times Earth's gravity is applied to a material of density, ρ, then the vertical stress, $\sigma_{v,}$ at depth, h_m, in the model is given by (Taylor, 1995):

$$\sigma_{vm} = \rho N g h_m \tag{2.2}$$

And the vertical stress in the prototype, is given by:

$$\sigma_{vp} = \rho g h_p \tag{2.3}$$

Therefore:

$$\sigma_{vm} = \sigma_{vp} \tag{2.4}$$

Then:

$$h_m = h_p N^{-1} \tag{2.5}$$

And the scale factor (model:prototype) for linear dimensions is; 1:N. Therefore, for example, a model with a scale of 1:50 has to be accelerated to 50 times earth's gravity, or 50 G, in order to create the correct stress distribution (Jacobsz, 2013a).

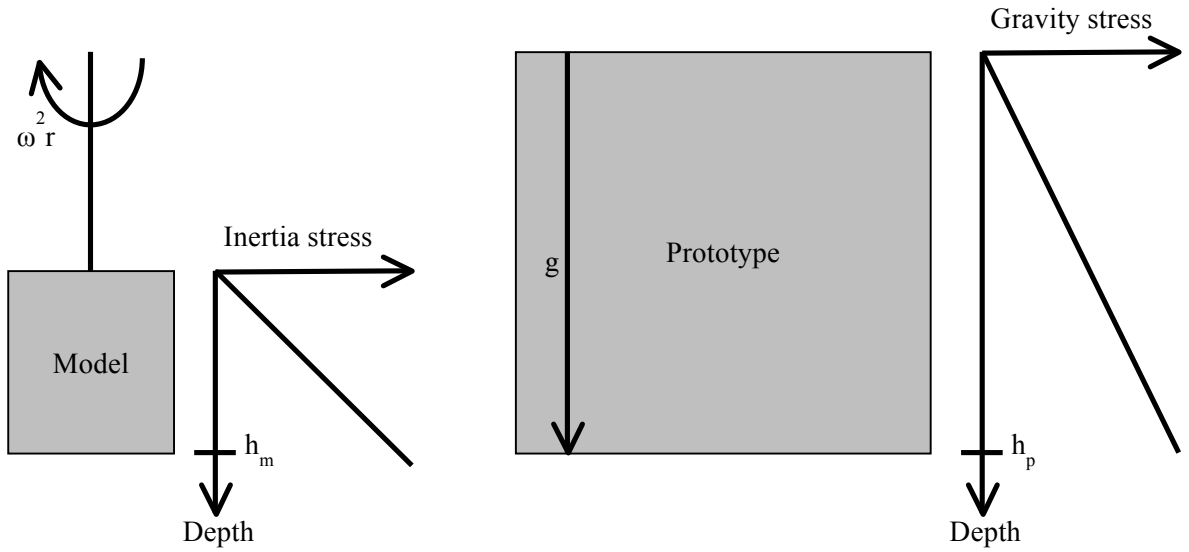

Figure 2.1 Inertial stresses in a centrifuge model induced by rotation about a fixed axis correspond to gravitational stresses in the corresponding prototype (Taylor, 1995).

Due to this linear scaling law for model dimensions, other physical properties can subsequently be derived and scaled. The scaling law for force is derived by considering Newton's second law (Jacobsz, 2013a), $F_p=m_p a_p$, where m_p is the mass, and a_p is the acceleration of the prototype (subscript p). If the material to be scaled is assumed to be a cube with density, ρ, and side length, l_p, and it is stationary on earth's surface, Newton's second law can be expressed as (Jacobsz, 2013a):

$$F_p = \rho\, l_p^3\, g \tag{2.6}$$

Where, g is gravitational acceleration. Newton's second law for the model can be written as:

$$F_m = m_m a_m \tag{2.7}$$

Where, F_m is the force at model scale, m_m is the mass of the model, and a_m is the acceleration at model scale. Standard practice in geotechnical centrifuge modelling is to use the same material that occurs in the full-scale situation, in the model, such that the material properties remain identical. Therefore, if the prototype material with density, ρ, is used in the model, and the model is N times smaller than the prototype, and therefore accelerated to N times earth's gravitational acceleration, equation 2.7 can be rewritten as (Jacobsz, 2013a):

$$F_m = \rho\, l_m^3 Ng \tag{2.8}$$

And equation 2.8 becomes:

$$F_m = \rho \left(\frac{l_p^3}{N}\right)^3 Ng = \frac{\rho l_p^3 g}{N^2} = \frac{F_p}{N^2}. \tag{2.9}$$

Therefore, proving the scaling law for force. It is on the same scaling basis that all physical properties can be scaled. Table 2.1 summarises some of the scaling laws for various physical quantities (Jacobsz, 2013a).

Table 2.1. Scaling laws for various physical properties (Jacobsz, 2013a).

Property	**Scale factor**
Model scale	N
Acceleration (G)	N
Linear dimensions	$1/N$
Stress	1
Strain	1
Density	1
Mass	$1/N^3$
Force	$1/N^2$
Time (consolidation)	$1/N^2$
Time (dynamic)	$1/N$
Pore fluid velocity	N

2.3 Department of Civil Engineering, University of Pretoria's geotechnical centrifuge

The University of Pretoria's laboratory is fitted with a 150 G-ton Actidyn C67-4 centrifuge (Figure 2.2). This centrifuge is a beam centrifuge, with a swinging platform. The platform surface will always be normal to the resultant acceleration, provided the hinges remain frictionless and the platform symmetrically loaded. The centrifuge radius is 3 m from the rotation axis to the model platform. The model platform measures 0.8 m x 1.0 m and the available free space above the model platform is 1.3 m. An aerodynamic shield has been fitted to the front of the platform to minimise the drag during testing. A plan and elevation of the centrifuge are presented in Figure 2.3. The centrifuge

is capable of carrying a payload of 1500 kg to 100 G, and thereafter 950 kg, up to 130 G. At its maximum capacity the rotational speed is 208 RPM (Jacobsz *et al*, 2014).

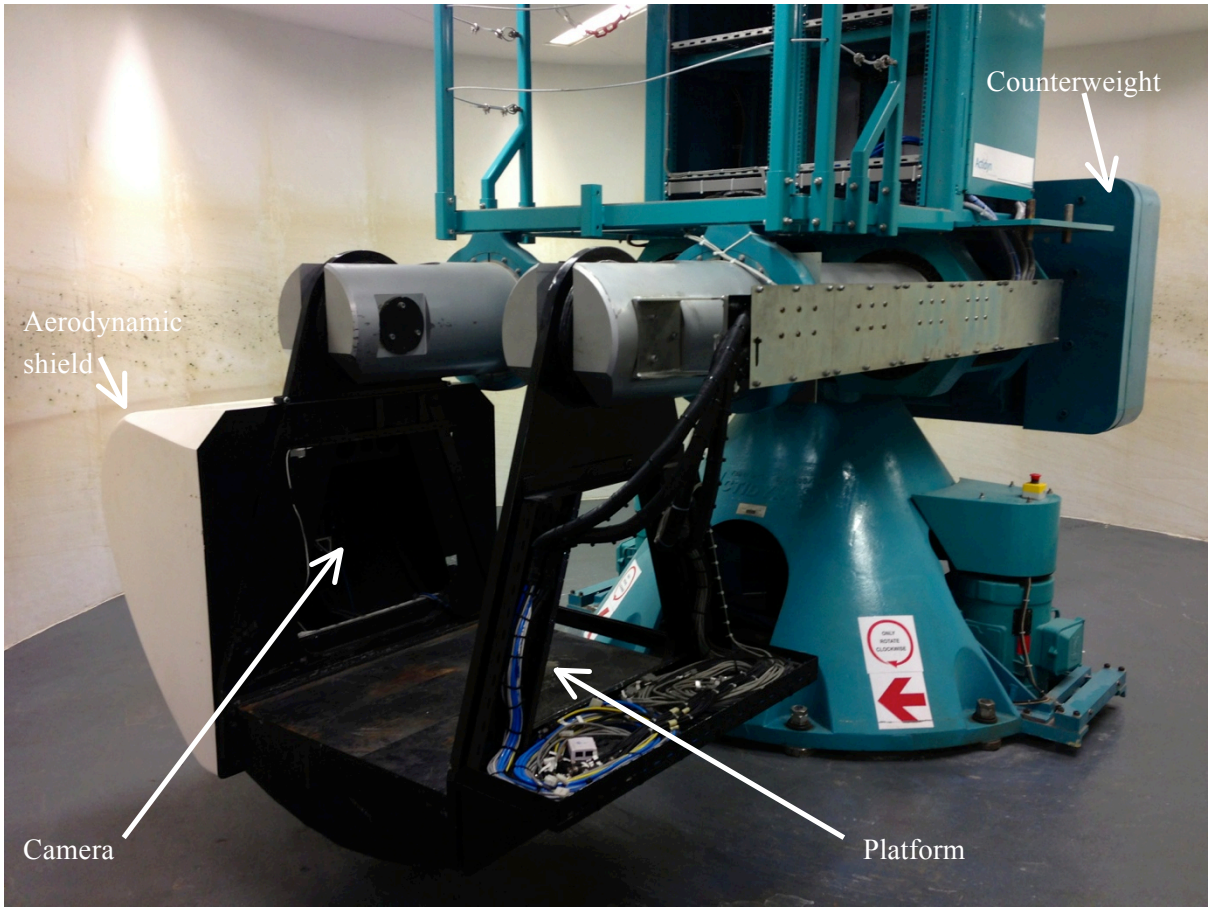

Figure 2.2 The Department of Civil Engineering's geotechnical centrifuge, at the University of Pretoria.

The drive assembly comprises twin AC variable speed induction motors with a maximum combined output of 120kVA operating by means of a belt and pulley transmission system. During testing a constant temperature in the centrifuge enclosure is required and therefore a powerful cooling system has been installed which has sufficient capacity to dissipate the heat released by the drive motors at maximum power. The air is introduced above the machine and withdrawn from vents below the centrifuge base before being cooled and recirculated (Jacobsz *et al*, 2014). The centrifuge is balanced by an adjustable counterweight, which is automatically adjusted from the centrifuge's control computer. The model weight, desired acceleration and position above the swing platform where the g-level should be balanced are used to estimate the required position of the counterweight before the test commences. The counterweight will then adjust to the calculated position while the centrifuge is still stationary. When the test commences the centrifuge will accelerate to 4.5 G where minor adjustments are made to the counterweight. Once the out-of-balance sensors in the centrifuge pedestal indicate satisfactory balance, acceleration to the desired level will begin. Thereafter, minor fine-tuning of the centrifuge balance during testing occurs via moveable masses inside the hollow centrifuge arms (Jacobsz *et al*, 2014).

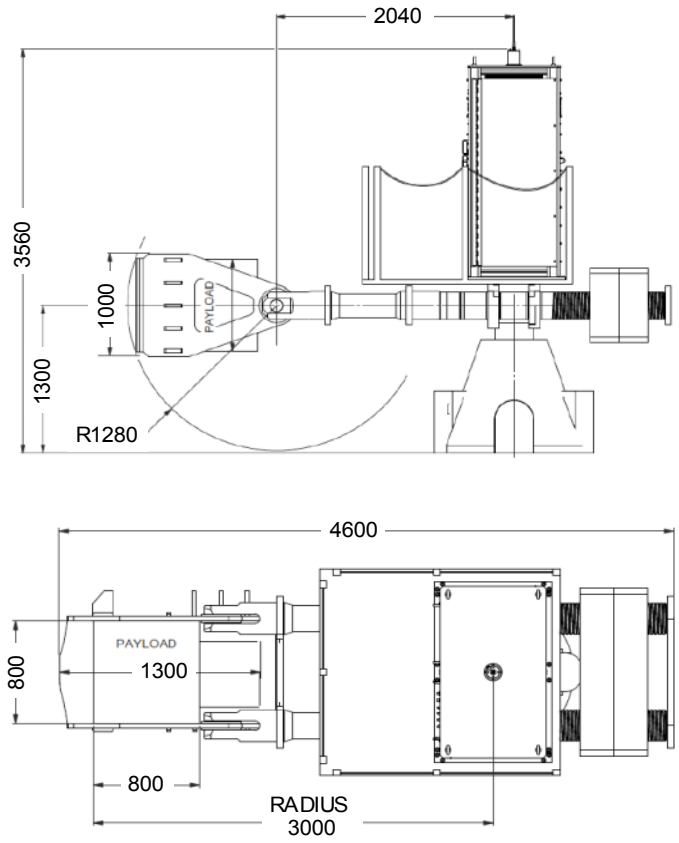

Figure 2.3 Elevation and plan on of the geotechnical centrifuge at the University of Pretoria (Actidyn 2011).

The centrifuge enclosure is fitted with fluorescent lights, installed radially around the rotation axis in the ceiling. LED strip and spot lighting, both above and on the side of the model platform has been installed to enhance viewing of the model during testing. These are controlled from the control computer (Jacobsz *et al*, 2014). Two cameras have been installed on the centrifuge to observe models during testing. One camera is housed inside the aerodynamic shield and observes the model's cross sectional profile, and can be adjusted according to the elevation relative to the model, as well as further and closer to it. This camera may be detached from its mounting and fixed anywhere on the model itself. The second camera is installed near the axis of rotation and looks down onto the model in plan view, when the model has swung up (Jacobsz *et al*, 2014). The centrifuge laboratory also has two portable Go-Pro cameras, which can be placed at any position on the model.

Two model container boxes, called strongboxes, are available to be used for the models to be constructed and tested in. Both are aluminium containers, with internal dimensions of 600 mm x 400 mm x 400 mm. One of the containers is fitted with a transparent window so that the model can be viewed from a cross sectional profile (Figure 2.4).

The centrifuge's operation is managed via a personal computer which controls the three-phase power system driving the machine. In addition to defining the input values for the automatic balancing (desired acceleration and model mass), the rate at which the centrifuge accelerates to the required G-level (in G per minute) can also be controlled. The screen displays a number of system checks,

warning messages and presents general data like temperature and humidity in the centrifuge enclosure (Jacobsz *et al*, 2014).

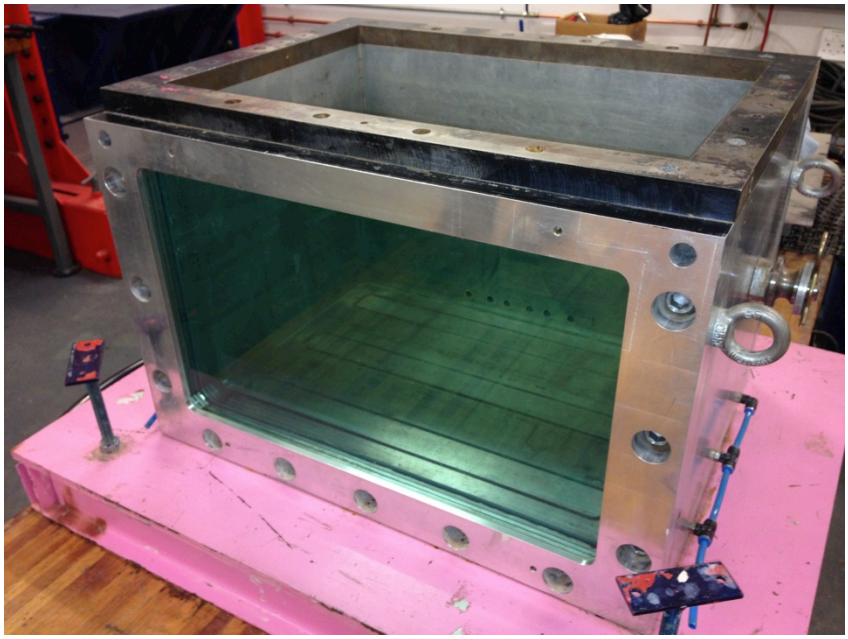

Figure 2.4 Model test container with transparent glass window.

The centrifuge is equipped with electric power slip rings as well as fluid slip rings mounted at the centrifuge base. The fluid slip rings allow water, pneumatic systems, as well as hydraulic systems to be supported. A large instrumentation cabinet, rotating with the centrifuge, is mounted above the centrifuge axis of rotation and provides space for data acquisition and control systems (Jacobsz *et al*, 2014). Electric power is supplied to the centrifuge instrumentation cabinet via these slip rings, which are rated to provide 50 A at 380 V (Jacobsz *et al*, 2014). A step down transformer in the instrumentation cabinet converts the power to 220V. Currently a 12 V 400 VA transformer and a smaller 24 V transformer have been installed to provide power to utilities on the model platform (Jacobsz *et al*, 2014).

Power to various utilities on the model platform, including the data aquisition system, is controlled via two six-channel digital input/output controllers operating a total of 12 relays. It is controlled via a 1 Gbit local area connection to the centrifuge through a fibre optic rotary link, which provides excellent noise immunity (Jacobsz *et al*, 2014).

The centrifuge is also fitted with a fluid rotary joint enabling hydraulic and pneaumatic connection to the model to drive actuators of various types. The seamless fibre optic network link to the centrifuge enables electric actuators to be controlled from the control room. The control room is equipped with the pneumatic and hydraulic control panel from which hydraulic and pneumatic pressure, applied to the centrifuge model, are controlled. Flow meters and pressure regulators are installed to monitor and control flow rates (Jacobsz *et al*, 2014).

All communication between the data acquisition systems and the control room occurs via the centrifuges Ethernet network. The centrifuge is equipped with three modules of the Digidaq data

acquisition system developed by the University of Western Australia (Gaudin et al. 2010), providing a total of 24 channels. This system is capable of logging a range of instrumentation at a wide range of frequencies and provides the user with much flexibility. The Digidaq system is complemented by a 24 channel HBM QuantumX System. This adds to the capabilities of the Digidaq system as the HMB system supports LVDTs, bender elements, 4-20 mA sensors and others. A HBM CX22W solid state computer, a modular system capable of being expanded to the user's requirements, was installed on the centrifuge. It currently controls the on-board cameras for image processing (Jacobsz *et al*, 2014).

2.4 Summary

Centrifuge modelling has become a powerful physical modelling tool in the geotechnical profession. The most fundamental reason for this is that it replicates the *in situ* stresses in a ground profile, which other small-scale physical models cannot do. This is achieved by placing the model at the end of the centrifuge arm, and thereafter subjecting it to an increased gravitational field, which creates the correct stress distribution within the model. This is necessary to ensure realistic ground behaviour. The 3 m balanced beam geotechnical centrifuge housed at the Department of Civil Engineering, University of Pretoria is capable of accelerating a payload of up to one ton to 150 G. The centrifuge is equipped with a 48-channel data acquisition channel, as well as hydraulic and pneumatic connections to model various ground models and situations.

CHAPTER 3 LITERATURE REVIEW

3.1 Introduction

Due to the experimental nature of geotechnical centrifuge modelling, practical considerations need to be made in the design and construction of any centrifuge model test. These considerations need to be taken from the large quantity of experience gained from previous studies, using proven apparatus and techniques, in order to provide a valid set of results. In order to gain a better understanding of the procedure to construct a model, it was important that a thorough perusal of existing literature was completed. Due to the unique nature of the study, most literature pertains to reinforced foundation sand for strip footings. Very little research has previously been attempted on reinforced foundation sand under a loaded platform, on a two-layer soil system comprising reinforced sand overlying a weaker clay horizon. No studies have attempted simulating this situation in a geotechnical centrifuge. This chapter presents the literature relevant to conducting an appropriate model, which addresses all properties of the most fundamental issues. The concept of soil reinforcement is discussed together with the subsequent modes of failure of reinforced soil. Techniques for modelling various elements of the model are also discussed.

3.2 Soil reinforcement

3.2.1 Concept

Soil shearing resistance stems from frictional contact between soil particles subject to effective compressive stress. Soil deforms when it is loaded in shear. In addition to any elastic distortion of the soil particles themselves, shear deformation occurs as soil particles realign their contacts to mobilise a shearing resistance. The deformation is observed as an overall strain in the soil, and both compressive and tensile strains usually develop when soil shears (Jewell, 1996).

When reinforcement is placed in soil it can develop bond through frictional contact between the soil particles and the planar surface areas of the reinforcement, and from bearing stresses on transverse surfaces, which exist in grids or ribbed strips (Jewell, 1996). Deformation in the soil causes tensile forces to develop in the reinforcement, when the reinforcement is inclined in a direction of compressive strain in the soil. The mobilised reinforcement force, ultimately limited by the available bond, acts to alter the force equilibrium in the soil (Jewell, 1996). The performance of reinforced soil foundations depends not only on soil and reinforcement properties but also on the interaction between the soil and reinforcement (Sharma *et al*, 2009). While a geotextile relies on the adhesion between itself and the adjacent soil to mobilise tension, a geogrid is able to mobilise tension mainly by generating passive resistance from the column of the soil confined between its large apertures (Sharma and Bolton, 1996). Figure 3.1 illustrates the mobilised tension along the geogrid reinforcement. Essentially soil reinforcement is the interaction between the reinforcement and soil by friction or mechanical interlock and the resistance to tensile strain and subsequent failure can be

provided by the reinforcement (James, pers comm, 2010). As a surcharge load is applied, stress is transferred at the interface through friction between the soil and the reinforcement, providing a lateral restraint on the reinforced soil, as illustrated in Figure 3.2 (James, pers comm, 2010).

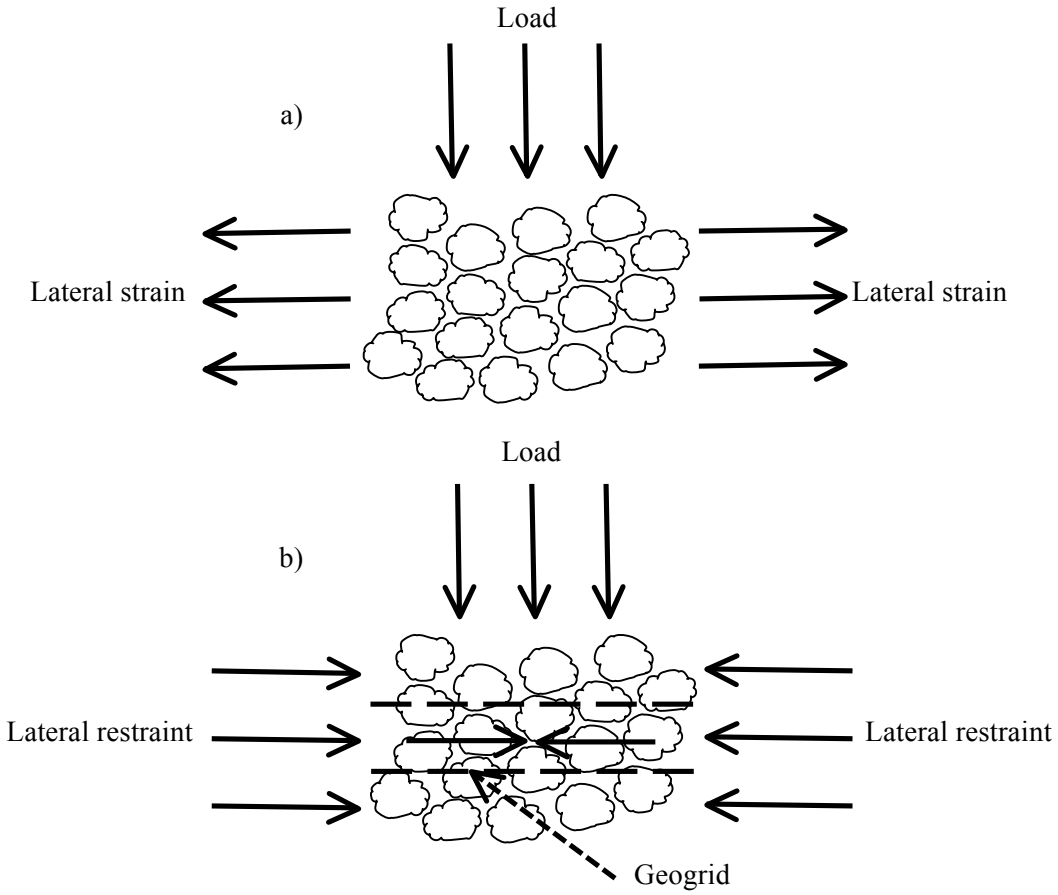

Figure 3.1 The concept of soil reinforcement. Lateral strain occurs when reinforcement is not used (a), while the use of reinforcing produces a lateral restraint (b), as the stress from the load is transferred through friction between the soil and the reinforcement (James, pers comm, 2010).

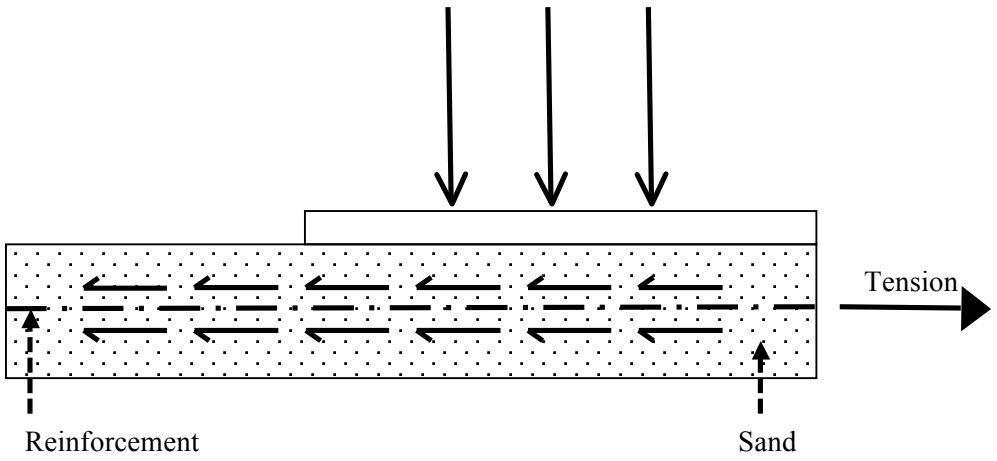

Figure 3.2 Basic mechanism of tension mobilisation in reinforcement (modified after Sharma and Bolton, 1996).

Sharma *et al* (2009) compiled an extensive literature review on the ultimate bearing capacity of geogrid reinforced soil foundations. They noted that geogrids with higher tensile modulus performed better than geogrids with lower tensile modulus, and that a geogrid reinforced soil foundation performed better than geotextile-reinforced soil foundations. This is the most notable difference between the reinforcing behaviour of the two materials, as the adhesion between a geogrid and adjacent soil is usually poor because of its smaller surface area (Sharma and Bolton, 1996). Binquet and Lee (1975) were also the earliest researchers to show that a failure load could be increased by the use of multiple layers of reinforcement.

Geogrids, which are arranged in a grid structure with an aperture geometry allows for soil particles to penetrate from one side of the geogrid to the other. Therefore the confinement effect is the dominant reinforcing mechanism in geogrid reinforced sandy soil (Sharma *et al*., 2009). As mentioned and illustrated, the confinement effect of reinforcement can restrain the lateral deformation or potential tensile strain of the soil. This will result in increasing the bearing capacity of the reinforcing sand, which is being utilized as the founding horizon.

3.2.2 Reinforcement mechanisms

Sharma *et al* (2009) summarised three reinforcement mechanisms of a reinforced soil foundation, under strip footings. The first is the rigid boundary mechanism. This mechanism occurs when the depth of the first layer of reinforcement is greater than a certain value. The reinforcement then acts as a rigid boundary, and the failure would occur above the top layer of reinforcement. The second mechanism, termed the membrane effect, is characterised by the downward movement of the footing and soil beneath the footing under the applied load. This results in the reinforcement deforming and tensioning. Due to the geogrid stiffness, the curved reinforcement develops an upward force to support the applied load. A certain amount of settlement is needed to mobilise the tensioned membrane effect, and the reinforcement should have enough length and stiffness to prevent it from failing by pull-out and tension. The third and final mechanism Sharma *et al* (2009) defined was the confinement effect or lateral restraint effect. A frictional force is induced at the soil-reinforcement interface, due to the relative displacement between the soil particles and the reinforcement. Consequently, lateral deformation or potential tensile strain of the reinforced soil is restrained and as a result, the vertical deformation of soil is reduced. Improved lateral confinement can increase the modulus or compressive strength of the soil and thus improve the bearing capacity of the reinforced soil.

3.2.3 Behaviour of reinforced foundation sand at failure

Huang and Tatsuoka (1990) and Miyazaki and Hirokawa (1992) both conducted studies showing how the mechanisms of deformation under a footing are affected by reinforcement. Huang and Tatsuoka (1990) systematically examined the effects of the length, the arrangements and the rigidity and rupture strength of the geogrid within the reinforcing layer.

For reinforcement, which has a width equivalent to the footing width, Huang and Tatsuoka (1990) found that in the zone reinforced beneath the footing, only small strains were induced. Along the lateral faces of this zone, intensely sheared bands were formed. These results indicate that the reinforced zone behaved like a part of the rigid deep footing. This means that the potential strains, had been restrained effectively and the shear bands formed in the unreinforced sand had moved outwards due to the effects of reinforcing. They concluded that by densely reinforcing sand with stiff tensile-reinforcement having a length similar to the footing width, a failure occurs in sand beneath the reinforced zone, and the bearing capacity characteristics become very similar to that of unreinforced sand loaded with a rigid deep footing having an equivalent depth.

Huang and Tatsuoka (1990) highlighted that there is an obvious increase in the bearing capacity when the geogrid reinforcement are wider than the footing width. They suggest that the increase in the bearing capacity by using long reinforcement layers can be considered due to two factors. Firstly from the deep footing effect, as is observed in the case of reinforcing with short reinforcement layers, and secondly from the effects contributed by the portions of reinforcement placed in the zone beyond the footing width. They termed this the 'wide slab' effect. Their test results showed that the wide slab effect contributed by about 10 - 50% of the total increase in the bearing capacity. Huang and Tatsuoka (1990) also concluded that the degree of contribution also increased with a larger covering ratio above the reinforcement, and the number of reinforcing layers present. Khing *et al* (1994) confirmed this, by concluding that the optimum width of the geogrid layer required to mobilize the maximum possible bearing capacity for a given reinforced sand layer over clay, is about six times the width of the foundation.

Michalowski and Shi (2003) also suggested that mechanisms are modified by the presence of reinforcement. They suggested that although the distribution of vertical displacement is similar to that in unreinforced soil, horizontal displacement of sand above the reinforcement is inhibited by the presence of a geogrid. Relative sliding of the reinforcement and sand occurs only at the geogrid bottom interface, and only in the more advanced phase of deformation is the interface shear fully mobilized. They found that this is demonstrated by the occurrence of distinct shear bands along the reinforcement. Since the rate of soil-geogrid relative displacement at the bottom interface is different from that at the top interface, the rate at which the work is dissipated is different at the two interfaces of the reinforcement. Michalowski and Shi (2003) suggested that this is different from the common assumption that the two interfaces contribute equally to stability.

Sharma *et al* (2009) identified four possible failure modes for reinforced soil foundations based on their literature review and the results of experimental study conducted by Chen (2007) and Abu-Farsakh *et al.* (2008). These failure modes are illustrated in Figure 3.3. The first failure mode was identified when failure occurs above the top layer of reinforcement (Binquet and Lee, 1975), whilst the second failure mode occurs between reinforcement layers (Wayne *et al*., 1998). The third failure mode is indicative of footings on a two-layer soil system, such as when a strong soil layer overlies a weaker soil layer (Wayne *et al*., 1998). This is much the same as a case where a stronger reinforced sand foundation overlies a weaker clay horizon. The final failure mode is where failure occurs through the reinforced zone and ruptures the reinforcement.

The first two failure modes can be avoided by keeping the top layer spacing and the vertical spacing between reinforcement layers small enough (Chen, 2007; Abu-Farsakh *et al*., 2007), and therefore for all research purposes the last two failure modes are important.

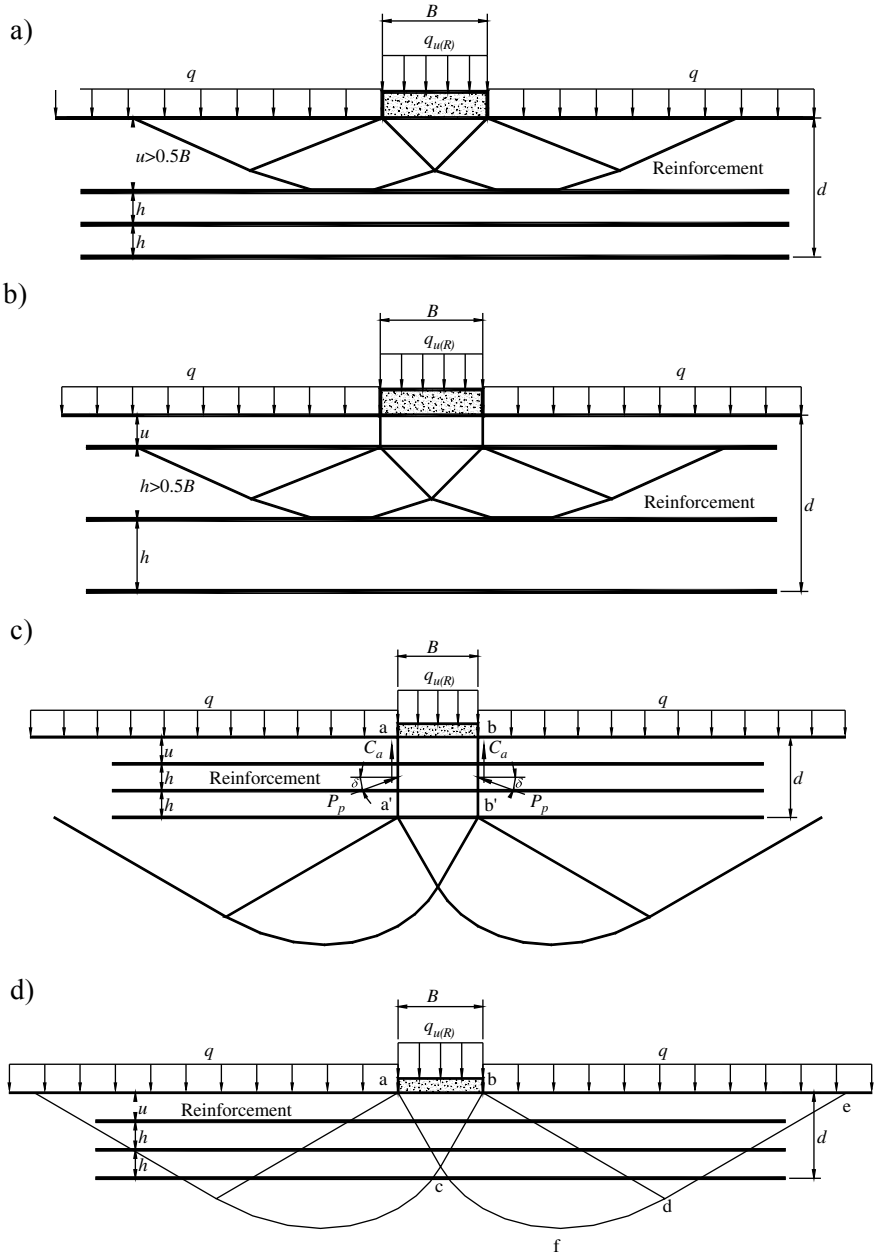

Figure 3.3 Failure modes of reinforced soil foundations. (a) Failure above the top layer of reinforcement (after Binquet and Lee, 1975a,b). (b) Failure between reinforcement layers (after Wayne *et al*., 1998). (c) Failure similar to footings on a two-layer soil system (after Wayne *et al*., 1998). (d) Failure within reinforced zone (Sharma *et al*., 2009).

3.3 Centrifuge modelling of materials

The most important aspect of designing and constructing a geotechnical centrifuge model, for soil, is to ensure a correct representation of the effective stress profile. The effective stress history, the

current effective stress state and the effective stress path followed during the test will dictate the behaviour of the model (Phillips, 1995). Ensuring a correct simulation of these input properties, will guarantee a meaningful output from the behaviour of the model when tested. Due to the generic and experimental nature of this study, techniques used for undisturbed soil will not be considered.

For these conditions reconstituted laboratory soils are normally used with well-defined properties, which can then be altered to produce the required material behaviour. The fundamental reason to doing this is so that the models are well controlled, and aids in the comparison of model results with numerical results (Phillips, 1995).

3.3.1 Sand

Dry pluviation techniques have been used for uniformly graded dry sands. Pluviation involves dry sand particles being rained-down into the model container. The density of the sand can be controlled by the energy imparted to the sand particles during placement, via a sand hopper (Phillips, 1995). Denser samples are created by pluviating the sand slowly from a larger drop height, whilst looser samples can be created by pluviating the sand quicker from a lower drop height. Huang and Tatsuoka (1990) describe how their model was constructed via a slit in a hopper, which was moved over the sand box repeatedly. The falling height was adjusted so that it was kept at a constant height from the surface. By this method, homogeneous sand models having a constant relative density value were obtained. They also describe that for their reinforced sand layer in the model, when geogrids needed to be installed, pluviation of the sand was temporarily ceased and a layer of reinforcement was placed on the surface of sand, at each prescribed depth. After this, sand pluviation was continued. Jacobsz (2013a) describes how sand was placed via pluviation for modelling a soil nail retaining wall. Maintaining a constant drop height and flow rate, resulted in a relative density of approximately 55% of the placed sand.

For saturated sand models, Phillips (1995) suggested that pluviated samples are better saturated after construction. The pore fluid is introduced via a header tank through a base drainage layer into the dry model. He noted that it is important to keep the driving head below the hydrostatic head to saturate the sand sample, and movement of the saturation front should be controlled to prevent air pockets becoming trapped within the saturated material. Furthermore, Arnold *et al* (2010) ensured stability of their model during transport to the centrifuge by flooding the model with water after preparation, thereafter draining the model to create suction, and ensure that no disturbance took place.

3.3.2 Clay

Phillips (1995) suggested that for better defined stress histories, clay samples should be reconstituted from a slurry. In many instances, researchers have made use of reconstituted kaolin powder to create clay for centrifuge modelling tests (Kutter *et al*., 1988; Stewart and Randolph, 1991; Köning *et al*., 1994; Sharma and Bolton, 1996; Sharma and Bolton, 2001; Ilyas *et al*., 2004; Arnold *et al*., 2010). In all instances the slurry is mixed at approximately twice the liquid limit of the dry kaolin powder with deionised water. This minimises any chemical effects and bacterial growth within the sample (Taylor,

1995). In all instances the clay slurries were mixed under at least partial vacuum for an extended period of time to de-air the slurry and create a smooth liquid.

Clay slurries can be consolidated in the centrifuge, while others can be consolidated in a consolidometer (Phillips, 1995). In some cases both techniques are used to achieve the required stress history, mostly for clay samples which required an overconsolidated stress history. Kutter *et al.*, (1988) consolidated the clay slurry in two stages, firstly in a consolidometer and then in the centrifuge. The second consolidation stage was used to 'heal' the disturbances caused by the instrumentation installed into the clay. Stewart and Randolph (1991) prepared two clay samples for their testing. The samples were consolidated by a vertical surcharge of 60 kPa and 100 kPa, before self-weight consolidation in the centrifuge at 100 G and 110 G, respectively. In both sample preparation procedures a 5 mm layer of sand was placed on top of the clay during self-weight consolidation, to prevent the clay swelling at the surface and to aid in drainage. Sharma and Bolton (1996, 2001) consolidated the slurry to a maximum vertical pressure of 100 kPa in a consolidometer. Two days before a centrifuge test, the slurry was unloaded and trimmed to the dimensions of the model container. Arnold *et al* (2010) utilised both methods to create their required stress history. The clay slurry was preloaded for four weeks up to a vertical stress of 200 kPa prior to the planned model tests. After the preconsolidation phase, the sample was reconsolidated in the centrifuge for 12 hours and 50 G., by monitoring the surface settlements and the excess pore water pressures. Ilyas *et al* (2004) utilised a similar method to prepare an overconsolidated clay sample for their experiments. They imposed a surcharge of 60 kPa, which was gradually placed on top of the clay slurry in the model container at 1 G, for approximately a week. The clay was then further consolidated under its self-weight in the centrifuge for about 6 h to achieve an average degree of consolidation of at least 95%. The preparation of overconsolidated clay samples is time consuming and arduous, and requires appropriate consolidation before centrifuge tests can be conducted.

For normally consolidated clay however, it is unnecessary to go to such lengths. The smaller preconsolidation stress in normally consolidated clays is not as large, and therefore to correctly model their stress history, a preconsolidation phase is generally not as lengthy. Nakase *et al* (1984) investigated the bearing capacity of strip footings on normally consolidated clay. The clay material was obtained from a block sample which was then remoulded. The clay sample was placed in the model container, and surcharge bags placed over the clay, and placed in the centrifuge. The container was accelerated to 10 G, where water was inserted into the bags. The amount of water was enough so as to load the clay to a stress not more than what was required when the load was applied with the footing. Ilyas *et al* (2004) prepared a normally consolidated kaolin clay sample by placing the clay slurry into the model container. They then consolidating it under self-weight in the centrifuge at 70 G to allow the excess pore water pressure in the clay to dissipate through the clay surface and the openings located close to the bottom of the container via a bottom sand layer. Ground settlements and pore water pressures in the soil were measured to monitor the progress of consolidation. Six hours consolidation time was typically required for Ilyas *et al* (2004) to achieve an average degree of consolidation of at least 95%.

3.3.3 Geogrids

Scaling down of geosynthetic materials is essential in any small-scale physical modelling studies, in order to obtain the correct response of prototype structure. Several researchers have conducted centrifuge testing with geogrids over a broad scope of application. Viswanadham and König (2009) used geotechnical centrifuge testing to model geotextile-reinforced slopes, while Sharma and Bolton (1996, 2001) researched the use of reinforced embankments on soft clay. Viswanadham and Jessburger (2005), and Rajesh and Viswanadham (2009) researched the use of geogrids as a reinforcement layer beneath clay based engineered barriers.

These researchers have based their choice of geogrid on the work conducted by Springman *et al*., (1992), and the more recent study by Viswanadham and König (2004), on scaling and instrumentation of a geogrid in small scale physical modelling. The scaling down of geosynthetic materials is essential in small-scale physical modelling studies in order to infer the correct response of prototype-soil structure. Because of the involvement of several complex factors, perfect scaling-down of the prototype materials to the desired scale factor may not be feasible and no model can be a precise equivalent of any particular structure in the field (Springman *et al*., 1992; Viswanadham and König, 2004). An ideal geosynthetic material (geotextile or geogrid) for model studies needs to be selected by considering a model material representing the band width of the existing commercially available prototype geosynthetic material characteristics. However, in order to model soil–geosynthetic behaviour satisfactorily, there is a substantial requirement of appropriate modelling of geosynthetic materials for studies pertaining to the behaviour of reinforced soil structures (Viswanadham and König, 2004). Springman *et al* (1992) suggested that it is necessary to quote significant prototype dimensions, groups and properties, by multiplying up the model parameters by the scale factor and then separately consider whether these structures are broadly representative of realistic conditions.

The main emphasis of the paper presented by Viswanadham and König (2004) was to provide a set of guidelines for selecting a model geogrid for physical model studies, especially in a geotechnical centrifuge. They deduced that in order to correctly model a geogrid, two basic requirements need to be considered. The first was the correct scaling of the frictional bond behaviour, and secondly, to model the tensile strength-strain behaviour. Based on the results of their study the selection of model geogrids can be carried-out by (Viswanadham and König 2004):

(i) Scaling ratio of rib cross-sectional area to the grid opening size,
(ii) Scaling of tensile strength–strain behaviour (Figure 3.4), and
(iii) Maintaining identical percentage open areas in both the model and commercially available geogrids (Figure 3.5).

By maintaining the ratio of rib cross sectional area to the grid opening sizes, as well as the percentage open area, the scaled down geogrid is able to generate the same amount of passive resistance from the column of the soil confined between its apertures as the prototype geogrid (Viswanadham and König, 2004). This, together with the scaling down of the geogrid tensile strength-behaviour, ensure that the two most valuable properties of increasing the bearing capacity of a reinforced soil are represented in the model.

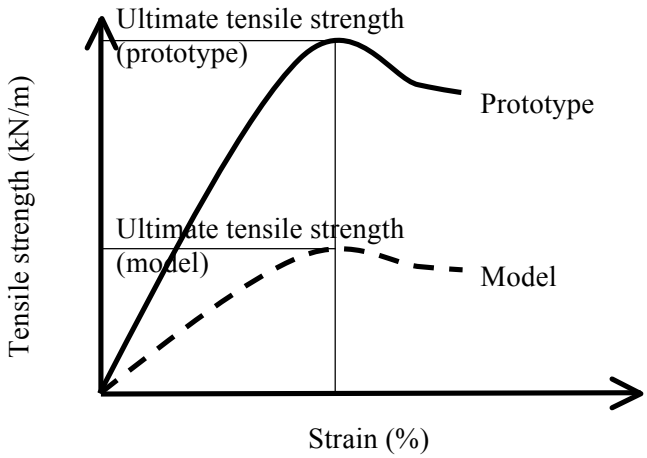

Figure 3.4 Idealised tensile strength-stain behaviour for scaling geogrids from prototype to model (Viswanadham and König, 2004).

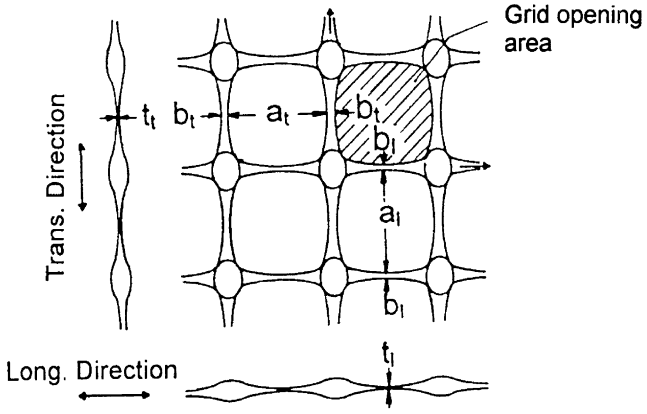

Figure 3.5 Ideal scaling of a geogrid should involve maintaining the identical percentage of open areas in the geogrid, as shown in the hatched area (Viswanadham and König, 2004).

Sharma and Bolton (2001) successfully scaled down the prototype reinforcement used in their study of reinforced embankments on soft clay. At 40 G, their model geotextile represented a prototype geotextile having a tensile strength of 380 kN/m at 10% axial strain. For their research on geogrids as a reinforcement layer in clay based engineered barriers, Rajesh and Viswanadham (2009) selected a model geogrid which was in agreement with the available prototype geogrids. The model geogrid that they chose had a percentage opening area of 68%, which compared successfully to the average values for available prototype geogrids in the range of 60 – 85%. The model geogrid selected in their study had an average tensile strength of 4.51 kN/m at 5% strain. This corresponded to a tensile strength of 180 kN/m at 40 G, which is in agreement with the average tensile strength of 75 – 250 kN/m at 5% strain for commercially available geogrids. It is not always necessary to identically simulate the model geogrid properties with the prototype geogrid properties, when researching the behaviour of materials when reinforcement is included. This is highlighted by the research conducted by Viswanadham and König (2009), who did not select a model geofabric which was necessarily representative of prototype conditions. Instead the model geogrids were chosen to understand the response of geotextile-reinforced slopes specifically subjected to differential settlement.

3.4 Summary

A perusal of literature was conducted to gain knowledge on previous studies surrounding geotechnical centrifuge modelling. Particular emphasis was placed on understanding the techniques previously used for the modelling of sand, clay and the scaling down of geogrids. The concept of soil reinforcement was also presented together with previous research conducted on geogrid reinforced sand foundation. The concept of soil reinforcement is that lateral strain in a soil cause by an imposed load becomes a lateral restraint when reinforcement is included. Soil reinforcement is essentially the interaction between the reinforcement material and the soil by friction or mechanical interlock and the resistance to tensile strain by the reinforcement. It is this interaction and strength of the reinforcement that increases the bearing capacity of the ground profile. Dry pluviation techniques for preparing sand in a centrifuge model involves adjusting the drop height and flow rate from a sand hopper to adjust the density of the sand particles. Clays samples are best prepared from a reconstituted powder and mixed to twice its liquid limit. The stress history and subsequent consolidation of the clay can be conducted via a consolidometer, or in the centrifuge via self-weight of the soil. When modelling a prototype geogrid in the centrifuge, the scaling of the tensile strength-strain behaviour and maintaining identical percentage grid opening sizes, are the fundamental issues when deciding on the model geogrid.

CHAPTER 4 NUMERICAL ANALYSES

4.1 Introduction

Standard procedure in the geotechnical profession when designing foundation solutions for complex structres upon unfavourable soil profile, would be to predict the stress-deformation in a Finite Element (FE) analysis package. The following chapter will present a simple qualitative FE analysis run on SIGMA/W. Conducting a complicated numerical analysis falls out of the scope of work for this research, however by conducting a simple FE analysis some comparison can be made between what the results of the simple qualitative numerical analysis and the observation from the centrifuge model tests, in the later chapters of this dissertation.

4.2 SIGMA/W Analyses

The numerical analyses were completed using SIGMA/W, which forms part of the Geostudio package, developed by GEOSLOPE. Sigma/W is finite element software which was developed to carry out stress-strain analysis of geotechnical problems.

The FE analysis was constructed on the scaled-up dimensions and properties of the model and materials. A total stress analysis was conducted. A linear-elastic numerical analysis was conducted at first, however it was realised that the loads achieved in the analysis were too high. This was explained by the clay horizon not being able to reach a yield point, and subsequently unable to behave as a plastic material when it fails. As such a liner elastic-perfectly plastic analysis was conducted. The input parameters for the materials and boundary conditions are listed in Table 4.1. A total of a 100 steps where conducted in the analyses and a maximum 100 iterations specified for the convergence. The reinforcement layers were modelled as a structural beam, with no flexural stiffness. Therefore the moment of inertia was specified as zero. The geofabric had a E-modulus of of 1 800 000 kN/m and a cross sectional area of 0.381 m^2. A frictional strength was added above and below the reinforcement. The angle of internal friction for this material was set as 30° with no cohesion. The geogrid had a tensile capacity, but no compressive capacity, and as such no compression was allowed for the geogrid during the analysis.

The analysis was displacement controlled to a vertical displacement of 0.75 m. This corresponded to a vertical displacement of 15 mm in the centrifuge at 50 G. The total applied load under the foundation was recorded at each of these displacement intervals, enabling comparison to the applied stresses achieved in the centrifuge at the corresponding vertical displacements. Figure 4.1 shows the FE mesh used in the analyses. The ground profile was modelled using a mesh with 186 four-noded linear elastic – plastic strain quadrilaterals and three-noded linear elastic – plastic strain trianglular elements

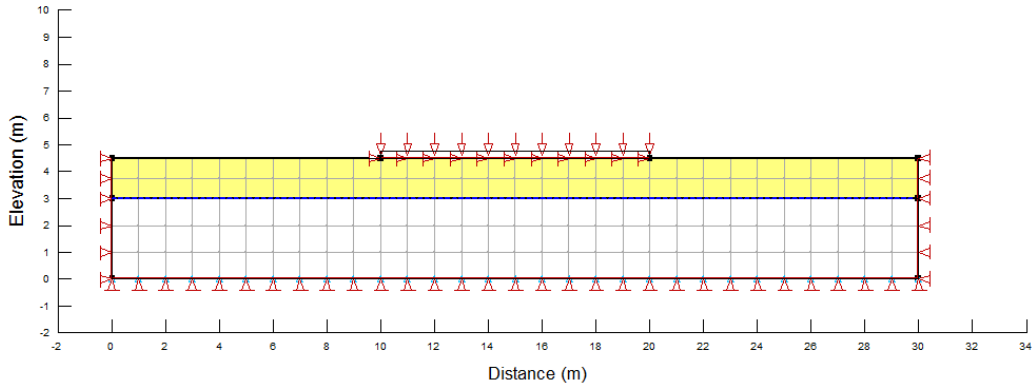

Figure 4.1 Finite element mesh used in the numerical analyses.

Table 4.1 Input parameters for the analyses, materials and structural beam used in the FE analyses.

Analyses	Convergence: Max no. of iterations	100
	Tolerance: Displacement norm:	0.1%
	Duration	100 sec
	No. of steps	100
Sand	Material category	Total stress parameters
	Material model	Elastic-plastic
	Total E-Modulus: Constant	60 000kPa
	Total cohesion: Constant	0 kPa
	Unit weight	8 kN/m^3
	Total phi	37°
	Poisson's ratio	0.25
	Dilation angle	0°
Clay	Material category	Total stress parameters
	Material model	Elastic-plastic
	Total E-Modulus: Constant	2 888 kPa
	Total cohesion: Constant	3.05 kPa
	Unit weight	20 kN/m^3
	Total phi	0°
	Poisson's ratio	0.495
	Dilation angle	0°
Friction (top and bottom of reinforcement)	Material category	Effective-drained parameters
	Material model	Slip surface
	Interface C'	0 kPa
	Interface Phi'	30°
	G (shear modulus)	1 000 kPa
	Unit weight	0 kN/m^3
	Poisson's ratio	0.334
Geogrid	E-modulus	1 800 000 kPa
	Cross-sectional area	0.381 m^2
	Moment of inertia	0 m^4

A FE analysis was run for each test completed and the results compared to those obtained from the centrifuge modelling tests. Figure's 4.2, 4.3, 4.4, 4.5 and 4.6. The deformation mechanisms from the centrifuge tests, are compared with the mechanisms obtained in the numerical analyses. The loads achieved at the respective vertical displacement intervals are tabulated in Table 4.2.

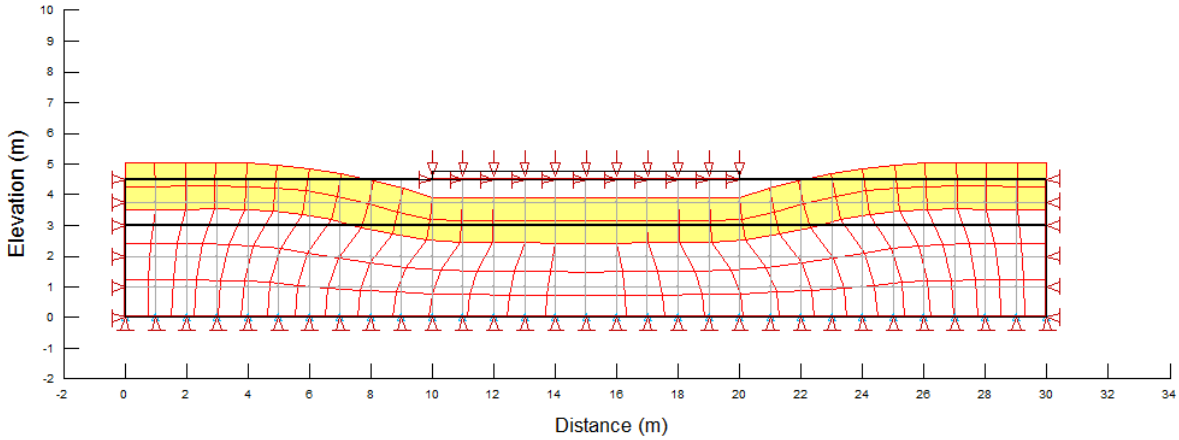

Figure 4.2 Numerical results for the test with no reinforcement present.

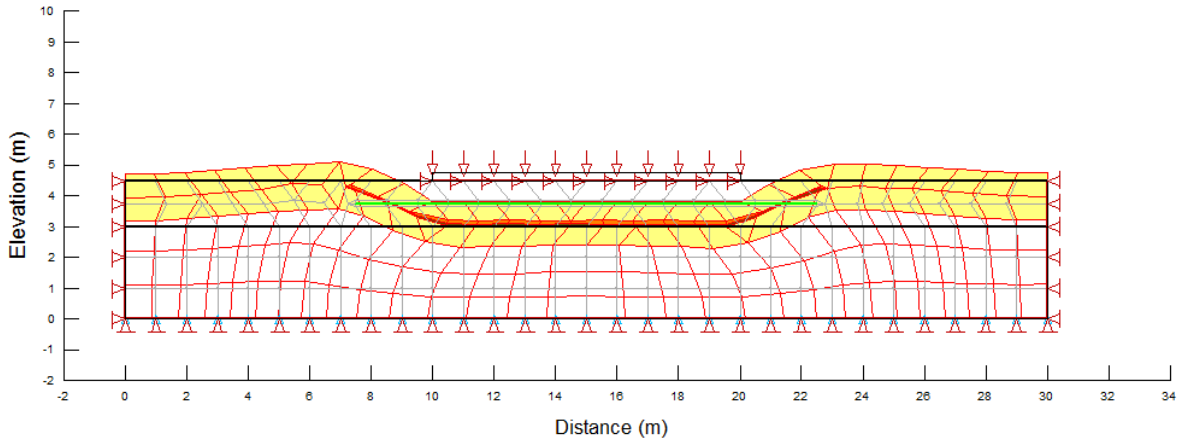

Figure 4.3 Numerical results for test with a single reinforcement layer (short width) present.

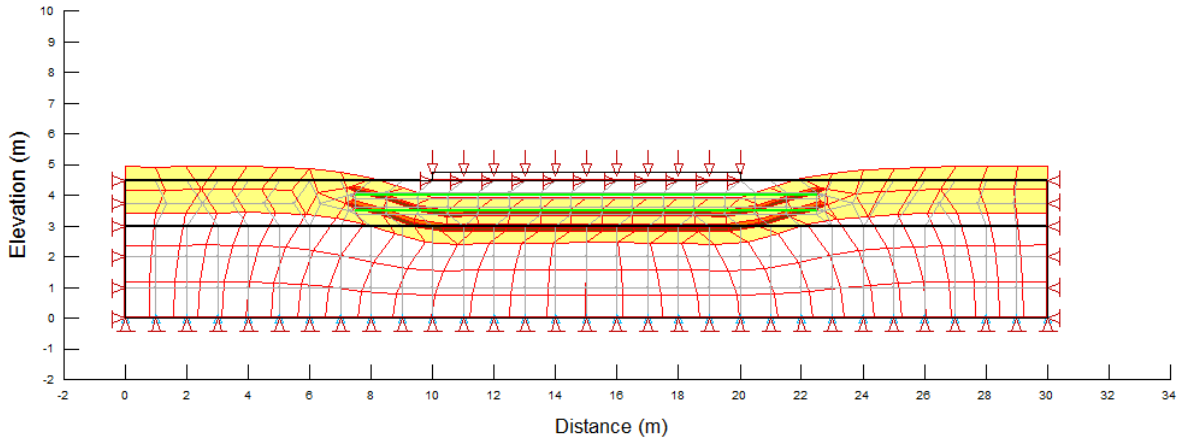

Figure 4.4 Numerical results for test with two reinforcement layers (short width) present.

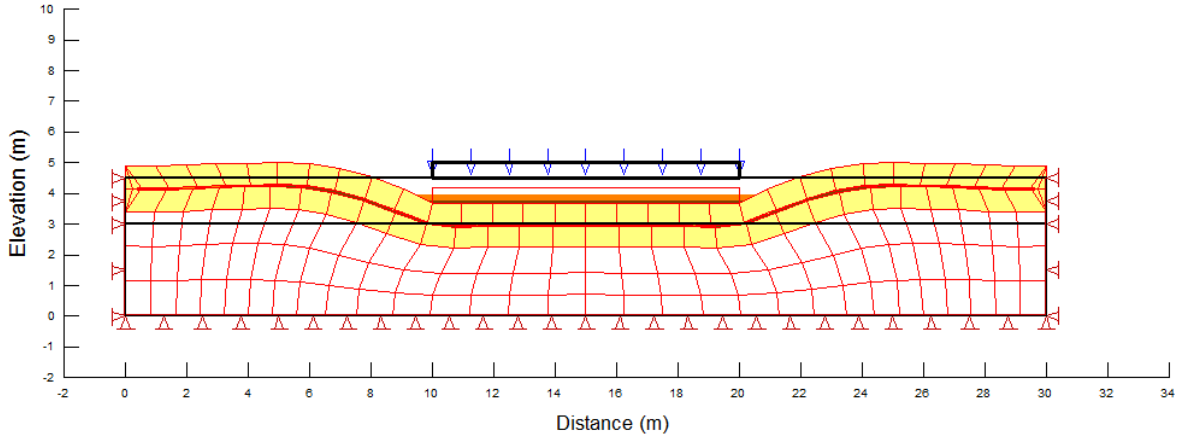

Figure 4.5 Numerical and centrifuge results for test with a single reinforcement layer (extended width) present.

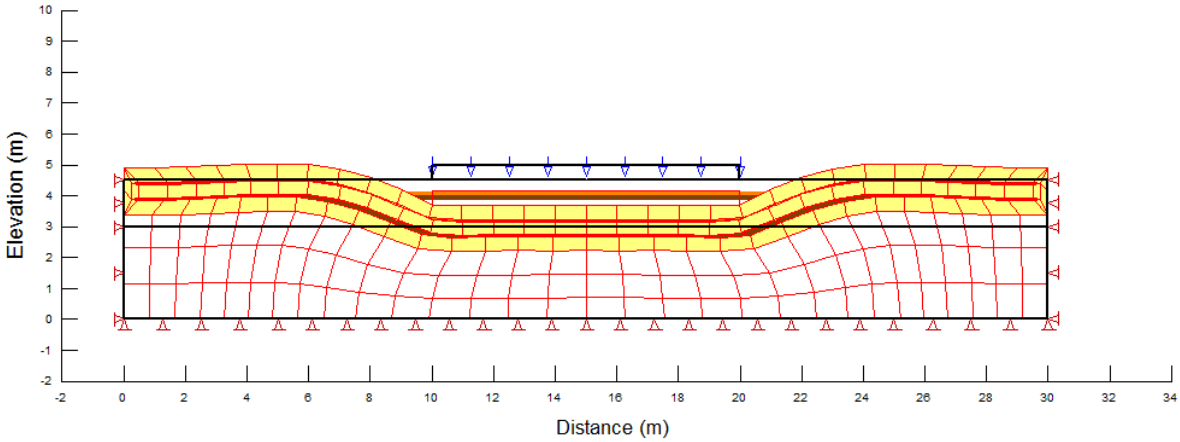

Figure 4.6 Numerical and centrifuge results for test with two reinforcement layers (extended width) present.

Table 4.2 Total applied stress achieved under the foundation at 0.75 m vertical displacement.

	Applied stress (kPa)
Unreinforced	16.72
1 Geogrid (Short width)	22.40
2 Geogrids (Short width)	31.20
1 Geogrid (Extended width)	2049.28
2 Geogrids (Extended width)	1696.12

The FE analysis computed substantial deformation under 0.75 m displacement. The zone of deformation of the clay layer is extensive, and the entire width of the clay horizon is vertically deformed for all numerical tests conducted. The maximum height of the vertical deformation bulge is approximately 0.5 m for all the numerical models computed. The portion of sand directly beneath the platform load behaves as a rigid horizon and displaces vertically down with the platform. There is no distinctly clear difference in deformation behavior between the unreinforced and reinforced tests, and furthermore no distinction between deformation behavior in the reinforced models.

The test with 1 geogrid layers with a short width has an slight bulging effect, compared to the rest of the numerical models. The loads achieved are expected for the clay horizon with such a soft consistency. There is an improvement in the load carrying capacity at 0.75 m when reinforcement is included. The applied stress values calculated for the extended width reinforcement tests are high. This is not unbelievable however, when considering that the program will recognize the high tensile strength geogrid as a flexural beam which will be able to withstand a large load. This is assuming that the modeled geogrid is well anchored over the width of the numerical model, which is is. The poor performance of the shorter width geogrid numerical models could be explained by the lack of surface area to 'anchor' the geogrid into the adjacent sand material. As such, the tensioned membrane effect is not mobilized along the width of the geogrid, thereby not allowing the full tensile strength capacity of the geogrid to withstand a large load upon displacement of the platform foundation.

The lower applied stress calculated for the 2 geogrid model with extended width, compared to the single geogrid with an extended width may be ascribed to an a small interaction problem. This would have occurred if the numerical model calculated that there was not sufficient sand at the interface of each of the geogrids, for the tensile strength in the geogrid to mobilise with the sand. This would have lead to an interface slip between the two geogrids at the bottom interface of the upper geogrid and the upper interface of the lower geogrid interface. Nevertheless, the high calculated applied load of this model is not a concern.

4.3 Summary

A simple qualitative FE analysis was constructed to provide a set of results which could be compared to what the centrifuge data obtained. The numerical analysis was displacement control to a vertical displacement of 0.75 m. This would enable comparison with the centrifuge model at 15 mm vertical displacement. The applied stresses recorded are realistic considering the soft nature of the clay material. The unreinforced test performed the worst, while the extended width geogrid numerical models performed the best, most likely due to the programs recognition of such a high tensile strength geogrid being able to withstand large imposed loads.

CHAPTER 5 CENTRIFUGE MODEL

5.1 Introduction

Necessary consideration needs to be given to all aspects of the centrifuge model, from the conceptualisation stage, through preparation of the materials, subsequent test set up and the final testing phase. This chapter presents the process, which was followed for each centrifuge model. The preparation procedure adopted to obtain the required parameters of each material is described and an account is given of the centrifuge testing procedures carried out. The diffculties encountered during preparation and testing are also discussed.

5.2 Model test set-up

Once a clear understanding of what fundamental questions were needed to be answered from the centrifuge tests, a conceptual model was planned. Knowledge gained from the perusal of the literature of previous studies, as well as several trial models, ensured a good understanding of how each model needed to be constructed.

As discussed in Chapter 3, the geometric scale factor of the model was selected to fit the prototype situation, specifically for this study, into the model container. The scale was chosen to ensure separation between elements of the model and the walls of the strongbox to ensure minimal boundary effects. The appropriate centrifuge acceleration level was chosen to satisfy several important aspects. The height of the model was chosen such that the length of the model was maintained at less than twice the height of the model. The height from the floor of the strongbox to the surface of the model was 190 mm, with a strongbox length of 600 mm. It was also required to choose a scaling factor to accommodate the stiffness, which the geogrids would add to the upper reinforcing sand. A centrifuge acceleration level of 50 g was decided to be the most appropriate scaling factor.

Figure 5.1 shows the conceptualised model set-up. The height of each soil stratum is displayed, with the bottom sand having a height of 100 mm, the overlying clay a thickness of 60 mm and the upper reinforced sand a thickness of 30 mm. The load would be applied via a jack attached to the model platform. This jack was placed above the centre of the model so that the 200 mm wide platform applied the load to the centre of the model, with 200 mm between the platform edge and the strongbox wall. Three pore pressure transducers (PPT's) were installed at 3 locations within the clay layer of the model. The first PPT was installed underneath the centre of the platform (PPT 1), and the second PPT at the edge of the platform (PPT 2), 100 mm away from the first PPT. The third PPT was installed 100 mm from the edge of the platform (PPT 3). All PPT's were positioned such that they occupied approximately the middle of the clay layer at 30 mm from the boundaries between the upper and lower sand horizons.

Figure 5.2 illustrates the configuration for each test conducted on the centrifuge model. The unreinforced test had only the upper sand horizon. The tests with reinforcement involved adjusting the number of reinforcement layers and the width of the geogrid, in the upper sand horizon.

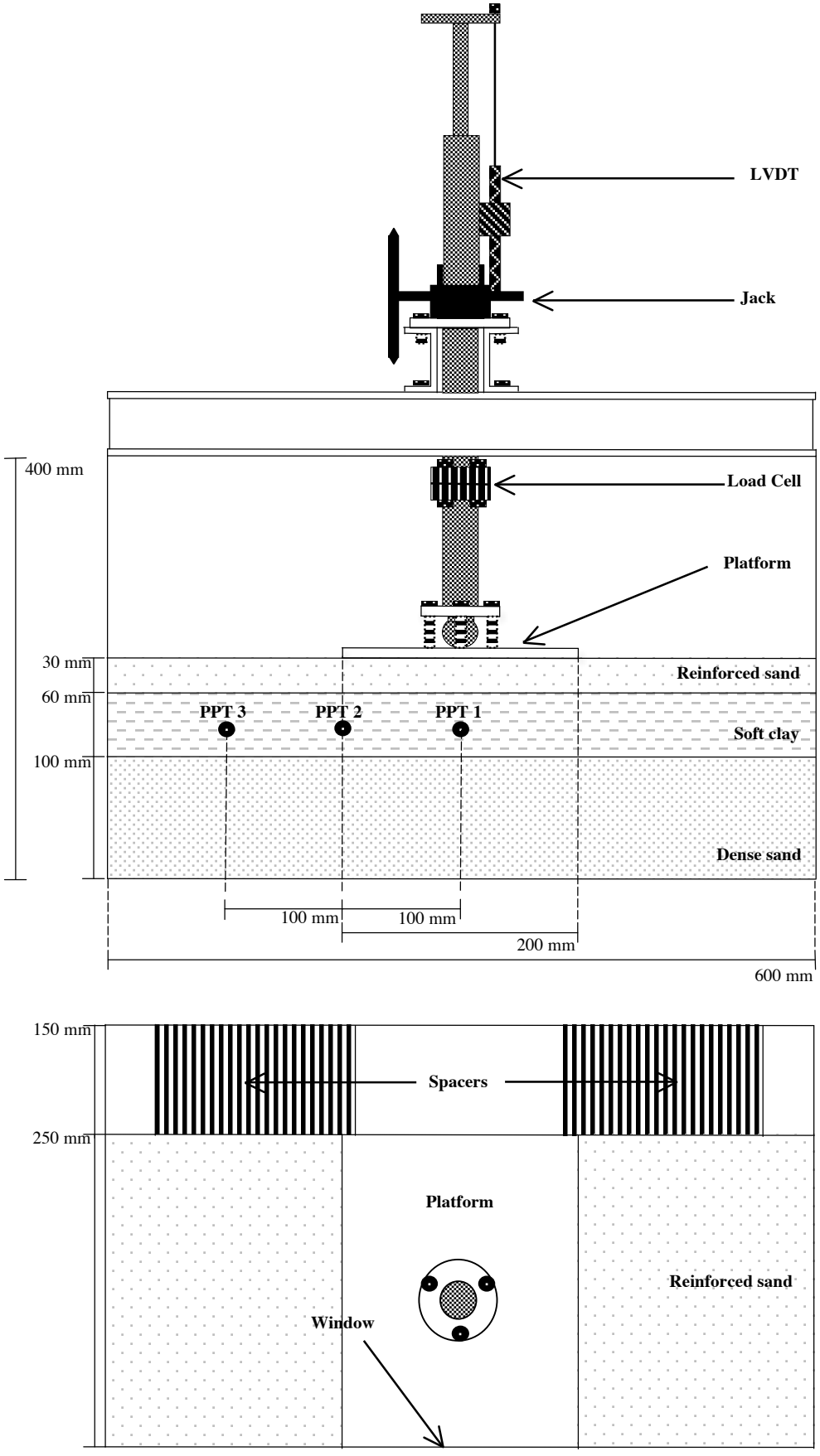

Figure 5.1 The centrifuge model set-up.

Tests with a geogrid width 50 mm past the edge of the platform are referred to as having a short width. The tests with a geogrid width which approximately spanned the length of the strongbox (180 mm from the edge of the platform), are referred to as extended geogrids. When a single geogrid was placed in the upper sand horizon, it was placed in the centre of the horizon, such that 15 mm sand was present on the top and below the geogrid. When two geogrids were placed in the upper sand, they were spaced 10 mm apart from each other, and 10 mm from the bottom and top of the reinforced sand horizon, respectively.

5.3 Strongbox

The strongbox used consists of 50 mm thick aluminium panels. The front panel is thicker and has a 80 mm thick glass window to allow a cross-sectional observation of the testing carried out in the box. The base of the box contains six drainage holes (3 on each side) to enable water to flow in or out of the box. Rectangular grooves are cut between these holes to ensure drainage or saturation, from the floor of the container. A transparency with a grid printed on it was placed between the glass and the model, which would assist in determining the dimensions of the deformation behaviour. Each square on the grid measured 5 mm x 5 mm.

The top of the strongbox is fitted with a 25 mm thick by 50 mm wide steel collar which allows for specific customisation for attaching instrumentation and loading apparatus. It was unnecessary to utilise the full width of the strongbox, and therefore a spacer was included for the tests conducted. This spacer allows for a model with a width of 250 mm. Once the spacer was placed in the strongbox, duct tape was placed around the edges to seal the modelling compartment from the spacer compartment. This also ensured that saturation of the model only occurred through the base holes in the floor of the box, and therefore minimising disturbance of the bottom sand layer. A non-woven continuous filament needle-punched geotextile with a high drainage capacity was placed on the floor of the box to ensure an even distribution of water during saturation. This also ensured that the bottom sand layer was not disturbed under the hydraulic head during the saturation process.

5.4 Sand

The sand used for the models was a local fine alluvial sand obtained from a commercial source near Cullinan, Gauteng. Typical soil properties of the sand are summarised in Table 5.1. The particles lager than 200 μm were usually well rounded , with the finer fraction being more angular to sub-angular, with an angle of internal friction of 37° (Jacobsz, 2013a). The grading curve for the sand is presented in Figure 5.3.

Table 5.1. Typical properties of the sand used during model construction.

	Value
Dry unit weight, γ_d	16 kN/m^2
Maximum dry unit weight, $\gamma_{d(max)}$	16.69 kN/m^3
Angle of internal friction, φ	37°

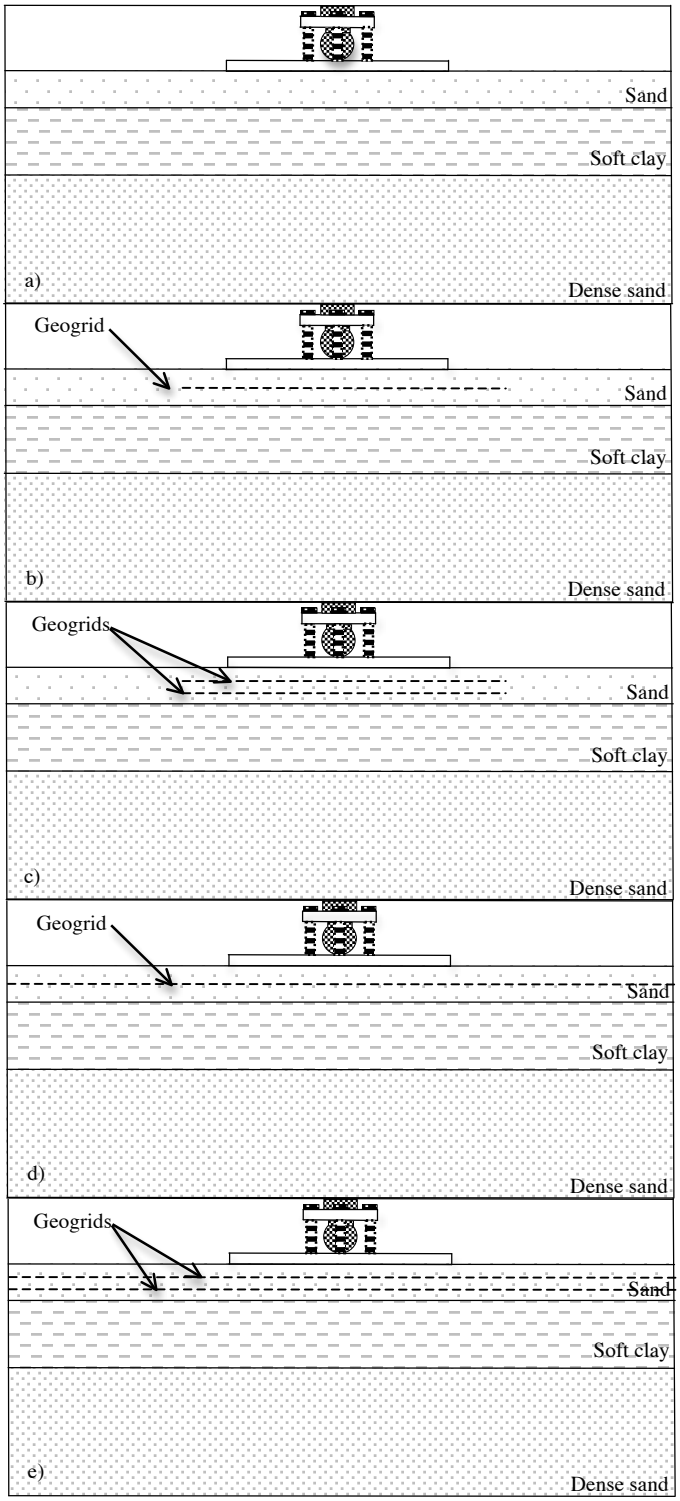

Figure 5.2 The configuration for each test on the centrifuge model.

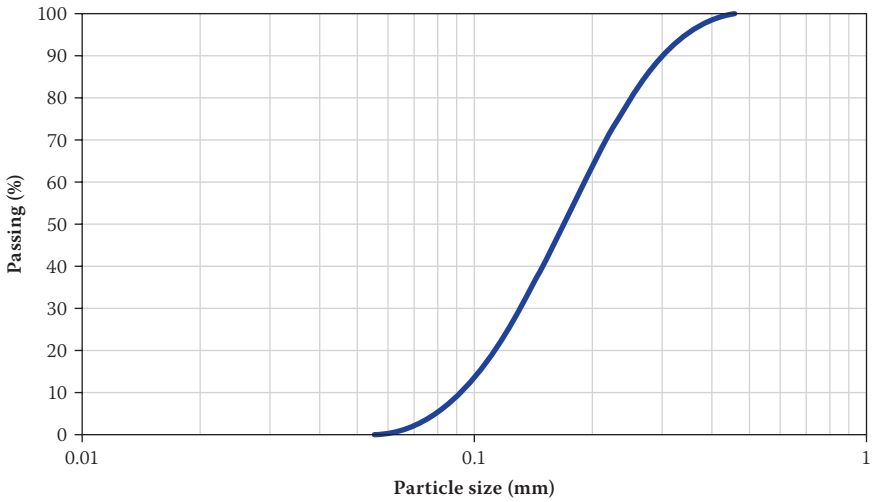

Figure 5.3 Grading curve for the sand used during the model preparation (Jacobsz, 2013a).

5.4.1 Pluviation

A dense packing was required for the basal sand horizon of the model. To ensure this, the sand was pluviated from an automated hopper. A higher drop height of sand particles and a slower flow rate from the opening of the hopper ensures a more dense packing, whilst a lower drop height and faster flow rate will ensure a more loosely packed sand layer. A number of trial runs ensured the optimal drop height and flow rate of the sand from the hopper. Table 5.2 gives an example of adjusting the drop height and flow rate and their respective relative densities. It was decided that the optimal pluviation height was 1.00 m, with an opening at the bottom of the hopper of approximately 1.65 mm. This allowed a relative density of approximately 69 % for all the tests conducted, with a minimum of 69 % and a maximum relative density of 75 % to be obtained. Table 5.3 summarises the relative densities achieved for each centrifuge model test. Figure 5.4 a) and b) show the pluviation process. Levelling of the sand once poured was done by using a vacuum system and light mechanical shaping using a leveller. Localised regions of less dense sand occurred in some of the corners of the strongbox, due to corner edge effects of the strongbox when placing the sand form the hopper. When this did happen, sand was placed by hand pluviation.

Table 5.2. Variation of the relative density of the sand pluviated during the trial stage.

	Drop height (mm)	**Hopper opening (mm)**	**Dry density (kg/m^3)**	**Relative density, R_D (%)**
Trial 1	700	2.40	1498	38
Trial 2	500	1.00	1558	60
Trial 3	1000	1.65	1592	72

5.4.1 Saturation

Once the sand layer had been pluviated, it was necessary to saturate it before placing the clay layer on top. Saturation was conducted by firstly pouring water into the unused portion of the strongbox,

where the spacer was placed. This compartment acted as a header tank. This created a hydrostatic head necessary to saturate the sand. The pore water was introduced via the base holes in the floor of the strongbox, which connected the spacer compartment and testing compartment filled with the pluviated dry sand. The driving head was kept to below the hydrostatic head in order to minimise any disturbance to the sand. Figure 5.4 c) shows saturation of the sand occurring from the base of the strongbox. Importance was given to ensuring that the sand was completely saturated before continuing with the model construction, and that no pockets of partially saturated or unsaturated sand remained. There was however, a fine balance between ensuring complete saturation and allowing too much water to pond over the sand surface. An excess amount of water on the sand surface would create difficulties when pouring the clay in the following stage, which would lead to excessive disturbance between the clay and basal sand boundary.

Table 5.3. Relative density achieved for each centrifuge model test.

	Dry density (kg/m^3)	**Relative density, R_D (%)**
Unreinforced	1583	69
1 Geogrid (Short width)	1583	69
2 Geogrids (Short width)	1600	75
1 Geogrid (Extended width)	1583	69
2 Geogrids (Extended width)	1583	69

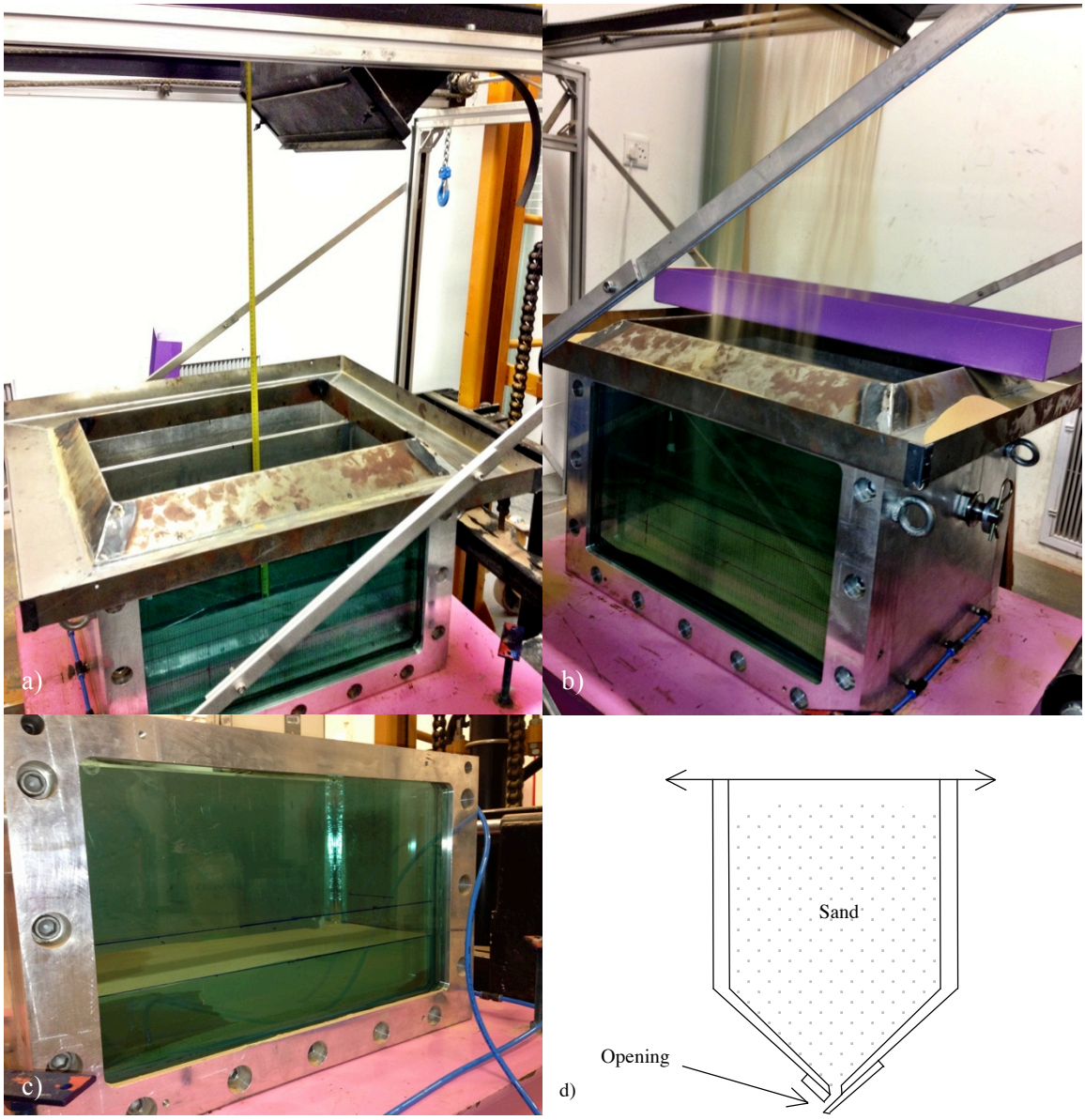

Figure 5.4 Preparation of the basal sand horizon. a) The sand is pluviated from the automatic sand hopper from a height of 1.00 m. b) The hopper opening is adjusted to 1.65 mm to ensure an optimal flow rate, while it moves back and forth over the strongbox to pluviate the sand particles to the required density. c) Once the sand is placed and levelled off, pore water is introduced from the floor of the strongbox. d) Sketch of the automated sand hopper indicating the opening gap to control the flow of sand to be pluviated onto the model.

5.5 Clay

Selection of the clay was based specifically on perusal of previous research conducted in centrifuge studies. Reconstituted kaolin powder was used. The properties of the clay are summarised in Table 5.4. The clay has a liquid limit of 47%, a plastic index of 25%, and was prepared to a very soft consistency with an undrained shear strength of 6 kPa, which was measured by a hand vane shear test.

Table 5.4 Typical properties of the clay used for centrifuge model construction.

	Value
Liquid limit (%)	47
Plasticity index (%)	25
Undrained shear strength	6.09 kPa

5.5.1 Mixing

The clay was mixed to a slurry at approximately twice its liquid limit. Figure 5.5 shows photographs taken during various stages of the preparation of the clay slurry. De-ionised water was poured into a large bucket and a defoaming agent added to minimise air in the slurry. This was then mixed for approximately 5 minutes before the clay was added to the fluid. The dry clay was added in three stages to the liquid, in order to mitigate the formation of lumps The first stage involved adding a third of the dry clay mass to the liquid. The container was shut and mixing continued under a partial vacuum for 30 minutes. Thereafter, the next third of the clay mass was added gradually again while mixing slowly for the initial few minutes. Once again the container was closed, and the clay mixed under partial vacuum. Once the last third of dry clay was added, the slurry was mixed under partial vacuum for another hour, until a smooth consistency was achieved. This process was repeated to create 7 batches. Each batch was left for 24 hours and mixed under partial vacuum thereafter for a further 30 minutes. Once all batches had been mixed, each batch was divided between 2 larger containers. After all the batches of clay slurry had been poured into the larger containers, they were thoroughly mixed together, and each container sealed tightly to avoid any moisture loss. The clay slurry was again mixed before clay was removed for a test.

5.5.2 Consolidation

The prepared slurry was carefully poured into the model container on top of the saturated sand. Initially small quantities of clay where placed over the sand by a scoop, to mitigate any disturbance to the boundary between the sand and the clay. Once this initial clay was placed, the rest of the slurry was poured into the container and levelled off with minimal mechanical disturbance. As the clay would consolidate by approximately 20 to 30% of the initial height, the clay was poured to a thickness of 90 mm. This allowed for enough clay to be available for the required thickness for each test after the consolidation phase.

Pore pressure transducers were then pushed into the clay at the three specific locations within the model. Refer to section 5.7 for details on the specifications of the pore pressure transducers. Each pore pressure transducer (PPT) was attached to a wire anchor, which was the required height for the PPT to be located in the clay, 30 mm from the base of the horizon. This would prevent them from floating in the clay during consolidation and guaranteed that the PPT would remain stationary during the consolidation stage. Filter paper was placed on the surface of the clay to separate the overlying sand. 7.65 kg of sand was poured over the filter paper to give an overburden load of approximately 25 kPa in the centrifuge during consolidation at 50 G (Figure 5.6). The sand also acted as a drainage medium during consolidation.

Figure 5.5 Photographs showing the sequence of preparing the clay to a slurry. a) De-ionised water was mixed with a defoaming agent. b) Dry clay powder was added gradually to the water. c) The slurry was mixed under a partial vacuum. d) Each batch was divided between 2 larger containers, mixed again and sealed for storage.

The strongbox was placed in the centrifuge to consolidate the clay at an acceleration of 50 G for 14 hours. Once consolidation was completed, the overburden sand was removed, and a hand vane shear

apparatus was used to measure the undrained shear strength of the clay after consolidation. Each test measured an average undrained shear strength of approximately 5-7 kPa. Figure 5.7 shows an example of the pore pressure dissipation during consolidation of the clay in the centrifuge over the 14 hours.

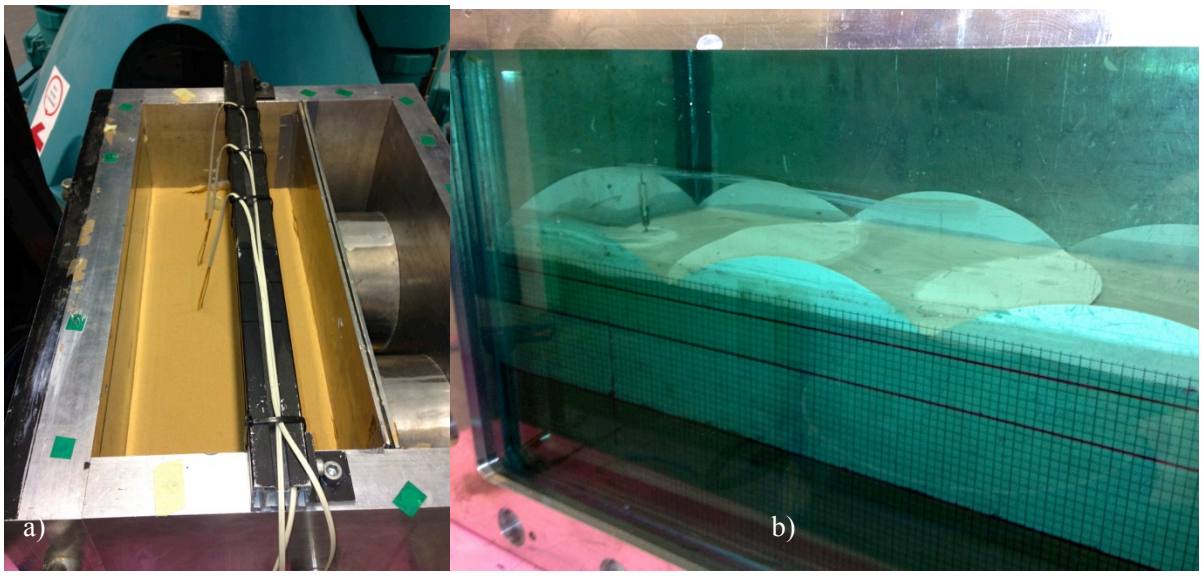

Figure 5.6 Once the clay slurry had been poured, a layer of filter paper was placed on the surface (a), and 7.65 kg of sand was placed over the clay (b).

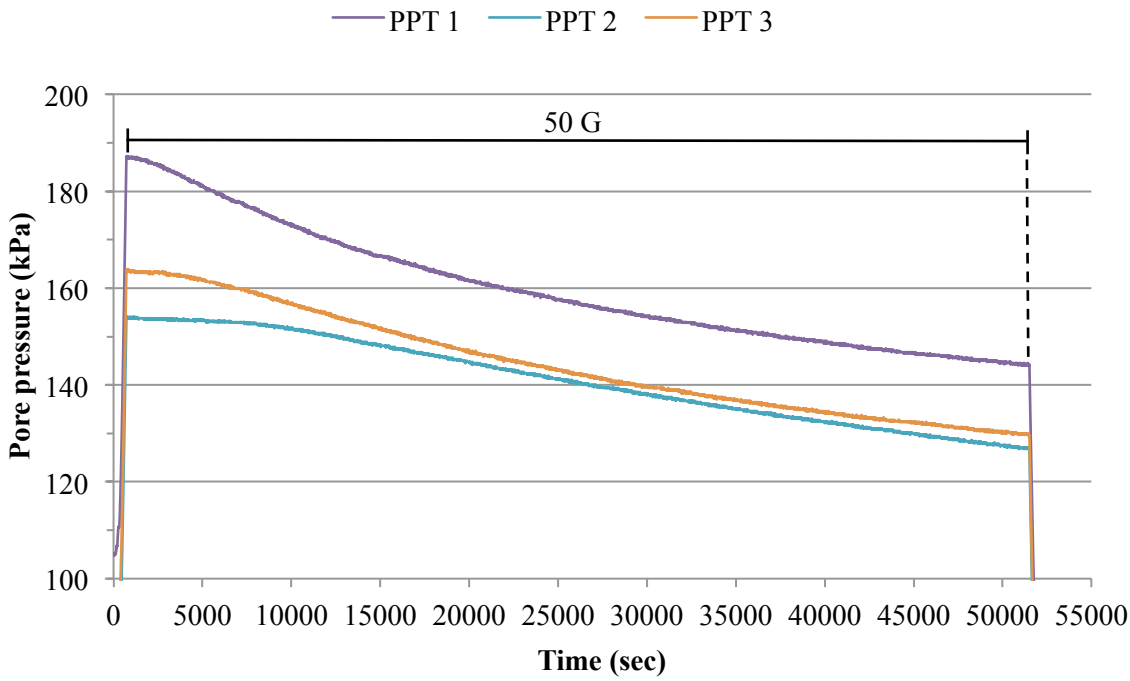

Figure 5.7 Typical dissipation of pore water pressure at 50 G during consolidation of the clay horizon.

It was common for most plots of the pore water pressure dissipation for each consolidation phase of every test to exhibit some sort of inconsistent behaviour during the early stages of consolidation (not evident in Figure 5.7). These inconsistencies usually involved a slight increase in pore water

pressures at some of the PPT localities. Thereafter the pore pressure recordings would decrease as dissipation begun. Most of these inconsistencies were due to localised adjustment of pore water adjacent to the transducer, either because there was an air or water pocket. This disturbance would have occurred during insertion of the pore pressure transducers. The maximum time period that the consolidated clay stood prior to testing was kept to a minimum. Preparation following the consolidation commenced immediately after the model was removed from the centrifuge in order to mitigate any external factors which could have influenced the clay and transducers while waiting.

5.5.3 Preparation for testing

After the consolidation stage, the clay was prepared for testing. The overlying sand which had provided a normal load during consolidation was removed, as well as the excess clay. Once the required thickness of 60 mm was left, the surface of the clay was smoothed off with as little disturbance as possible (Figure 5.8a). The cables attached to the pore pressure transducers where neatly lead and tied to the side of the box, where they would later be attached to the data acquisition system (Figure 5.8b).

Figure 5.8 After the consolidation phase, the sand, filter paper and excess clay was removed, the surface smoothed off (a), and cables from the pore pressure transducers neatly tied to the side of the box (b).

5.6 Reinforced sand

The last layer of the soil profile was the upper sand which would be reinforced with the geogrids. The same sand was used as in the bottom sand layer and therefore upper sand layer would exhibit the same properties.

5.6.1 Pluviation

Again, the upper sand horizon was constructed using a hopper to pluviate the sand. A more dense packing was required for the upper layer. To assist in creating a dense packing, the sand layer was constructed in increments. Two increments for the unreinforced model as well as the models required a single geogrid, and 3 increments for the models which required 2 geogrids. Firstly the sand was pluviated from the specified drop height and flow rate and then lightly compacted and levelled. The drop height of the sand was adjusted to 700 mm, with a opening of 1.00 mm for each incremental layer, in order to achieve the required state of packing. An average relative density (D_r) of 79 % was achieved for the upper reinforced sand horizon for all the centrifuge model tests.

At the prescribed thickness, the pluviation was ceased and the geogrid was placed on the surface of the sand. Thereafter pluviation continued.

5.6.2 Geogrid

The choice of geogrid was based on the perusal of the literature of previous studies. A punched and extruded polypropylene biaxial geogrid was used for the testing (Figure 5.9). Table 4.5 summarises the properties of the selected model geogrid, along with its projected prototype values corresponding to 50 G and the average range of commercially available geogrids used in basal reinforcement applications.

Table 5.5 Properties of the selected model geogrid for centrifuge testing, compared with the commercially available geogrids, used in basal reinforcement applications. (BBA, 2010; Maccaferri, 2012).

Property	**Model geogrid**		
	In model dimensions	**Dimensions corresponding to 50 G**	**Prototype geogrid (average values)**
Ultimate tensile strength (kN/m)	20	1000	103 – 1 390
Strain at ultimate tensile strength (%)	13	13	10.5 ± 1
Percentage open area (%)	76	76	8 – 51
Secant modulus (kN/m)	154	7692	981 – 13 238
Mesh opening size (mm)	38 x 38	1900 x 1900	98 x 940 – 9 x 940
Thickness (mm)	1.27	63.5	1.8 – 4.4

As can be seen the model geogrid has an ultimate tensile strength of 20 kN/m at 13% elongation, which represents a prototype geogrid with an ultimate tensile strength of 1000 kN/m at 13% at 50 G. The secant modulus of the model geogrid is 154 kN/m which corresponds to a secant moduls of 7692 kN/m at 50 G. This is in good agreement with the respective available prototype geogrids. Although the percentage open area of the model geogrid does not necessarily correspond to those used in basal reinforcement applications, it was decided that modelling the tensile strength-strain was the most important property to simulate in order to increase the stiffness of the upper reinforced sand horizon. The model geogrid was therefore chosen specifically to understand how an increase in stiffness of the upper reinforced sand horizon, affects the behaviour of the underlying clay horizon under a wide loaded platform

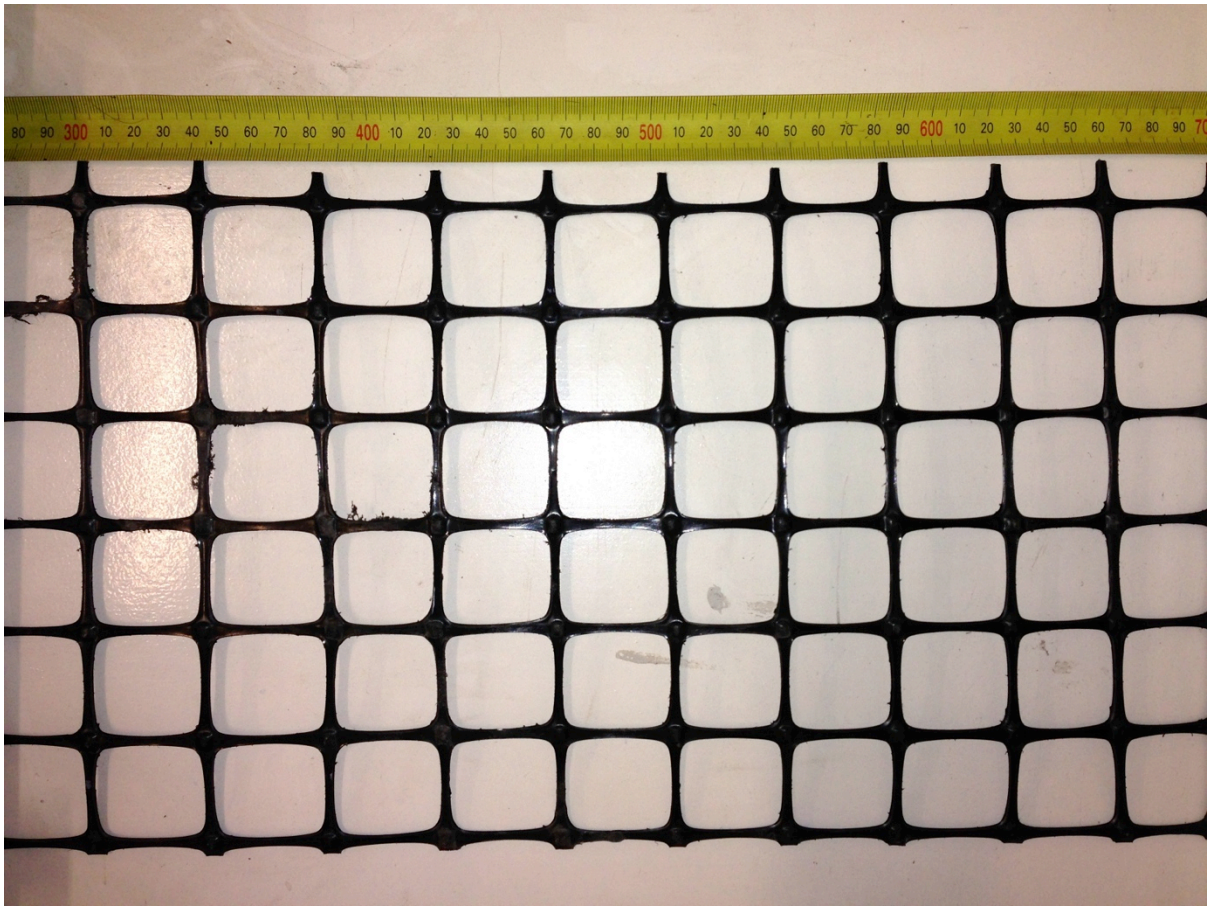

Figure 5.9 The model geogrid used in the centrifuge tests.

5.7 Loading system and instrumentation

5.7.1 Pore pressure transducers

The pore pressure transducers consisted of a miniature pressure sensor and a high-air-entry ceramic disc assembled together to form a small water reservoir between them, with a structural epoxy that forms the body of the device. Its small size enables it to be used in many laboratory and physical modelling applications (Le Roux, 2013). The design of the pore pressure transducer is shown in Figure 5.10.

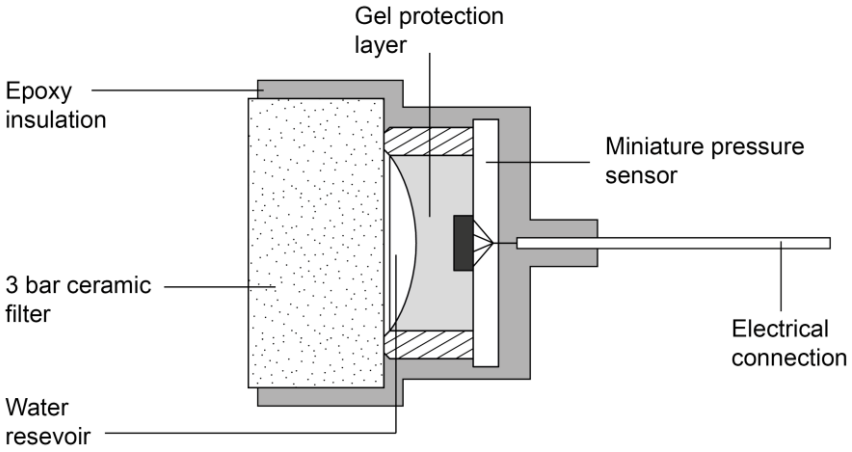

Figure 5.10 The design of the pore pressure transducer (Le Roux, 2013).

The pressure sensor within the pore pressure transducer was a MS5407-AM high sensitivity Miniature SMD pressure sensor, constructed by Measurement Specialties and shown in Figure 5.11. It has a full scale pressure rating of 7 bar absolute pressure and is ideal for the use in centrifuge modelling due to its low cost, small size and high reliability. The sensor delivers a high sensitivity output at high linearity and is equipped with a layer of gel that protects it from humidity and water. The ceramic disk is a high air entry (HAE) ceramic with a nominal air entry valve (AEV) of 3 bar (Le Roux, 2013). The complete pore pressure tranducer is shown in Figure 5.12.

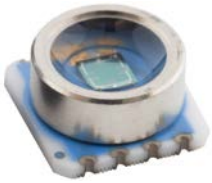

Figure 5.11 MS54XX Miniature SMD Pressure Sensor used in the pore pressure transducers (Measurement Specialities, 2012).

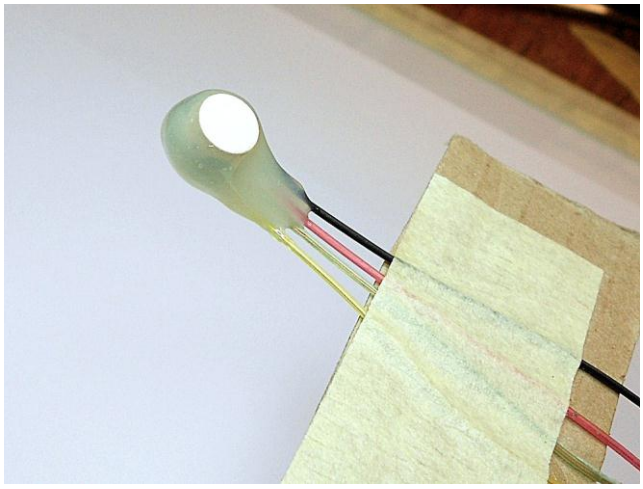

Figure 5.12 The assembled pore pressure transducer (Le Roux, 2013).

The pore pressure transducers were saturated and calibrated in a standard triaxial cell as outlined by Le Roux (2013). The pore pressure transducers were stored in water immediately after the saturation process, and placed back in water immediately after being removed from the clay horizon once a test was completed.

The pore pressure transducers were utilized to qualitatively identify whether the clay at the location of the PPT's would be influenced by the vertical displacement of the platform. This would aid in recognizing possible yielding of the clay, when the pore pressures reach a point were they do not rise with further displacement and loading of the platform. The PPT's would also be used to ascertain what the change in applied stress would be over the width of the clay layer when reinforcement is included.

5.7.2 Jack

The jack used to lower the platform was a PFAFF screw jack, fitted with a windscreen wiper motor which was provided with power from the centrifuge (Figure 5.13). The jack has a stroke of 150 mm, and was attached to 2 supporting beams which were fitted to the strongbox collar. The jack was fitted with a LVDT to measure the vertical displacement of the platform, and a load cell to measure the load against the platform. The jack was fitted with the aluminium platform which would apply the load to the surface of the model. The platform was attached to load cell which was subsequently attached to a cylinder. The platform had a width of 200 mm and was suspended from the jack approximately 5 mm from the surface of the model. Although a ball at the base of the cylinder with the ability to allow rotation of the platform was constructed, the platform was fixed by 3 screws so as to not allow rotation of the platform as the load was applied during the test. The jack displaced at approximately 0.07 mm/s once power was provided via the centrifuge during the test.

5.7.3 Load cell

The load cell fitted to the jack is an HBM U93 and is a force transducer used for monitoring force versus displacement curves. It had a load capacity of 50 kN. The load cell was attached to the data acquisition system. The load cell used is shown in Figure 5.14. The bottom of the load cell was attached to the cylinder by 3 screws which in turn was attached to the platform.

The load cell enabled the observation of the load achieved against the platform as it was displaced vertically onto the centrifuge model. This would enable the possible identification of the increase in load bearing capacity when reinforcement is added to the model. The loads recorded would also be compared visually with the deformation of the centrifuge models, as well as compared with the vertical displacement of the platform and the behaviour of the pore pressure with an increasing load.

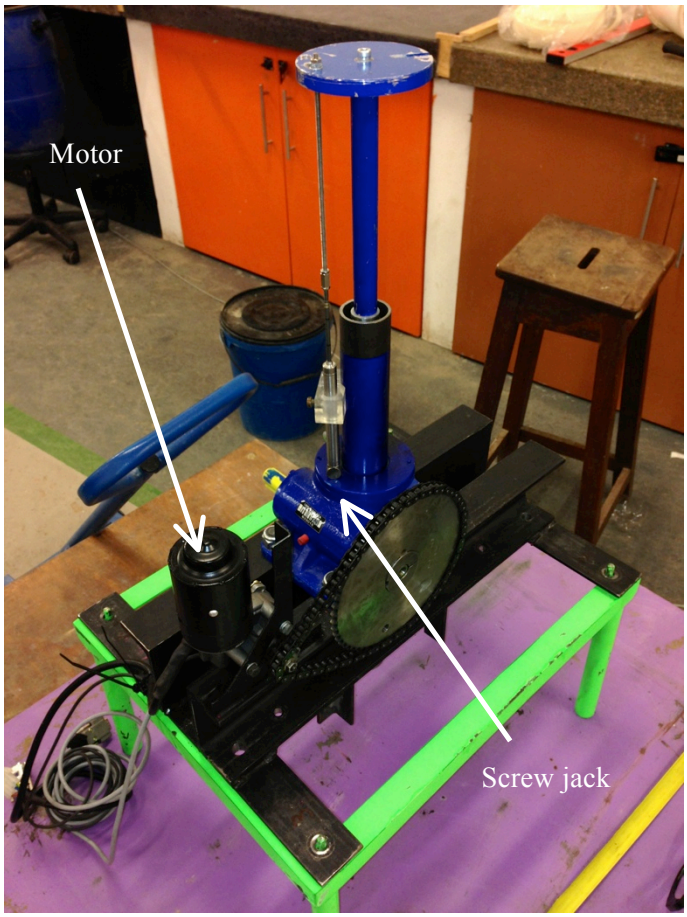

Figure 5.13 The screw jack used to lower the platform onto the model, fitted with a windscreen wiper motor.

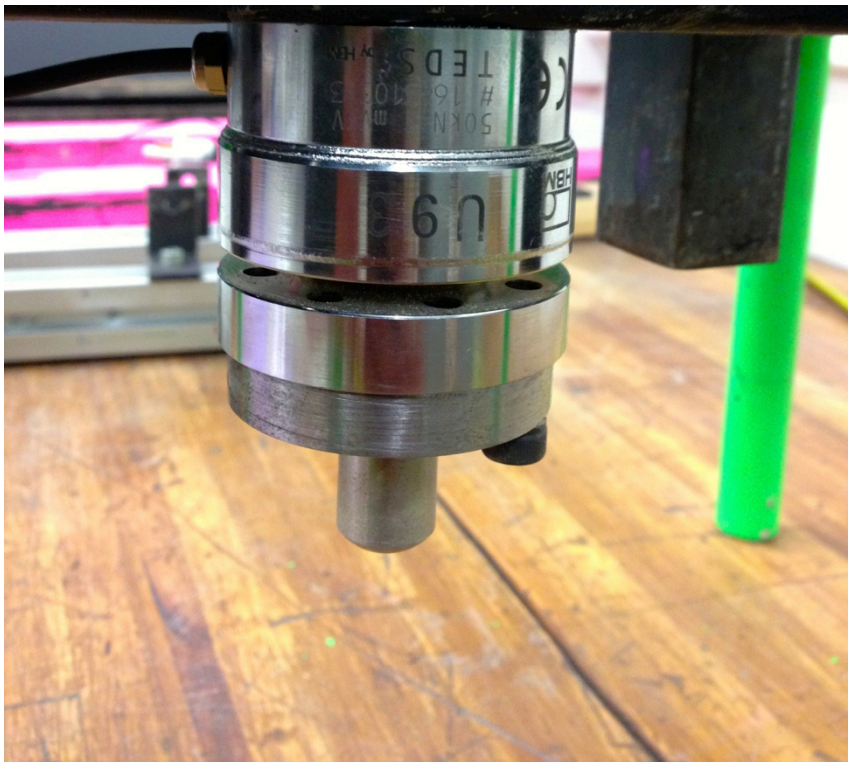

Figure 5.14 The HBM U93 load cell used in the centrifuge model tests.

5.7.4 LVDT

The LVDT was fitted to the side of the jack, and is a plunger inductive displacement transducer. The LVDT was also made by HBM and is a WA model. It was used to measure the vertical displacement of the screw jack as it lowered the platform onto the surface of the centrifuge model. The LVDT is shown in Figure 5.15.

The data recorded from the LVDT would be used to compare the difference in deformation behaviour at specific displacement intervals, to potentially explain the difference in deformation behaviour under various reinforcing conditons as well as the unreinforced scenario. Load data would also be observed against the vertical displacement in order to identify the difference between load-displacement curves for the separate scenarios of the unreinforced and reinforced situations.

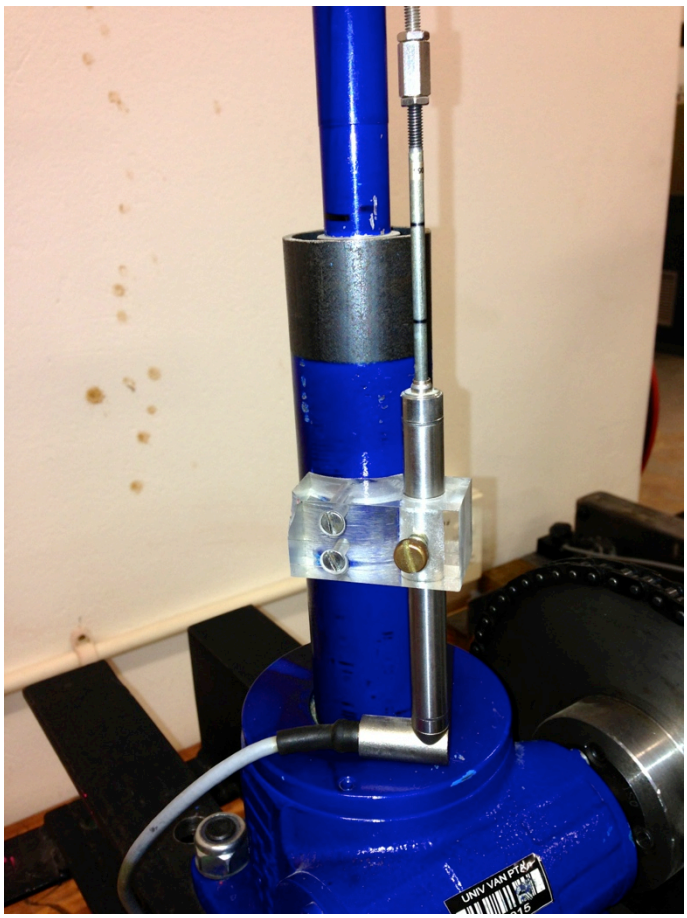

Figure 5.15 The HBM WA displacement transducer (LVDT) attached to the screw jack.

5.8 Centrifuge test sequence

Once all construction of the entire centrifuge model had been completed, the container was loaded onto the centrifuge platform and the data acquisition systems connected to the various instrumentation. Figure 5.16 shows the ready centrifuge model on the platform, just before testing commenced.

The following sequence was followed for each centrifuge model test:

i. The centrifuge enclosure was checked and secured,
ii. All data acquisition systems and cameras were reset and begun recording data,
iii. The centrifuge was started and the arm begun rotating,
iv. The acceleration was gradually increased until it reached the required level of 50 G. Figure 5.17 shows a top view of the centrifuge model at 50 G.
v. Once it had reached this level, the pore pressures were monitored until they stabilised. This usually took approximately 5 to 10 minutes,
vi. Once the pore pressures had stabilised, power to the jack was turned on and the platform was lowered onto the model soil surface,
vii. The loading stage was ceased for all tests between 20 – 25 mm vertical displacement,
viii. Thereafter, the pore pressures were observed, and the centrifuge test stopped once the pore pressures had reached a relatively constant value,
ix. Once the centrifuge arm had come to a complete stop, the enclosure was opened and the model removed from the centrifuge enclosure for observation.

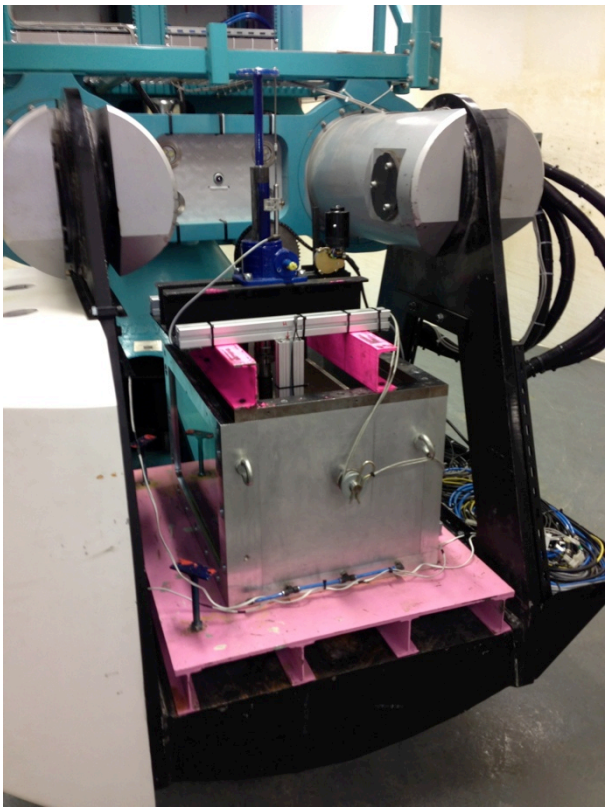

Figure 5.16 The complete model placed on the centrifuge platform before testing commenced.

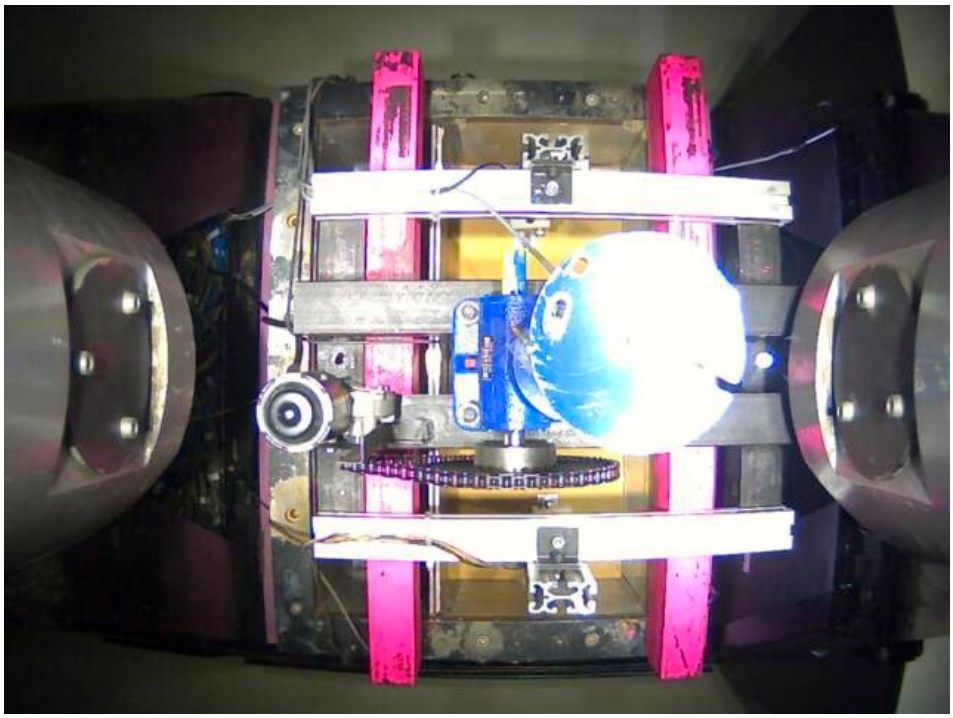

Figure 5.17 Top view of the centrifuge model at 50 G, during a test.

5.9 Summary

The background to the model preparation is presented. This covers all aspects from the conceptualised model design, through to the testing stage. Once a clear understanding of the testing that needed to be conducted in the model was gained, the appropriate materials were chosen and construction of the model commenced. This involved the preparation of the container for the model materials, followed by pluviating the underlying sand layer to the required density. The clay was prepared as a slurry, poured over the sand and pore pressure transducers installed. The clay horizon was then consolidated in the centrifuge overnight. Before testing, the reinforcing sand was pluviated, and the geogrids installed at each required interval. Lastly, the loading system was attached and the model was ready to be tested in the centrifuge.

CHAPTER 6 CENTRIFUGE MODEL RESULTS

6.1 Introduction

After completion of all five centrifuge tests, the data obtained from the data acquisition systems, as well as the recordings from the in-flight cameras, were organised. Each event in the test was analysed sequentially to define the load behaviour, vertical displacement and pore pressure data. Furthermore, the mechanisms of deformation were observed based on the video recordings. The following chapter presents the data from the five centrifuge model tests conducted.

6.2 Test 1: Unreinforced sand

6.2.1 Observed deformations

Figure 6.1 presents the mechanism of deformation for the model without reinforcement at 5 mm, 10 mm, and 15 mm vertical displacement of the model platform, respectively. It is evident that at 5 mm displacement there is little deformation of the clay horizon, with little disturbance or bulging of the clay horizon and the surface of the upper sand beyond 30 mm from the platform edge. Only the clay directly beneath the platform appears to strain.

At 10 mm vertical displacement, a shear zone appears to have formed through the upper sand horizon at the edges of the platform, and the clay horizon continues to strain underneath the platform, squeezing out laterally. There is no disturbance to the boundary between the basal sand and the clay horizon. Bulging of the upper surface of the clay horizon and the surface of the upper sand is evident at a horizontal distance of 30 to 90 mm from the edge of the platform and the width of the deformation zone is 380 mm. The bulge of the clay has a maximum height of approximately 5 mm, with approximately 3 mm on the surface of the sand horizon.

The extent of the deformation zone of the clay at 15 mm vertical displacement is wider. The bulging is seen approximately 125 mm laterally from the edge of the platform. However, there is no change in the maximum height of the bulge at the top of the clay horizon. The bulging on surface of the upper sand horizon has a maximum height of 5 mm, similar to that of the clay. The deformation is asymmetrical with respect to the middle of each deformation bulge, as the maximum height of the bulge is observed closer towards the platform. Most strain in the clay horizon seems to coincide with the width of the platform footprint.

In summary, at small displacements there is very little deformation of the clay horizon present. At increasing vertical displacements an asymmetrical deformation bulge develops, but the maximum height of this bulge does not seem to increase upon increased displacement up to 15 mm. Most of the vertical strain in the clay horizon is confined to the area directly beneath the loaded platform.

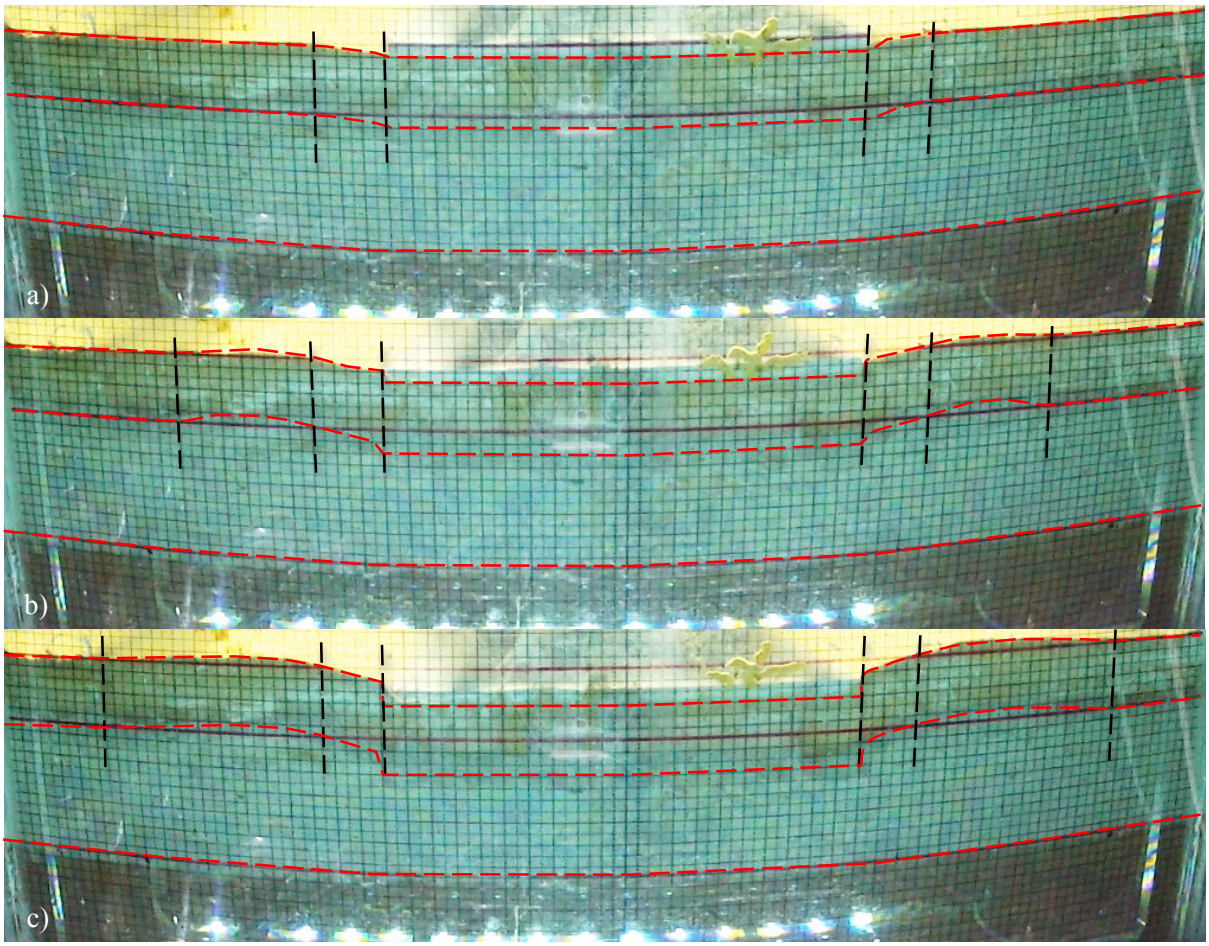

Figure 6.1 Deformation sequence for the model without reinforcement at a) 5 mm, b) 10 mm and c) 15 mm vertical displacementa (grid size is 5mm).

6.2.1 Instrumentation data

The data acquired from the test sequence is illustrated in Figure 6.2. The vertical displacement is a function of time, and therefore the relationship is linear. The applied stress recorded increases up to 13.4 kPa, at 1.1 mm vertical displacement. Thereafter the applied stress increases at a shallower gradient up to 23.9 kPa at 10 mm, subsequently increasing slightly until it reaches 35.3 kPa when vertical displacement was ceased at 20 mm.

The change in pore pressure in the clay horizon under the centre of the platform (PPT 1), reaches a peak of 18.7 kPa at 2.3 mm. Thereafter the pore pressure decreases to a change in pressure of 15.3 kPa at 9.3 mm, and subsequently increases again to 23.9 kPa at 20 mm.

The change in pore pressure recorded in the clay horizon at the edge of the platform (PPT 2) increases similarly to PPT 1 at 2.3 mm, however a change in pore pressure of 11.4 kPa, is recorded. The pore pressure then steadily increases to 16.6 kPa at 5.4 mm, and furthermore to 17.6 kPa at 13.2 mm. By the end of the loading stage at 20 mm, the change in pore pressure recorded is 19.8 kPa.

The pore pressure transducer placed in the clay horizon 100 mm from the edge of the platform (PPT 3), did not record any change in pore pressure until 1.5 mms after loading commenced. The change in pore pressure, thereafter only reaches 1.8 kPa at 5.4 mm, and subsequently 4.9 kPa at 10.1 mm. By the end of the loading stage, the pore pressure at PPT 3 had not changed by more than 6.7 kPa.

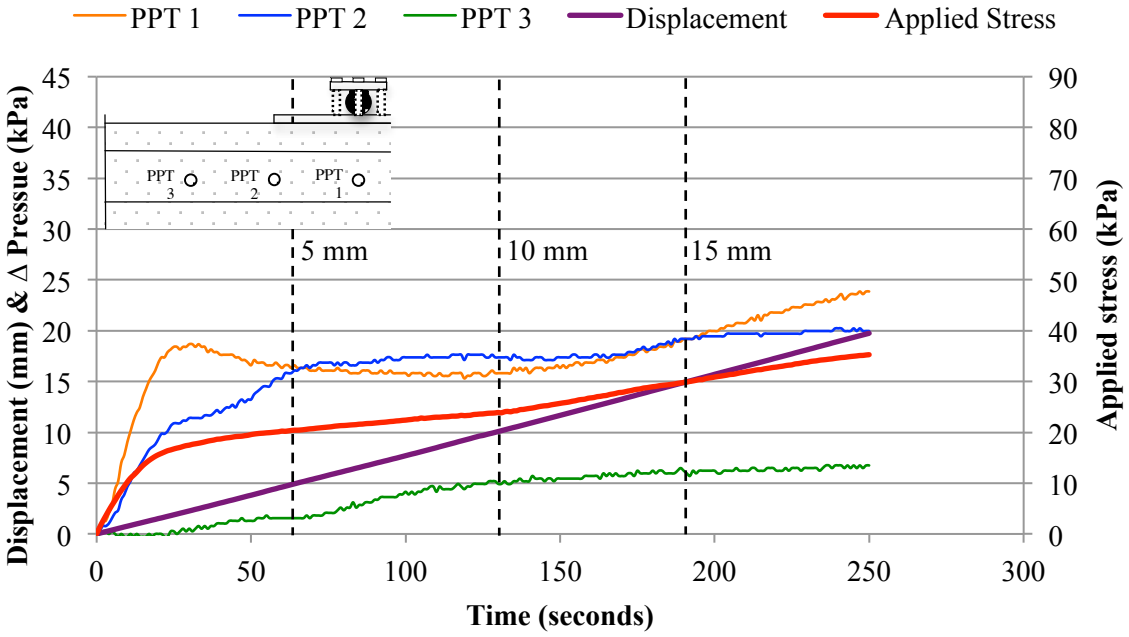

Figure 6.2 Vertical displacement, applied stress and the change in pore pressure measured at each pore pressure transducer (PPT), during the test sequence for the model without reinforcement.

6.3 Test 2: Reinforced sand - 1 geogrid with a short width

6.3.1 Observed deformations

Evidence of deformation and bulging of the clay horizon occurring at 5 mm vertical displacement is seen in Figure 6.3. Note, that for ease of comparison, the scales are identical to the results of all other tests for both the visual recordings of deformation, as well as the data from the instrumentation. There is also some disturbance and bulging of the surface of the upper sand beyond. The bulging occurs approximately between 30 mm and 110 mm from the edge of the platform with a zone of deformation of 420 mm width and attains a maximum height of approximately 2 mm.

At 10 mm vertical displacement, bulging of the upper surface of the clay horizon and the surface of the upper sand occurs at a horizontal distance of 25 to approximately 120 mm from the edge of the platform, with a deformation zone of 440 mm. The bulge of the clay attains a maximum height of approximately 4 mm, and is similar for the maximum bulge on the surface of the upper sand horizon.

The lateral extent of the deformation zone of the clay is the same at 15 mm vertical displacement. However, the deformation has a maximum height of 6 mm for both the upper surface of the clay horizon, as well as the surface of the upper sand horizon. There is no disturbance to the boundary

between the basal sand and the clay horizon. It seems that the clay directly beneath the platform has exhibited the most strain, but is not confined only to this portion as in the unreinforced test. It is evident that deformation within the clay is also present beyond the platform edge and coincides with the edge of the geogrid width. The deformation bulge is generally symmetrical, with the maximum height of the deformation occurring approximately in the middle of the bulge.

In summary, at small displacements there is already some deformation of the clay horizon present, unlike the unreinforced test. At increasing vertical displacements a symmetrical deformation bulge develops, and the maximum height of this bulge increases upon increased displacement up to 15 mm. The vertical strain that takes place in the clay horizon coincides with the region between the edges of the geogrid width.

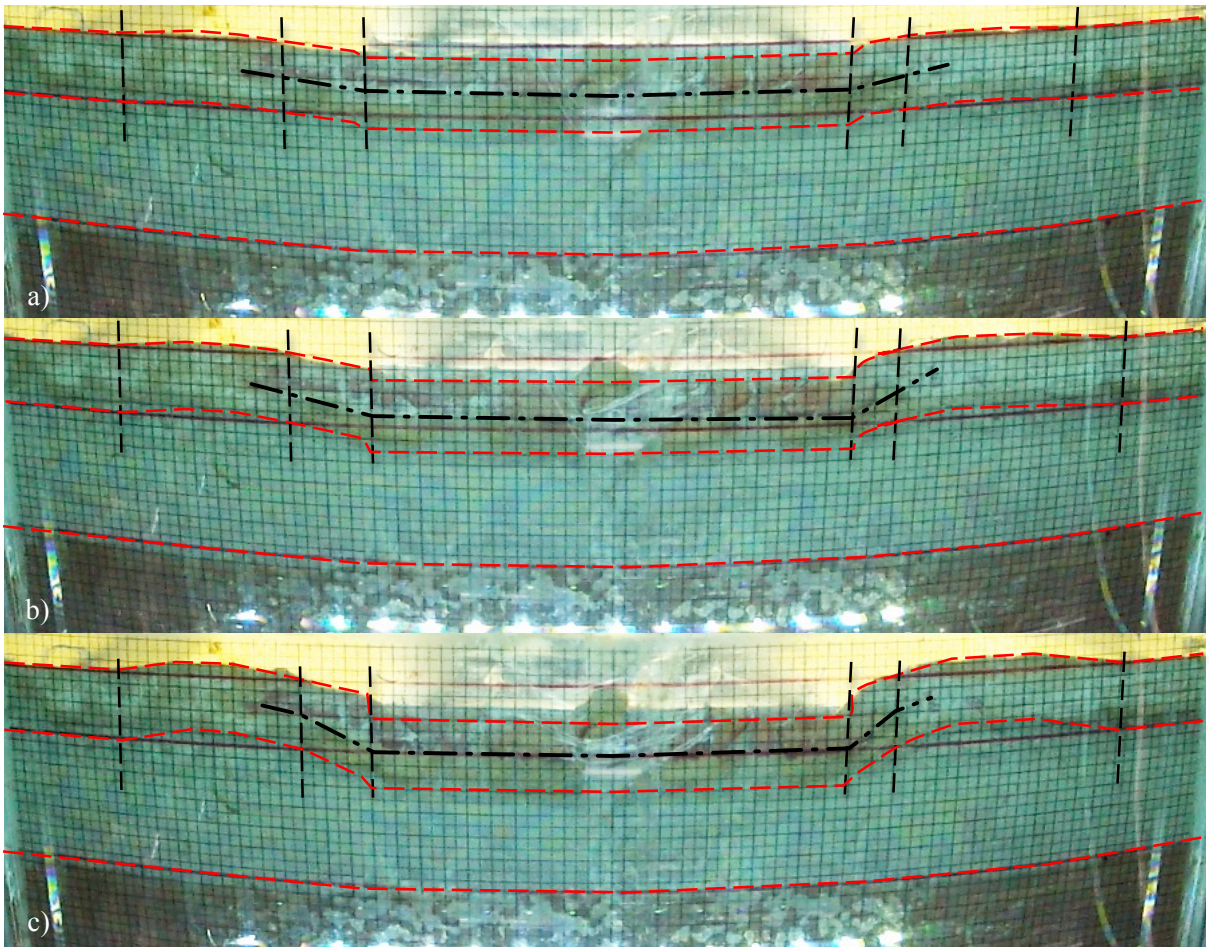

Figure 6.3 Deformation sequence for the model with one short geogrid installed, at a) 5 mm, b) 10 mm, and c) 15 mm vertical displacement.

6.3.2 Instrumentation data

The data acquired from the test with one layer of geogrid reinforcement is illustrated in Figure 6.4. The load recorded increases up to 1.6 kPa, at 1.5 mm vertical displacement after the loading commenced. Thereafter the load increases at a steeper gradient up 20.6 kPa at 2.2 mm. Subsequently

the load continues to increase until it reaches 53.2 kPa when vertical displacement was ceased at 21 mm.

The change in pore pressure in the clay horizon under the centre of the platform (PPT 1), reaches a peak of 15.3 kPa at 2.2 mm vertical displacement. Thereafter the change in pore pressure increases gradually to 18.9 kPa at 9.6 mm, and subsequently increases at a higher rate to 23.9 kPa at 21.0 mm displacement.

The change in pore pressure recorded in the clay horizon at the edge of the platform (PPT 2) increases sharply, similar to PPT 1, to 14.8 kPa at 3.6 mm displacement. By the end of the loading stage at 21 mm vertical displacement, the change in pore pressure recorded increased steadily to 27.5 kPa.

The pore pressure transducer placed in the clay horizon 100 mm from the edge of the platform (PPT 3), did not record any change in pore pressure until 0.5 mm displacement. The change in pore pressure thereafter only reached 1.8 kPa at 1.1 mm, and then 4.7 kPa at 2.2 mm. By the end of the loading stage, the pore pressure at PPT 3 had not changed by more than 11.4 kPa.

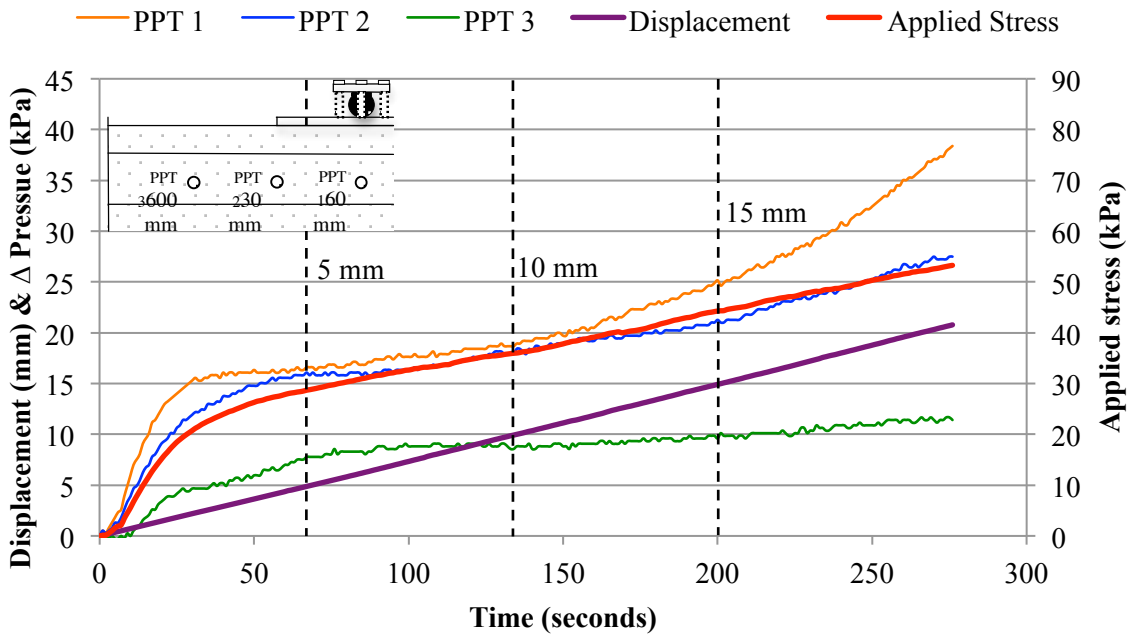

Figure 6.4 Vertical displacement, applied stress, and the change in pore pressure measured at each pore pressure transducer (PPT), during the test sequence for the model with one short layer of reinforcement in the upper sand horizon.

6.4 Test 3: Reinforced sand - 2 geogrids with a short width

6.4.1 Observed deformations

The test with 2 geogrids with a short width installed in the upper sand layer, and the subsequent mechanisms of deformation seen in the video recordings are shown in Figure 6.5. Some deformation

and bulging of the clay horizon occurring at 5 mm vertical displacement is seen together with some disturbance and bulging of the surface of the upper sand beyond the edge of the platform. The bulging occurs approximately between 25 mm and 80 mm horizontally from the edge of the platform, and attains a maximum height of no more than 2 mm with a deformation zone of 360 mm width.

At 10 mm vertical displacement, bulging of the upper surface of the clay horizon and the surface of the upper sand occurs at a horizontal distance of 25 to approximately 145 mm from the edge of the platform. The bulge of the clay has a maximum height of approximately 5 mm, and is similar for the maximum bulge on the surface of the upper sand horizon. The width of the deformation zone is 490 mm.

The extent of bulging of the clay occurs between 25 and 165 mm from the edge of the platform at 15 mm vertical displacement and the width of the deformation zone increases to 530 mm. The deformation attains a maximum height of 10 mm for both the upper surface of the clay horizon as well as the surface of the upper sand horizon. There is no disturbance to the boundary between the basal sand and the clay horizon. Similar to the test with only a single layer of geogrid, the maximum strain, which has occurred in the clay horizon, seems to coincide with the width of the geogrid. The deformation bulge is generally symmetrical with the maximum height of the deformation occurring in the middle of the bulge

To outline, at small displacements there is already some deformation of the clay horizon present, much the same as the reinforced test with a single geogrid layer. At increasing vertical displacements a symmetrical deformation bulge develops, and the maximum height of this bulge increases upon increased displacement up to 15 mm. Once again, the vertical strain that takes place in the clay horizon coincides with width of the geogrid.

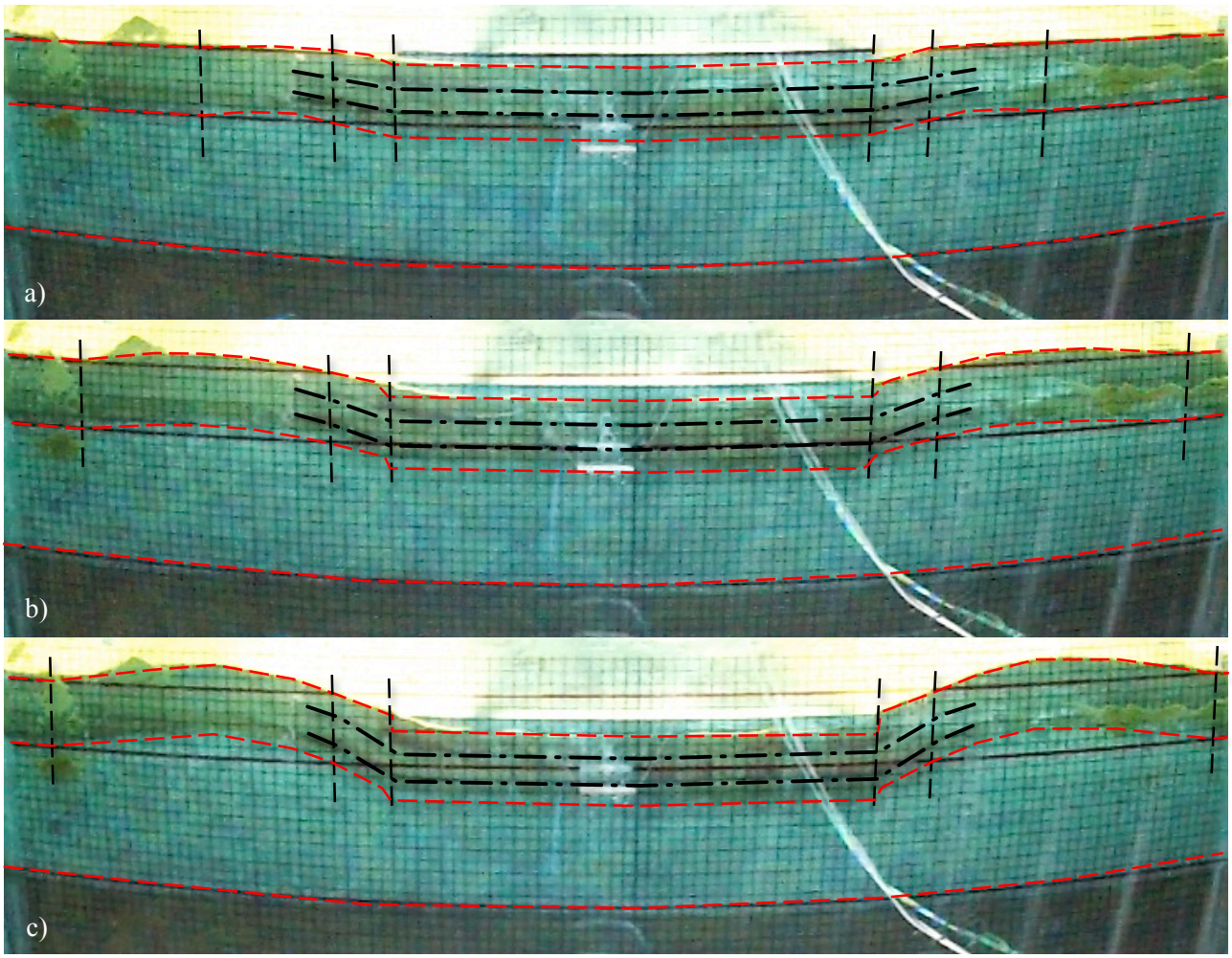

Figure 6.5 Deformation sequence for the model with two short geogrids installed, at a) 5 mm, b) 10 mm, and c) 15 mm vertical displacement.

6.4.2 Instrumentation data

Figure 6.6 shows the data acquired from the test with two layers of geogrid reinforcement. The load recorded increases up to 9.4 kPa, at 2.4 mm vertical displacement after the loading commenced. Subsequently the load continues to increase gradually until it reaches 46.0 kPa when vertical displacement was ceased at 24.0 mm.

The change in pore pressure in the clay horizon under the centre of the platform (PPT 1), reaches 4.9 kPa at 2.4 mm. Thereafter the change in pore pressure increases slowly to 13.2 kPa at 10.4 mm, gradually increasing to 24.4 kPa at 19.5 mm, and subsequently maintaining a steady rate to 25.9 kPa at 24.0 mm.

The change in pore pressure recorded in the clay horizon at the edge of the platform (PPT 2) increases, to 4.7 kPa at 2.4 mm, similar to PPT 1. There is not much change in the pore pressure, with a change in pressure of 5.4 kPa at 8 mm vertical dislpacement. By the end of the loading stage at 24.0 mm, the change in pore pressure recorded increased steadily to 12.7 kPa.

The pore pressure transducer placed in the clay horizon 100 mm from the edge of the platform (PPT 3), recorded a change in pore pressure, of 2.1 kPa at 2.4 mm and subsequently increases slightly to a change of pressure of 3.8 kPa at 6.4 mm. The pore pressure does not change until approximately 13.7 mm, and thereafter only increasing slightly, where at the end of the loading stage the change in pore pressure at PPT 3 was 7.0 kPa.

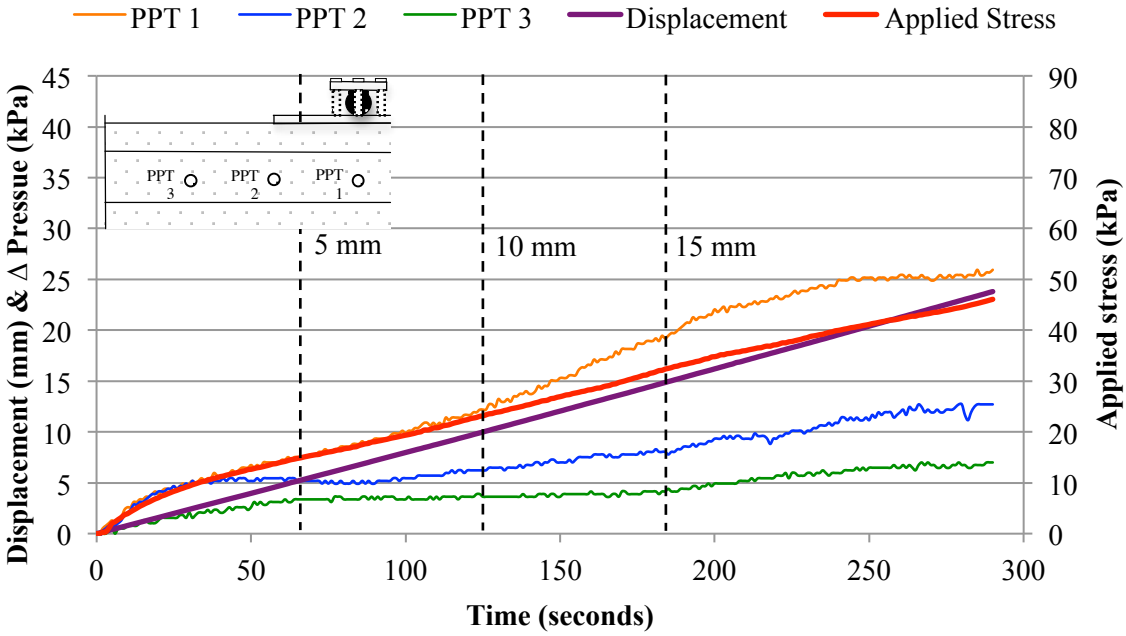

Figure 6.6 Vertical displacement, applied stress, and the change in pore pressure measured at each pore pressure transducer (PPT), during the test sequence for the model with two short layer of reinforcement in the upper sand horizon.

6.5 Test 4: Reinforced sand - 1 geogrid with an extended width

6.5.1 Observed deformations

Figure 6.7 shows the mechanisms of deformation identified for the model with a single layer of geogrid installed, extending the length of the box. At 5 mm displacement there is little deformation of the clay horizon, with little disturbance or bulging to the boundary of the clay horizon and the upper sand horizon, 30 mm from the platform edge.

At 10 mm vertical displacement, bulging of the upper surface of the clay horizon and the surface of the upper sand occurs at a horizontal distance of 30 to approximately 130 mm from the edge of the platform. The bulge of the clay has a maximum height of approximately 5 mm, and is similar to the maximum bulge on the surface of the upper sand horizon. The width of the deformation zone is 460 mm.

The lateral extent of the deformation zone of the clay is wider at 15 mm vertical displacement, with deformation occurring between 30 to 160 mm from the edge of the platform. The deformation attains a maximum height of 10 mm for both the upper surface of the clay horizon as well as the surface of

the upper sand horizon. No disturbance to the boundary between the basal sand and the clay horizon was observed. The inclusion of a single extended geogrid reinforcement in the sand in the upper horizon widened the zone of deformation in the clay, coinciding with the width of the geogrid. However, maximum strain still takes place beneath the platform. The deformation bulge is not symmetrical, as the maximum height occurs further away from the platform than the mid-point of the deformation bulge.

In summary, at small displacements there is already a large amount of deformation of the clay horizon present. At increasing vertical displacements an asymmetrical deformation bulge develops, and the maximum height and extent of this bulge increases upon increased displacement up to 15 mm. The vertical strain that takes place in the clay horizon coincides with width of the geogrid, which extends the entire length of the model.

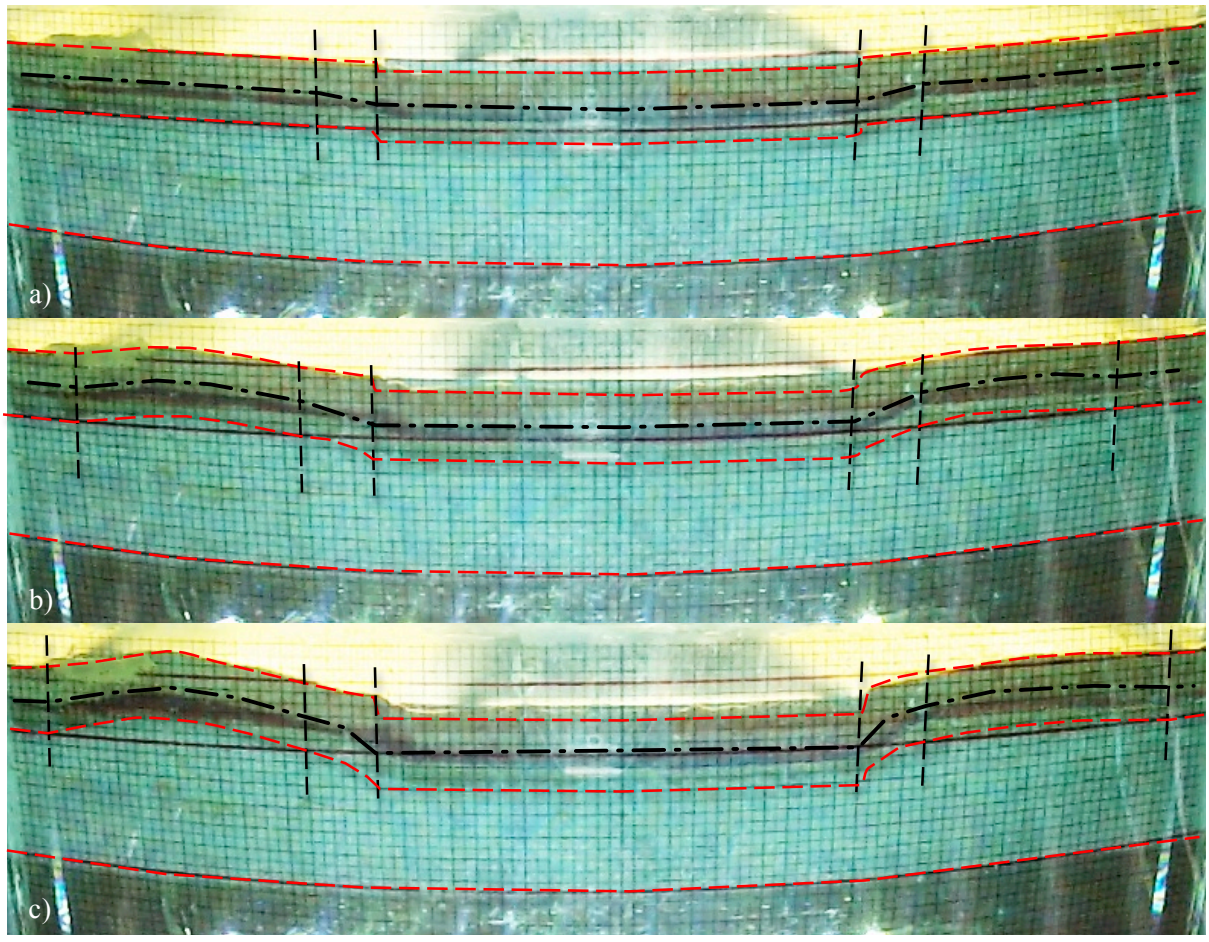

Figure 6.7 Deformation sequence for the model with one extended geogrids installed, at a) 5 mm, b) 10 mm, and c) 15 mm displacement.

6.5.1 Instrumentation data

The data acquired from the test sequence is charted in Figure 6.8. The load recorded increases up to 17.2 kPa, after 2.4 mm vertical displacement. Thereafter, the load increases at a constant rate up 46.0 kPa at 18 mm, when vertical displacement was ceased.

Pore pressure in the clay horizon under the centre of the platform (PPT 1), increases steeply to 14.2 kPa at 2.4 mm. Thereafter the pore pressure increases slightly to a change in pressure of 16.6 kPa at 10.8 mm. Pore pressure subsequently increases further to 22.8 kPa at 18.4 mm.

The change in pore pressure recorded in the clay horizon at the edge of the platform (PPT 2) increases similarly to PPT 1 at 2.4 mm. However, it only records a change in pore pressure of 8.6 kPa. Pore pressures recorded at PPT 2 then steadily increases to 17.1 kPa at 18.4 mm, at the end of the loading stage.

The pore pressure transducer placed in the clay horizon 100 mm from the edge of the platform (PPT 3), records a peak change in pore pressure at 6.6 mm of 7.8 kPa. The pore pressure drops, to an overall change in pore pressure of 5.1 kPa at 10.8 mm. Thereafter the pore pressure remains constant and records a change in pore pressure of 5.4 kPa at the end of the loading stage of the test.

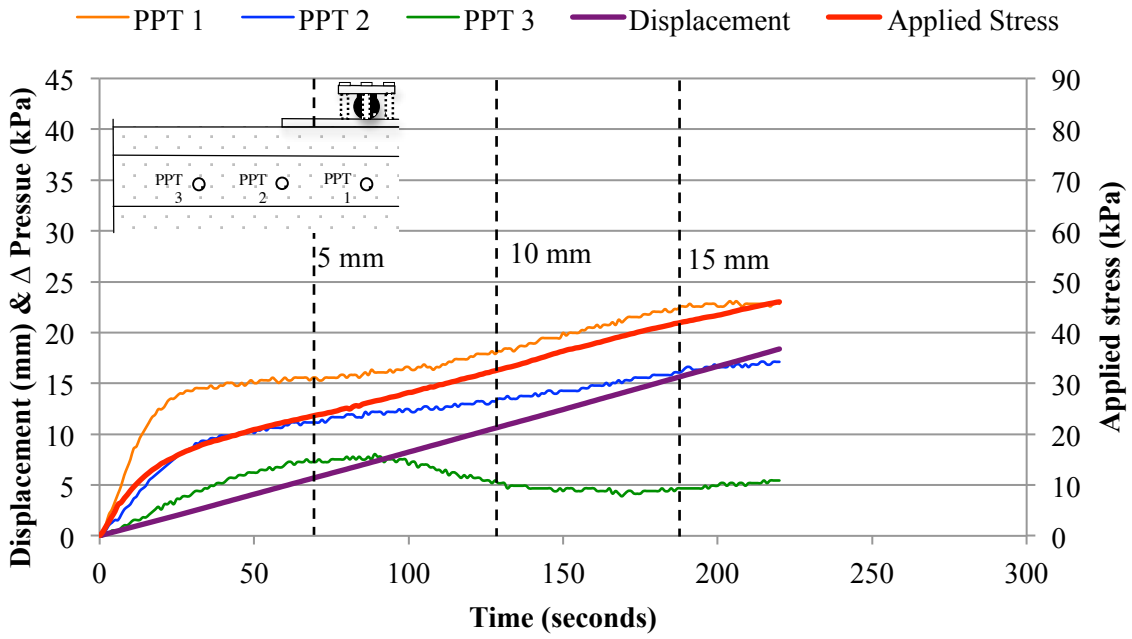

Figure 6.8 Vertical displacement, applied stress, and the change in pore pressure measured at each pore pressure transducer (PPT), during the test sequence for the model with one extended layer of reinforcement in the upper sand horizon.

6.6 Test 5: Reinforced sand - 2 geogrids with an extended width

6.6.1 Observed deformations

The test with 2 extended geogrids installed in the upper sand layer, and the subsequent mechanisms of deformation seen in the video recordings are shown in Figure 6.9. Some deformation and bulging of the clay horizon occurring at 5 mm vertical displacement is seen together with some disturbance and bulging of the surface of the upper sand beyond. The bulging occurs approximately between 30 mm

and 150 mm horizontally from the edge of the platform, with a zone of deformation width of 500 mm and attains a maximum height of no more than 3 mm. At 10 mm vertical displacement, the horizontal extent of the deformation zone does not change. However, the bulge of the clay has a maximum height of approximately 9 mm, and is similar for the maximum bulge on the surface of the upper sand horizon.

At 15 mm vertical displacement, the deformation attains a maximum height of 14 mm for both the upper surface of the clay horizon as well as the surface of the upper sand horizon. There is no disturbance to the boundary between the basal sand and the clay horizon. Once again, most of the deformation in the clay coincides with the width of the reinforcement. The deformation is asymmetrical as the maximum height occurs further away from the platform than the mid-point of the deformation bulge.

In summary, at small displacements there is a large amount of deformation in the clay horizon present. At increasing vertical displacements an asymmetrical deformation bulge develops, and the maximum height and extent of this bulge increases rapidly upon increased displacement up to 15 mm. The vertical strain that takes place in the clay horizon coincides with width of the geogrid, which extends the entire length of the clay horizon.

6.6.1 Instrumentation data

The data acquired from the test sequence is illustrated in Figure 6.10. The load recorded increases up to 18.8 kPa, at 2.4 mm vertical displacement. Thereafter the load increases at a constant rate up 58 kPa at 22 mm vertical displacement.

The change in pore pressure in the clay horizon under the centre of the platform (PPT 1), increases to 11.2 kPa at 2.4 mm. Thereafter the pore pressure increases gradually to a change in pressure of 29.6 kPa at 22 mm.

The change in pore pressure recorded in the clay horizon at the edge of the platform (PPT 2) increases similarly to PPT 1 at 2.4 mm. However, it only records a change in pore pressure of 9.1 kPa. Subsequently it continues to rise to a change in pore pressure of 12.5 kPa achieved at 4.8 mm, and then maintains a constant pressure until 9.0 mm vertical displacement. The pressure then steadily increases until a change in pore pressure of 20.8 kPa at 22 mm is attained, at the end of the loading stage.

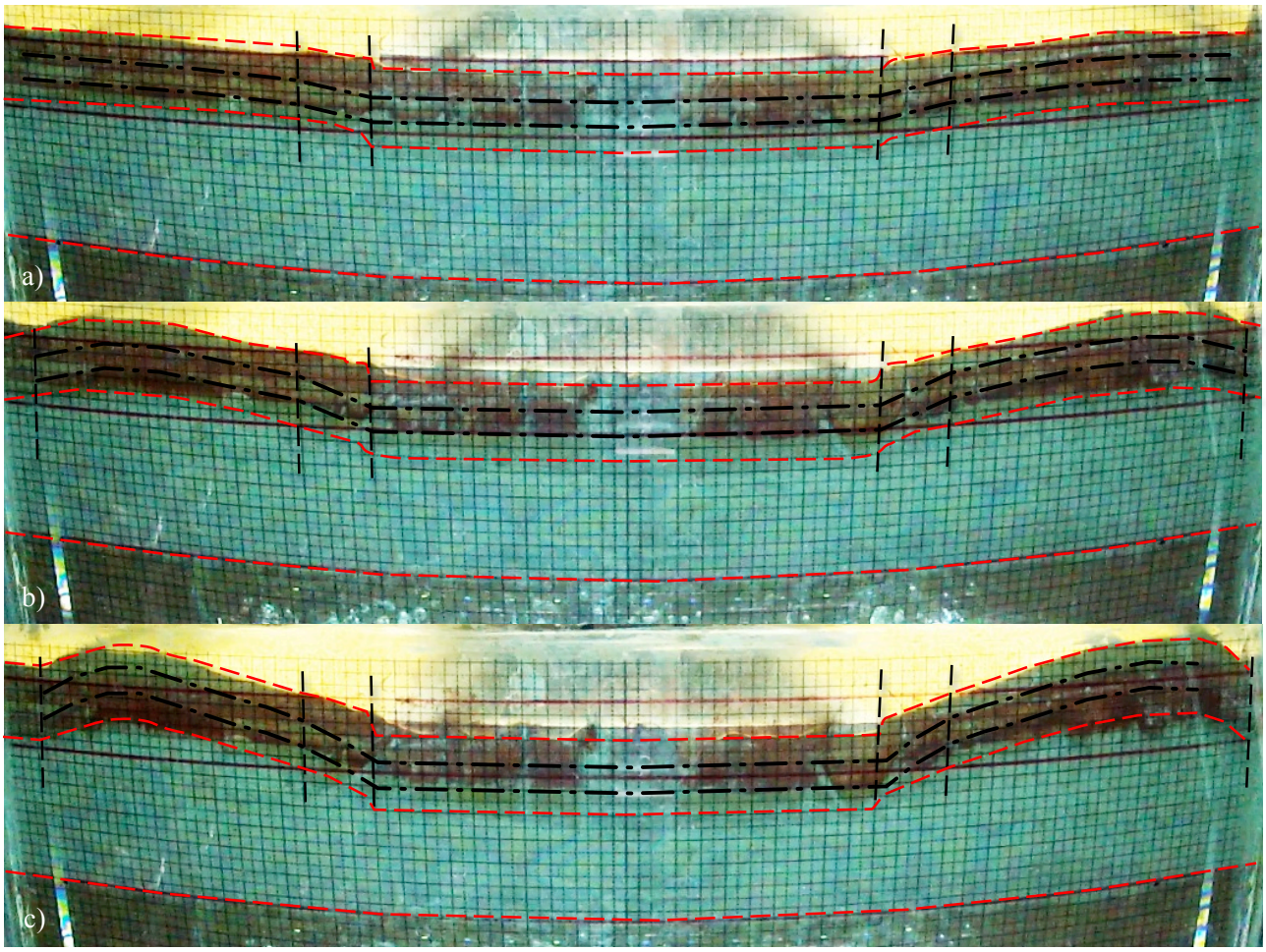

Figure 6.9 Deformation sequence for the model with two extended geogrids installed, at a) 5 mm, b) 10 mm, and c) 15 mm displacement.

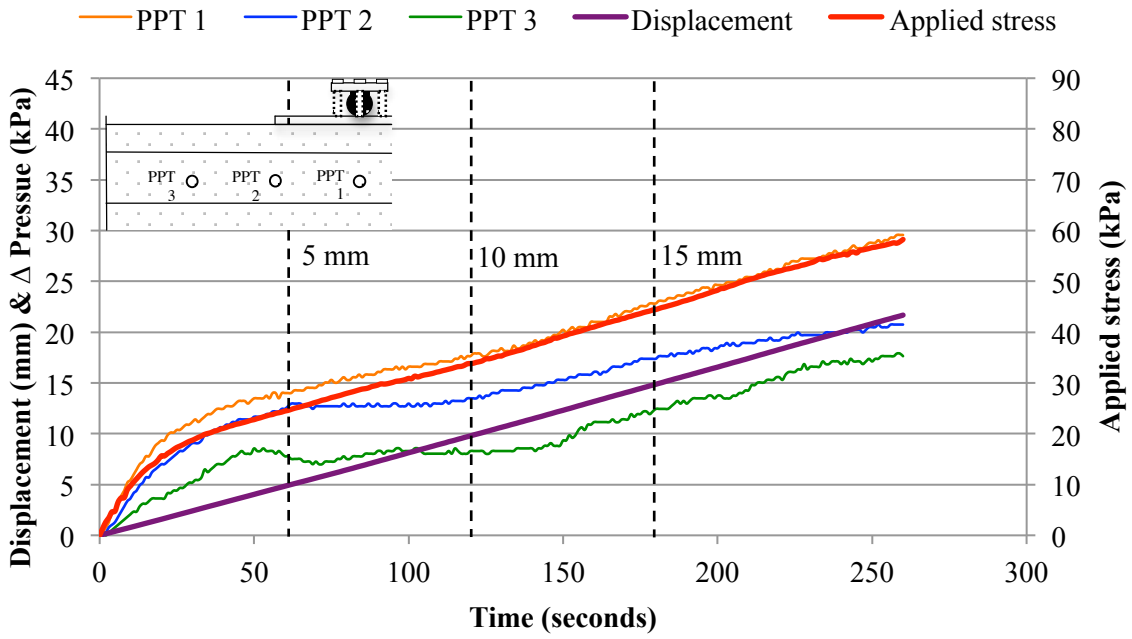

Figure 6.10 Vertical displacement, applied stress, and the change in pore pressure measured at each pore pressure transducer (PPT), during the test sequence for the model with two extended layers of reinforcement in the upper sand horizon.
The pore pressure transducer placed in the clay horizon 100 mm from the edge of the platform (PPT 3), records a peak change in pore pressure at 4.0 mm of 8.6 kPa. The pore pressure generally remains constant, until approximately 11.5 mm. Thereafter the pore pressure increases and a change in pore pressure of 17.6 kPa was recorded at the end of the loading stage of the test.

6.7 Post-load pore pressure behaviour

Data recorded after loading was stopped shows a gradual dissipation of pore pressures at all three locations where the transducers were installed. These pore pressures are shown in Figure 5.11.

The origin (0, 0) in each chart is set from the moment that the loading was stopped. Once power to the jack was closed, no more vertical displacement of the platform took place, and the platform hung from the jack against the soil model.

All of the pore pressures recorded at PPT 1 at the end of each test, recorded a lower pore pressure than what was recorded when the loading stage was began. This is most likely due to the large amount of clay that had been displaced beneath the platform. The platform was only stopped being lowered after 20 – 25 mm vertical displacement had occurred, in all the centrifuge tests.

Pore pressures from PPT 2 dissipated gradually until they stabilised, to within 10 kPa of their original pore pressure before the loading commenced. The pore pressure data recorded at PPT 3 for each test showed gradual dissipation to approximately the same pore pressure that was recorded before the loading stage.

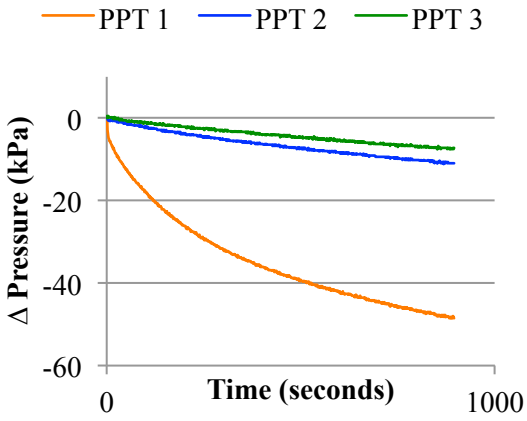

a) Test 1: Unreinforced

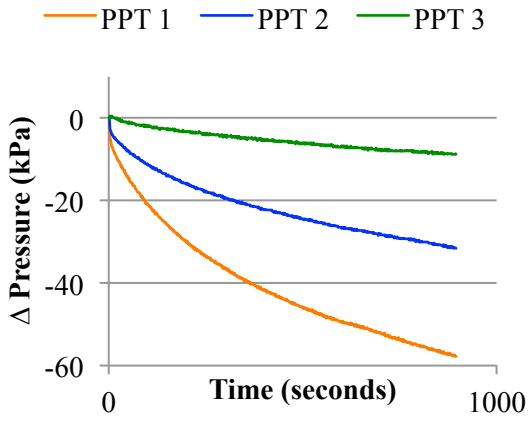

b) Test 2: 1 geogrid (short width)

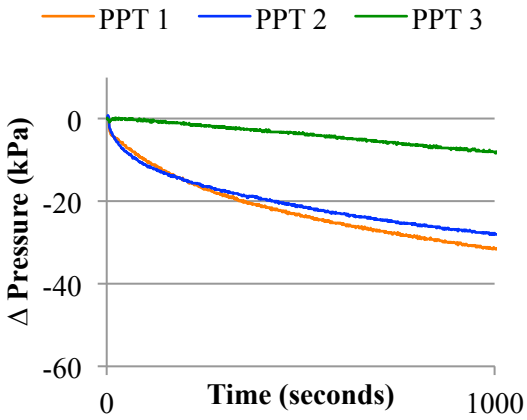

c) Test 3: 2 geogrids (short width)

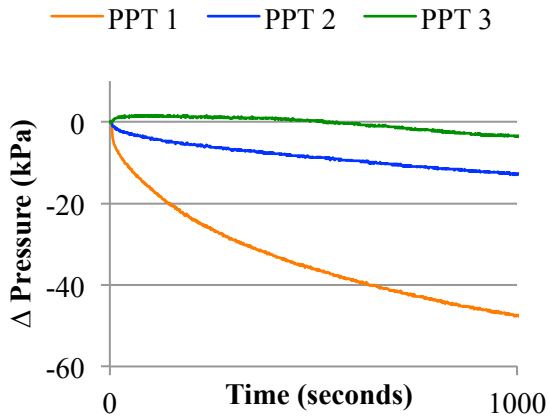

d) Test 4: 1 geogrid (extended width)

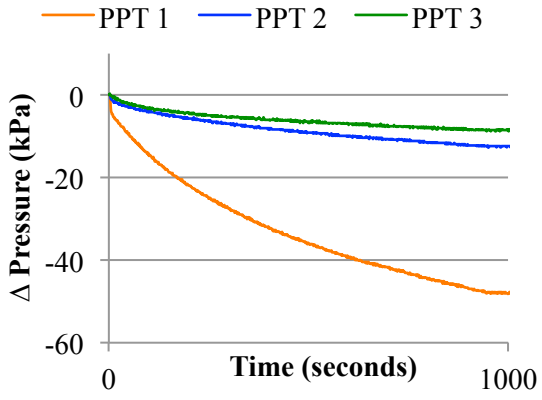

e) Test 5: 2 geogrids (extended width)

Figure 6.11 Dissipation of pore pressure, post-loading for each centrifuge model tests. The origin of each chart is the moment that loading was ceased.

6.8 Summary

Table 6.1 summarises the observations from the deformation and instrumentation data.

Table 6.1 Summary of the findings of the centrifuge model tests at 5, 10 and 15 mm displacement.

		Test				
		1	**2**	**3**	**4**	**5**
5 mm	**Applied stress (kPa)**	20.4	28.9	14.4	22.5	24.8
	Maximum height of bulge (mm)	1	2	2	1	3
	Offset of maximum height (mm)	40	70	50	75	70
	Width of deformation zone (mm)	320	420	360	340	500
	Δ PPT 1 (kPa)	16.3	16.6	7.2	15.3	14.0
	Δ PPT 2 (kPa)	16.1	16.1	5.4	10.9	13.0
	Δ PPT 3 (kPa)	1.6	7.8	3.1	7.3	7.5
10 mm	**Applied stress (kPa)**	23.8	36	23.2	31.3	34.1
	Maximum height of bulge (mm)	5	4	5	5	9
	Offset of maximum height (mm)	60	70	75	85	105
	Width of deformation zone (mm)	380	440	490	460	500
	Δ PPT 1 (kPa)	15.8	18.9	12.2	17.6	17.9
	Δ PPT 2 (kPa)	17.4	18.4	6.2	13.0	13.5
	Δ PPT 3 (kPa)	5.2	8.8	3.6	5.7	8.3
15 mm	**Applied stress (kPa)**	29.9	44.3	32.5	40.9	44.7
	Maximum height of bulge (mm)	5	6	10	10	14
	Offset of maximum height (mm)	50	70	75	95	110
	Width of deformation zone (mm)	450	450	530	520	500
	Δ PPT 1 (kPa)	19.2	24.6	19.5	22.0	23.1
	Δ PPT 2 (kPa)	19.2	21.0	7.8	15.8	17.6
	Δ PPT 3 (kPa)	6.0	10.1	4.4	4.4	12.5

At 5 mm vertical displacement the applied stress increases with the addition of reinforcement. Test 2, which contained a single geogrid with a short width performed the best, achieved an applied stress of 28.9 kPa. The maximum height of the deformation bulge that develops at 5 mm displacement increases with the addition of reinforcement, most notably with the addition of 2 extended width geogrids. The offset of this maximum height is further away from the edge of the platform for all the reinforced tests, compared to the unreinforced test (test 1) which is much closer to the edge of the platform. The width of the zone of deformation is the greatest for test 2 and test 5, which both tests recorded higher applied loads than any of the other tests. Pore pressures recorded directly beneath the platform (PPT 1) are generally similar for all tests with exception of test 3. The pore pressures at PPT 2 are similar for test 1 (unreinforced) and test 2 (1 geogrid with a short width), compared to the reinforced tests with extended geogrid widths which recorded lower pore pressures at 5 mm displacement. The pore pressures recorded at PPT 3 are comparable for all the reinforced tests, but is much lower for the unreinforced test (test 1).

At 10 mm vertical displacement all tests had recorded an increase in the applied stress from the platform, but the tests with reinforcement achieved higher applied stresses than the unreinforced test. Test 2 again records the highest applied stress, but it is evident that the tests with geogrids with extended widths (both single and double layers) record higher applied stresses. The maximum height

of the deformation bulge is comparable for all tests, except test 5 which has a maximum height of 9 mm. The offset of this maximum height from the edge of the platform is further away for the reinforced tests. The maximum height of the bulge moves further away with the addition of an additional layer of reinforcement, and furthermore with the increase in the width of the geogrid. With exception of test 3, the width of the zone of deformation increases from test 1 to test 5. The pore pressures recorded directly beneath the platform remain similar at 10 mm displacement, with the exception of test 3, the test with the lowest applied stress. It is evident that the pore pressure at PPT 2 is lower for the tests with reinforcement included which has an extended width, compared to the unreinforced test and reinforced tests with a short geogrid width. The addition of a secondary layer of reinforcement (both short and extended widths) evidently decreases the pore pressure recorded at PPT 3.

At 15 mm vertical displacement it is more noticeable that the tests with reinforcement included have achieved higher applied stresses, compared to the test without reinforcement. Test 5, which contained 2 geogrids with an extended width, recorded the highest applied load of 44.7 kPa. This test also has the largest maximum height of the deformation bulge. The addition of a secondary geogrid (short and extended width) increases the maximum height. . The offset of this maximum height from the edge of the platform increases from test 1 through to test 5. The pore pressures recorded directly beneath the platform remain similar at 15 mm displacement. Similar to the results at 10 mm displacement, the pore pressure at PPT 2 is lower for the tests with reinforcement included which has an extended width, compared to the unreinforced test and reinforced tests with a short geogrid width.

The load, vertical displacement, pore pressures and visual recordings of each test have been presented. In summary, most strain in the clay horizon coincides with the edge of the platform for the unreinforced test, while in the reinforced tests the zone of strain seems to coincide with the width of the reinforcement. The lateral extent of the zone of deformation is the largest for the tests with an extended reinforcement width, and is enhanced by the addition of a second layer of reinforcement. Pore pressure changes are the highest for the pore pressure transducer located beneath the centre of the load, and the lowest at the pore pressure transducer located the furthest away from the platform, while there is a distinct change in pore pressures at each location upon loading with the addition of reinforcement.

CHAPTER 7 ANALYSES AND DISCUSSION

7.1 Introduction

Data acquired from the five centrifuge model tests were reviewed and compared. Defining and comparing the deformation behaviour for each centrifuge test, outlines the differences in the geometry for each test at specific vertical displacement intervals. Data was compared to identify the changes in response to the load-displacement responses for each model. The response of the pore pressure transducers within the clay layer would aid in gaining a better understanding of how the material responded to different configurations of reinforcement in the upper sand horizon. The following chapter presents the findings of these analyses.

7.2 Load - deformation behaviour

The deformation behaviour of each centrifuge model, at 5, 10, and 15 mm displacement, is presented in Figure's 7.1, 7.2, and 7.3, respectively. The change in deformation behaviour at the same vertical displacement interval between each test is distinct. At 5 mm vertical displacement it is apparent that there is little disturbance to the boundary between the clay and overlying sand, as well as little disturbance to the surface for the model without reinforcement. Without reinforcement, distinct shear zones develop at the edge of the platform through the upper sand horizon. As such, the sand beneath the platform essentially behaves as a deeper rigid foundation extending to the top of the clay horizon. This is in agreement of the observation highlighted by Huang and Tatsuoka (1990) who concluded that the underlying sand of unreinforced footings act as a deeper rigid footing. Directly below this sand, an extremely shallow wedge of clay develops similar to the classic bearing capacity wedge which develops beneath footings. By 15 mm displacement it is obvious that most of the strain in the clay horizon is therefore confined to the portion below the overlying sand directly beneath the platform. The clay is squeezed laterally, with little disturbance to the boundary at the top surface of the clay horizon and the base of the upper sand horizon. Consequently, there is little disturbance at the surface of the model, as the lateral extent of the influence zone on deformation in the clay horizon is small, with the offset of the maximum height occurring closer to the platform. By 15 mm vertical displacement an applied stress of 29.9 kPa is achieved for the unreinforced test.

This is in contrast to the tests performed with geogrid reinforcement present. With the inclusion of geogrid reinforcement in the upper sand horizon the deformation behaviour changes. Deformation to the clay horizon is already observable at small displacements in some reinforced tests and clear at larger displacements for all reinforced tests.

With a single layer of reinforcement in the upper horizon with a short width (50 mm beyond the platform), the deformation of the clay horizon is 'enhanced' at all displacement intervals. The shear zone at the edge of the platform is unable to fully develop through the upper sand horizon, due to the presence of the geogrid. As such, the sand beyond the edge of the platform is deformed under the

load up to the edge of the width of geogrid. Consequently, the reinforcement places a wider portion of the clay under an applied stress, thereby increasing the lateral extent of the zone of deformation. The effect of the inclusion of a geogrid is evident in the deformation behaviour, as the deformation at the boundary between the upper clay horizon and the base of the upper sand horizon has a larger bulge of deformation than compared with the unreinforced test. This leads to more disturbance at the surface of the model. The width of the influence zone on deformation is laterally wider than the unreinforced test, with a vertically higher maximum height of the deformation bulge. At 5 mm vertical displacement the applied stress is 28.9 kPa, compared with the applied stress of 29.9 kPa at 15 mm vertical displacement in the unreinforced test. This highlights that an increased vertical load capacity is achieved at smaller displacements when reinforcement is added. The deformation behaviour at approximately the same applied stresses for each test is comparable, but occurs at different vertical displacements. The By 15 mm vertical displacement the applied stress is 44.3 kPa for the test with a single layer of reinforcement with a short width.

With an addition of a second geogrid layer with a short width, the deformation is intensified. The maximum height of deformation is greater at 15 mm displacement, compared to the test with one short width geogrid installed. The same length of sand is deformed with the inclusion of a secondary geogrid, but leads to further deformation of the clay. On comparison between the single and double layer of reinforcement with a shorter width, the offset of the maximum height of the bulge of deformation is closer to the edge of the platform for the test with two short geogrids installed. This could plausibly be attributed to an increase in stiffness provided by the addition of a secondary layer of reinforcement. As such, the movement of the reinforced sand beyond the foundation is more rigid upon loading. An applied stress of 23.2 kPa is achieved at 10 mm displacement, which is comparible to an applied stress of 23.8 kPa achieved in the unreinforced test at the same displacement. At the same applied stress level for both tests, the maximum height of the deformation bulge is the same. However, the lack of correlation with the deformation and applied stress levels with the other tests conducted, indicate that the test with 2 short layers of geogrid reinforcement may be an outlier.

In the model tested with extended geogrid widths (both 1 and 2 layers), the influence zone on deformation is wider, rather than a smaller deformation bulge in the tests with shorter reinforcement lengths as well as the unreinforced test. The deformation of the boundary between the clay and upper sand horizon is also laterally more extensive at 5 mm vertical displacement, for the model with 2 extended geogrids installed. As in the shorter geogrid tests, the addition of geogrid reinforcement with an extended width, contributes to an increase in stiffness of the reinforced sand. This increase in bearing capacity is in agreement with the work conducted by Huang and Tastuoka (1990) who concluded that an increase in bearing capacity can be attributed to an increase in the length (in this case width) of reinforcement. As Jewell (1996) and James (pers comm, 2010) highlight, when the load is applied, stress is transferred at the interface and the sand interacts with the geogrid, taking up the load laterally and becoming more rigid over the entire width of the geogrid. Subsequently a larger portion of the clay is strained beneath the entire length of the georid.

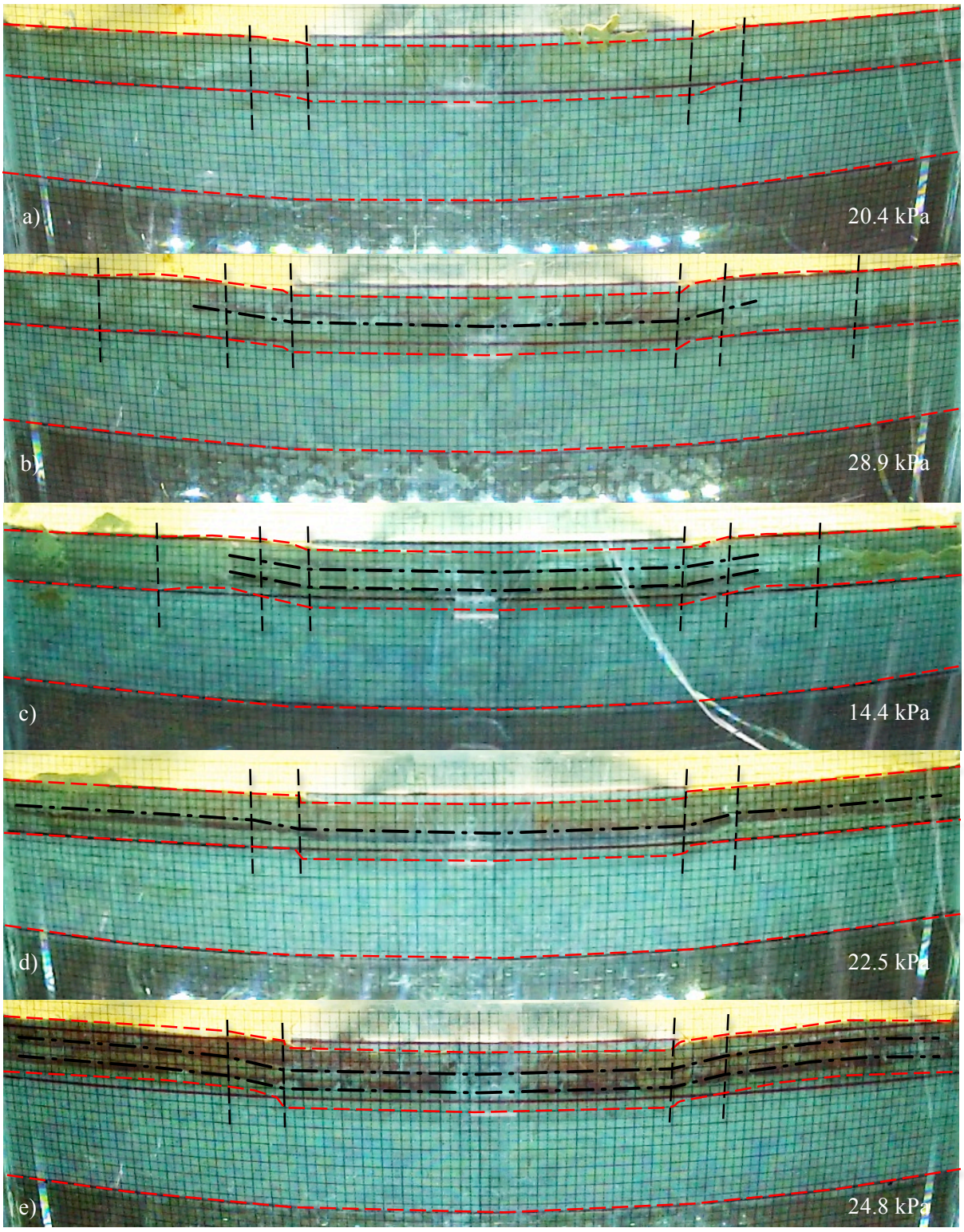

Figure 7.1 Comparison of load-deformation behaviour between a) unreinforced, b) 1 short geogrid, c) 2 short geogrids, d) 1 extended geogrid, and e) 2 extended geogrids, at 5 mm vertical displacement.

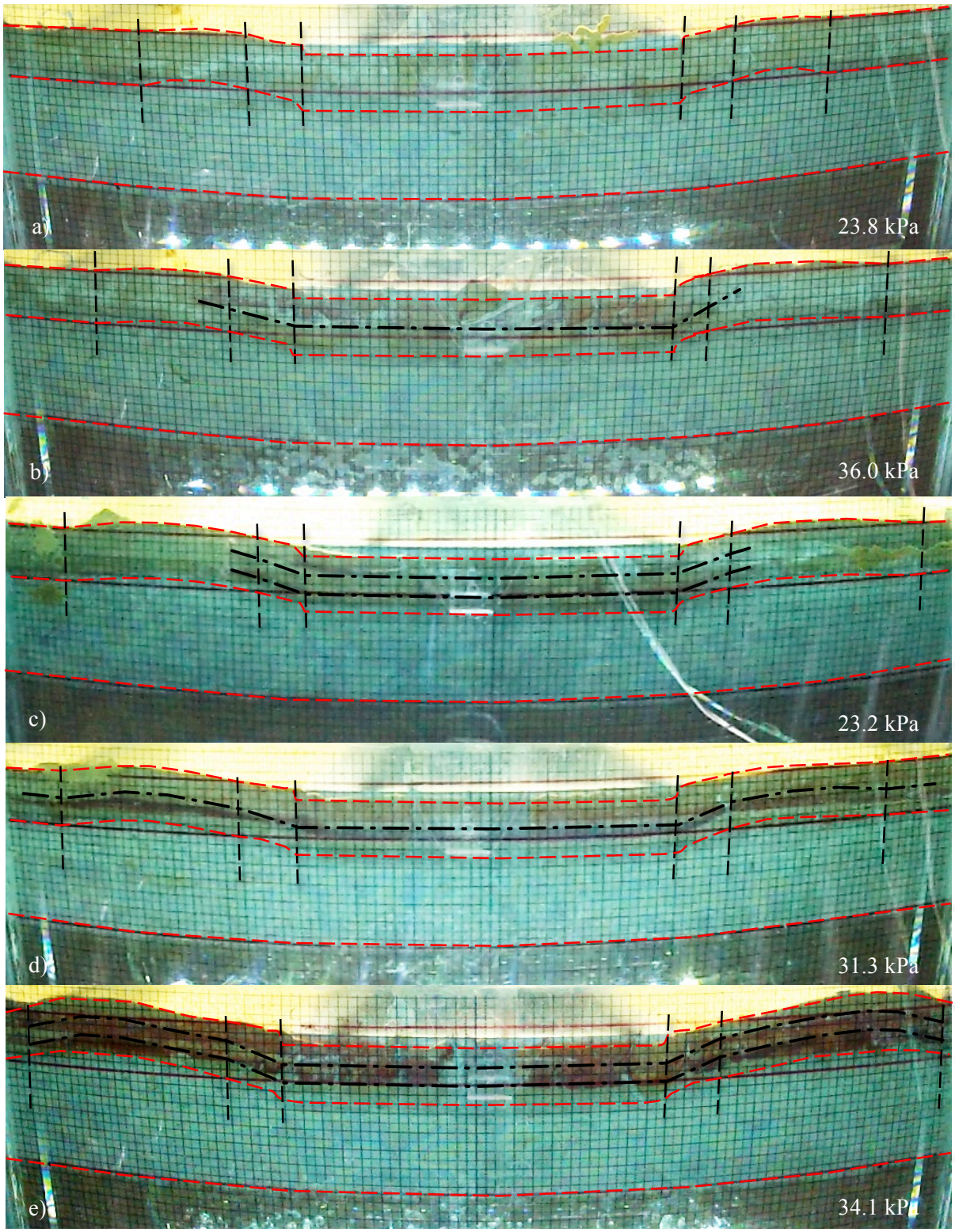

Figure 7.2 Comparison of load-deformation behaviour between a) unreinforced, b) 1 short geogrid, c) 2 short geogrids, d) 1 extended geogrid, and e) 2 extended geogrids, at 10 mm vertical displacement.

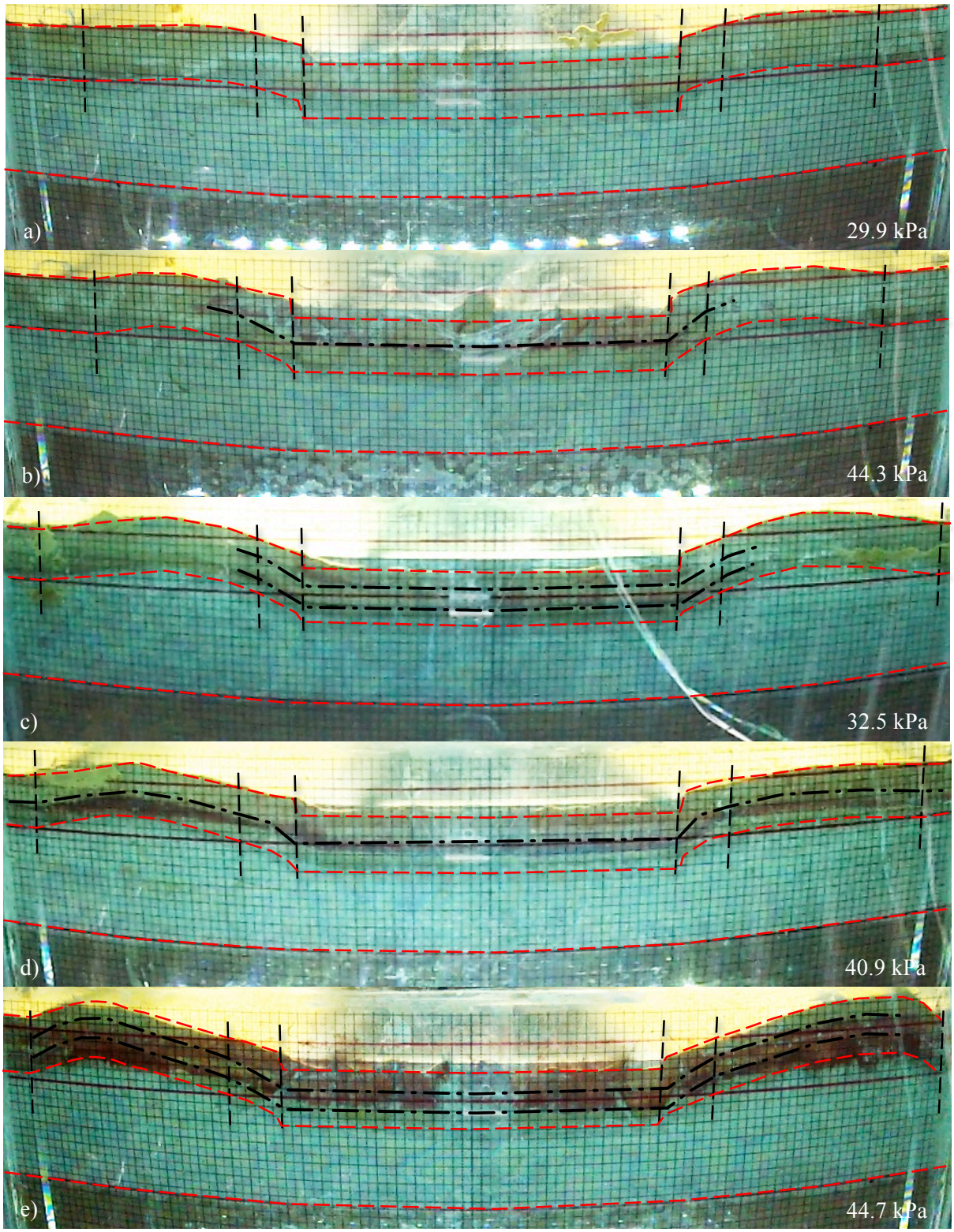

Figure 7.3 Comparison of load-deformation behaviour between a) unreinforced, b) 1 short geogrid, c) 2 short geogrids, d) 1 extended geogrid, and e) 2 extended geogrids, at 15 mm vertical displacement.

However, the increase in stiffness provide by the reinforcement allows for a larger vertical load capacity. At 15 mm displacement an applied stresss of 40.9 kPa and 44.7 kPa is achieved, for the single and double layer of geogrid tests with extended widths respectively. When comparing the deformation at similar applied stress levels between the extended width tests and the unreinforced

tests, there is a notable correlation. An applied stress of 24.8 kPa is achieved at 5 mm displacement in the reinforced test with 2 geogrids with an extended width, compared with the 23.8 kPa applied stress achieved for the unreinforced test at 10 mm displacement. The maximum height of the deformation bulge is similar (3 and 5 mm respectively) for both tests at approximately the same applied stress level, but different displacements.

The same comparison can be made between the unreinforced test at 15 mm displacement, and the reinforced test with a single layer of geogrid reinforcement with an extended width at 10 mm vertical displacement. These tests achieve similar applied stresses of 29.9 kPa and 31.3 kPa at these respective displacements. Once again, the maximum height of the bulge of deformation is comparable, with both recording a maximum height of 5 mm. It seems that the 'enhancement' of deformation when reinforcement it included, comes at the profit of an increased load capacity.

The extended width reinforcement tests are comparable to what Sharma *et al* (2009) call the membrane effect. Reinforcement is provided by the downward movement of the foundation and underlying soil under an applied load. This results in the reinforcement deforming and being placed under tension, as a curved shape develops in the reinforcement to develop an upward force to support the applied load. As Sharma *et al* (2009) mention, a certain amount of settlement is needed to mobilise the tensioned membrane effect. The extended width reinforcement tests achieve a higher applied load upon increasing displacement because there is enough length (in this case represented by width) and stiffness to prevent the geogrid from failing by pull-out and tension. The failure mode for all the reinforced tests is comparable to the failure mode researched by Wayne *et al* (1998) and very specific to reinforced sand foundations over a two-layer soil system, similar to the case when a strong soil overlies a weaker soil horizon (as shown previously in Figure 3.3 c).

It is clear that the offset of the maximum height of the bulge during deformation of the clay moves horizontally further away from the edge of the platform for each test. Deformation is enhanced with the inclusion of reinforcement at the gain of an increased load capacity. The deformation and load capacity is improved when additional reinforcement layers are included, and increases even more when the width of the geogrid is extended.

In all the tests conducted on the centrifuge model, there is no disturbance to the boundary between the basal sand horizon and the overlying clay horizon. As such, the interface between the two horizons behaves as a fixed boundary. Therefore the clay can be expected to move laterally at this boundary, should it deform.

This distinction that is observed when the geogrid has an extended width, can most certainly be best described by the 'wide-slab effect' as termed by Huang and Tatsuoka (1990) for their studies pertaining to footings over reinforced foundation sand. By including the reinforcement far beyond the platform footprint, even more of the upper sand horizon is mobilised under load as the extended geogrid takes up most of the load laterally. The deformation to the boundary between the top of the clay horizon and the base of the upper sand horizon, is vertically and horizontally larger than the test without reinforcement and with a short geogrid installation length. The deformation bulge at this boundary and at the surface of the model is laterally more extensive, with a larger maximum height,

horizontally further away from the platform edge. Once again, when a second geogrid is included at an extended length, the effect of this deformation behaviour is enhanced. The maximum height of the bulging effect and the extent of deformation to the clay horizon is the greatest of all the test conducted.

7.3 Load – displacement behaviour

The loads achieved for each centrifuge model test are plotted against vertical displacement of the platform in Figure 7.4 to show the behaviour (<5 mm) of the model during the tests. Figure 7.5 presents the load-displacement relationship for the tests up to 15 mm vertical displacement to highlight the subsequent loading behaviour under increasing displacement. The test without reinforcing initially reaches a load of 0.6 kN at 1 mm displacement. Two distinct gradients are evident for the model with a single layer of reinforcement with a shorter width. Initially, at 0.5 mm vertical displacement the load reached is 0.1 kN. However, this increases sharply to a steeper gradient of 0.5 kN at 1 mm vertical displacement. The gradient for the test with two layers of reinforcement with a shorter width has a typically shallow gradient, reaching a load of 0.3 kN at 1 mm vertical displacement. When a single layer of reinforcement is included with an extended width, the load achieved for the first 1 mm of vertical displacement was 0.5 kN. When an additional reinforcement layer is included with the same extended width, the relationship is similar, with a load of 0.6 kN at 1 mm vertical displacement during the test.

Up to approximately 1.4 mm vertical displacement, the gradients of the unreinforced, 1 geogrid (extended width), and 2 geogrids (extended width) tests are similar. The two geogrid reinforced gradients with a shorter width are also similar, but shallower than the other three tests, indicating a possible error. Thereafter the test with one geogrid with a shorter width exhibits a sharply increasing gradient, and reaches a load of approximately 1.3 kN at 3 mm displacement. Thereafter it follows a similar gradient to that of the test with two geogrid layers with a shorter width. This test maintains a larger load than any of the other tests, and it is likely that the test could be an outlier. This is likely an anomaly and could be explained by a modelling error, due to the differences in model construction and soil properties.

The poor load bearing performance of the test with 2 geogrid layers with a short width, could be explained by a combination of factors. If the distance between the 2 geogrids was such that the spacing was too close, there could have been an interaction problem. This would have occurred if there was not sufficient sand at the interface of each of the geogrids, for the tensile strength in the geogrid to mobilise with the sand. This would have lead to an interface failure between the two geogrids at the bottom interface of the upper layer and the upper interface of the lower geogrid interface. Coupled with the short width, this would have not given the geogrids enough surface area to anchor itself by interaction with the sand, as indicated by Sharma *et al* (2009) as a requirement to being a successful reinforcement mechanism. This gave rise to the worst preforming test in terms of load bearing capacity.

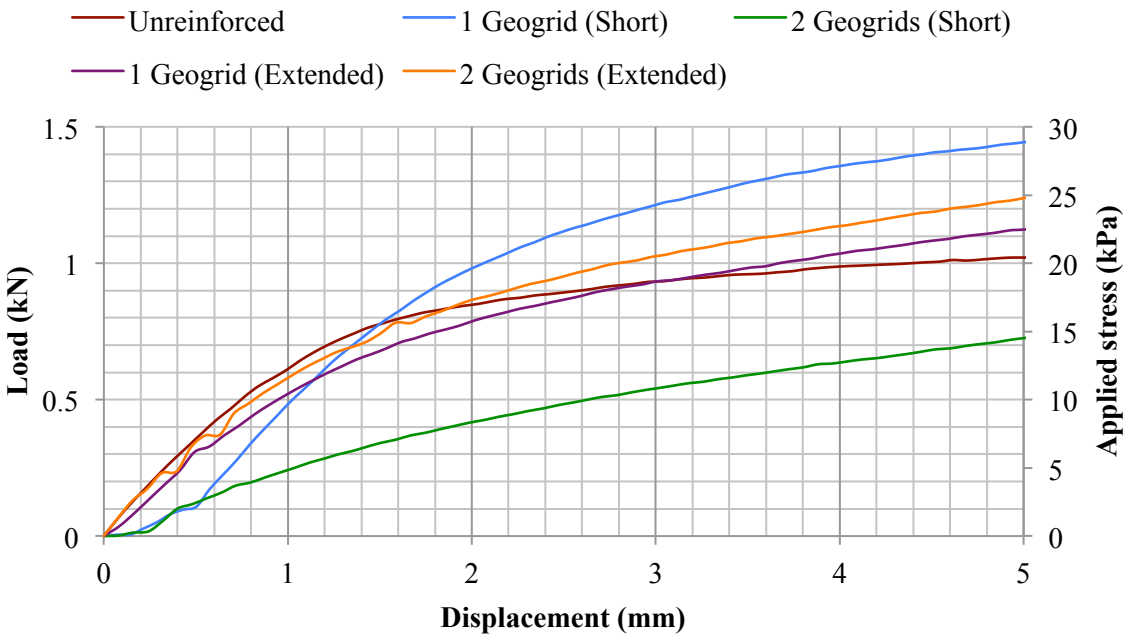

Figure 7.4 Load-displacement curves for the centrifuge model tests, for the initial 5 mm vertical displacement.

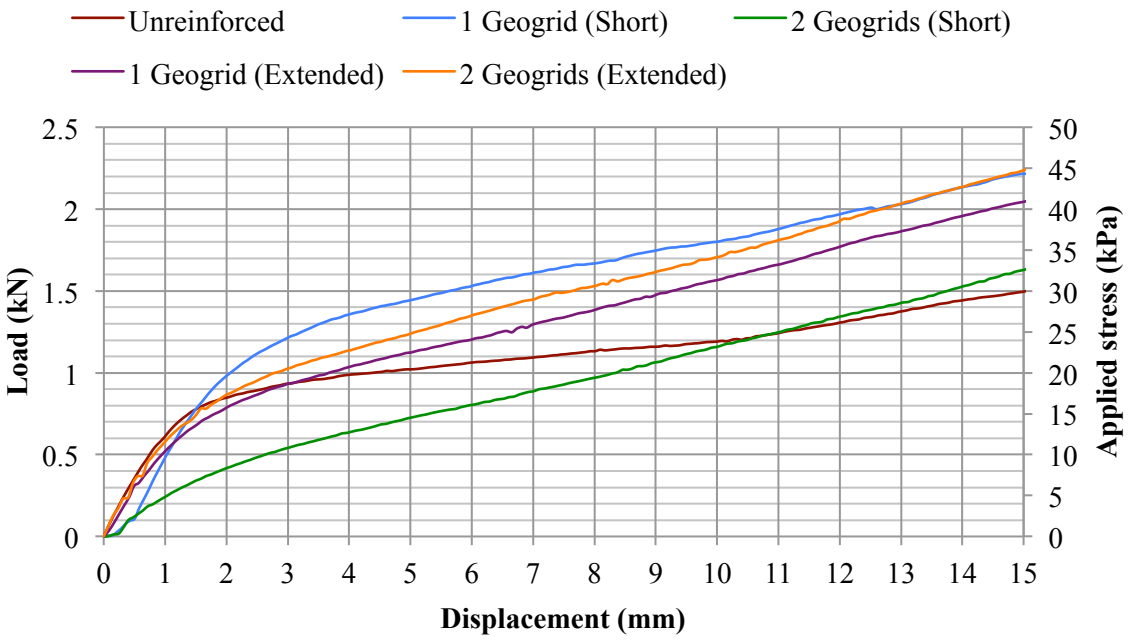

Figure 7.5 Load-displacement curves for the centrifuge model tests, up to 15 mm vertical displacement.

Between 1 and 4 mm displacement, the slopes of all the load-displacement curves change, and become flatter. The unreinforced model only reached a load of 1.0 kN at 4 mm displacement. The tests with one and two layers of reinforcement with a short width achieved loads of 1.4 kN and 0.6 kN, at 4 mm displacement respectively. When one layer of reinforcement was included with an extended width, the load achieved is 1.0 kN at 4 mm displacement. When an additional layer of

reinforcement with an extended width was included, a load of 1.2 kN at 4 mm displacement was achieved.

For the remaining tests (unreinforced, 1 extended geogrid and 2 extended geogrids) at small displacements all three load-displacement gradients remain constant up to increased loading where the extended reinforcement curves differ in their relationship with the unreinforced curve. Both unreinforced and reinforced (extended width) curves reach a load of approximately 0.7 to 0.8 kN, at approximately 1.5 mm displacement. Thereafter the reinforced gradients are much steeper than the unreinforced gradient. Both curves of the tests with extended width reinforcement (1 and 2 geogrid layers) exceed a 2 kN load and applied stress of 40 kPa at 15 mm displacement. At the same displacement the unreinforced test only reaches a load of 1.5 kN and an applied stress of 30 kPa. Similar load-displacement relationships exist for both the single and the double reinforcement conditions. However, the test with two geogrids installed performed better under load than that with a single layer of geogrid reinforcement.

Observations of the load-displacement curves suggest that the load-displacement behaviour is typically very similar for the initial displacements of all tests. It is only at relatively large displacements where a difference becomes apparent. This difference would be ascribed to the increase in vertical load capacity from the addition of geogrid reinforcement, as highlighted initially by Binquet and Lee (1975). Again these findings correspond well to the work conducted by Sharma *et al* (2009), in order to mobilise the tension membrane effect as a reinforcement mechanism when a geogrid is used in a reinforced sand foundation.

A failure to mobilise the tension membrane effect could explain the failure of the 2 geogrids with a short width as a successful reinforcement mechanisms. This could indicate why the load-displacement results from this test perform inadequately. The test with a single layer of short reinforcement which achieves a load capacity which was not expected may be regarded as an outlier, plausibly due to model contruction, soil properties, or experimental error.

7.4 Load – pore pressure behaviour

The applied stresses achieved throughout the test sequence were plotted against the change in pore pressure measured for each test. These graphs are displayed in Figure 6.6. Pore pressure transducer 1 (PPT 1) was located beneath the centre of the platform, PPT 2 at the edge of the platform, and PPT 3 placed at 100 mm from the edge of the platform. All the PPT's were placed in the middle of the clay horizon.

Observably, the pore pressure response for the unreinforced test is dissimilar to the rest of the tests. PPT 1 shows a clear point, at approximately 16 kPa where the pore pressure drops as the load continues to increases, and thereafter increases again. For both of the tests with only a single layer of geogrid reinforcement (short and extended widths), there is a point where the pore pressure remains constant under an increasing load. This is not observable for the response of PPT 1 for both tests with 2 layers of geogrid reinforcement (short and extended widths), as the pore pressure seems to increase in a generally linear relationship with an increasing load.

Data from PPT 2, does not show any clear evidence which distinguish the tests from one another. However, there is a slightly more immediate response in the pore pressure recordings for the geogrids with a shorter width (1 and 2 layers), compared to the geogrids with an extended width. This is plausibly due to the narrower width of the test with a shorter width geogrid, as the applied stress to the clay horizon may subsequently be less extensive.

PPT 3 shows no response under the initial load for the unreinforced test compared to the rest of the test with reinforcement included. Inclusions of geogrids place a larger area of the clay under strain, whereas only the portion of clay beneath the platform strains when reinforcement is not present. The pore pressure increase recorded at PPT 3, would coincided when the clay would have reached a yield point and was 'squeezed' out from beneath the platform. This point in the unreinforced test also coincides with the point (approximately 16 kPa) where PPT 1 records a drop in pore pressure.

Data acquired from PPT 1 can be used to distinguish differences between the tests. In the unreinforced test there is a clear yielding point where the pore pressure response in the clay ceases to behave in a linear fashion. This yield point is less distinct for the tests with 1 geogrid installed (both short and extended widths), but still identifiable.

Tests conducted with 2 geogrids installed (both short and extended widths) are also similar in their behaviour at PPT 1. The pore pressure data for these tests show the least clear evidence of yielding and have a near linear relationship between the increase in load and pore pressure.

Due to the undrained nature of the tests, no consolidation of the clay occurs under load therefore the pore pressure changes are due to the lateral squeezing of the clay. This evidence of yielding in the unreinforced test may be due to most of the vertical strain in the clay horizon occurring directly beneath the loaded foundation. It would be obvious that most of the load is concentrated directly beneath the platform and the clay reaches its yielding point quicker, subsequently squeezing out laterally. Only once the lateral squeezing occurs, does the pore pressure at PPT 1 increase linearly with the load.

The inclusion of reinforcement alters the load and the subsequent vertical strain in the clay horizon. The less clear yielding for the single layer of reinforcement (shorter and extended widths) may be due to the increase in stiffness and rigidity of the upper sand horizon. This upper sand horizon subsequently transfers the applied load to the clay horizon over a larger surface area. An additional reinforcement layer further enhances this, as the sand horizon is even more rigid. This places less direct load onto the clay horizon directly beneath the loaded platform. Subsequently, the yielding in the clay horizon is less evident (near linear) beneath the centre of the platform, as the application of the load to the clay is broader, acting over a larger surface area.

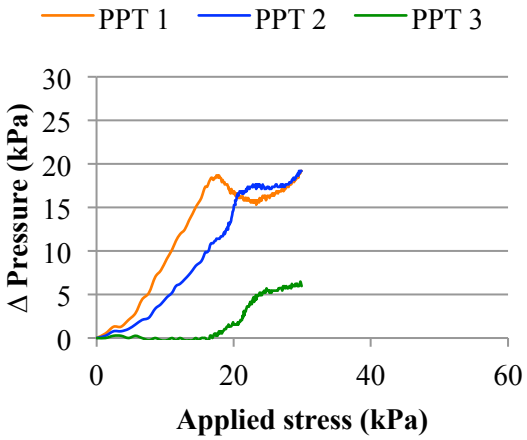

a) Unreinforced

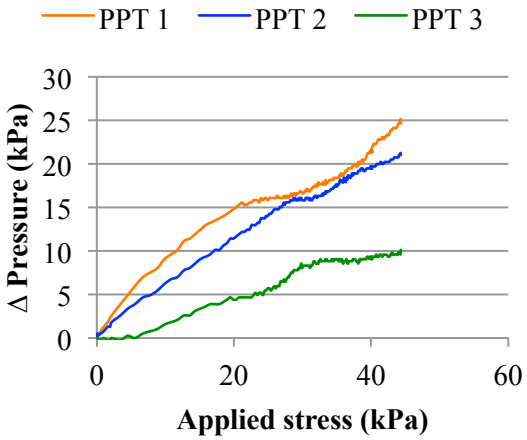

b) 1 Geogrid (short width)

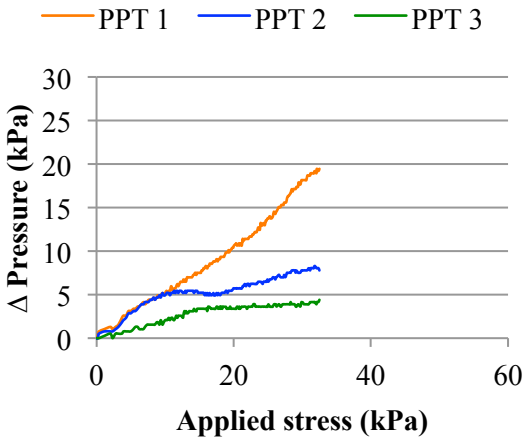

c) 2 Geogrids (short width)

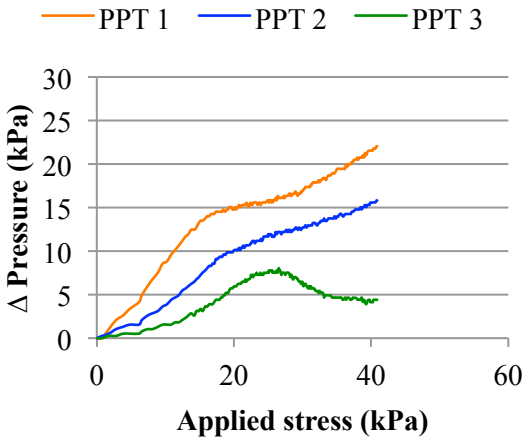

d) 1 Geogrid (extended width)

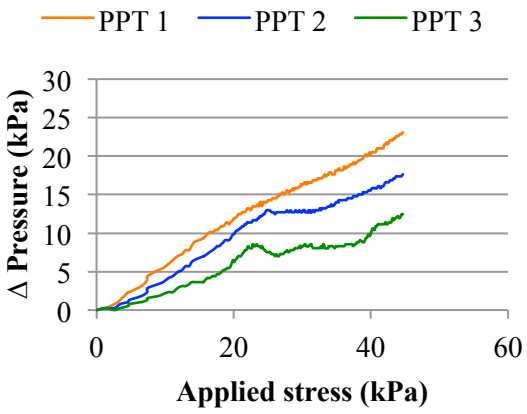

e) 2 Geogrids (extended width)

Figure 7.6 Change in pore pressure versus load curves, for each centrifuge model test.

The relationship between the change in pore pressures at PPT 1 and PPT 2 are different for both scenarios (single and double layers of reinforcement). The test with a single layer of reinforcement (both short and extended widths) maintains a similar response of pore pressure, with increasing load.

However, the tests with two layers of reinforcement (both short and extended widths) reach a load when the pore pressure response at PPT 2, deviates and becomes constant under increasing load. The applied stress at this point is approximately 10 kPa for the shorter width and 26 kPa for the extended width. This may enhance the idea that the initial load is applied over a larger portion of the clay, but at a certain load the increased stiffness of the sand directly beneath the foundation, influences the pore pressure and subsequently the yield point is less clear.

When comparing the pore pressures at each location, at similar applied stress levels for each test, this becomes even more clear. At an applied stress of 23.8 kPa in the unreinforced test, the change in pore pressures recorded at PPT 1, PPT 2 and PPT 3 are 15.8 kPa, 17.4 kPa and 5.2 kPa, respectively (refer to table 6.1 for tabulated values). When comparing these results to the pore pressure changes recorded at similar applied stress levels for the reinforced tests (both 1 and 2 layers of geogrid) with an extended width, the influence on the reinforcement becomes apparent. At an applied stress of 22.5 kPa the change in pore pressure recorded at location PPT 1, PPT 2 and PPT 3 are 15.3 kPa, 10.9 kPa and 7.3 kPa for a single layer of geogrid reinforcement. For the test with 2 extended width geogrids the change in pore pressures are 14.0 kPa (PPT1), 13.0 kPa (PPT 2) and 7.5 kPa (PPT 3).

It is clear that the change in pore pressure is lower at PPT 2 when a geogrid is installed with an extended width. Furthermore, the change in pore pressure recorded at PPT 3 is higher for the test with extended width reinforcement than for the unreinforced test.

The same is evident at a higher applied stress level. At an applied stress of 29.9 kPa for the unreinforced test, the change in pore pressures are 19.2 kPa (PPT 1), 19.2 kPa (PPT 2) and 6.0 kPa (PPT 3). For the test with a single layer of extended width reinforcement at an applied stress of 31.3 kPa the change in pore pressures recorded are 17.6 kPa (PPT 1), 13.0 kPa (PPT 2) and 5.7 kPa (PPT 3). The findings are identifiable but less clear for the tests conducted with reinforcement with a short width.

The pore pressure responses clearly indicate that the inclusion of reinforcement appears to spread and transfer the applied load into the adjacent soil. Subsequently, the applied stress to the clay horiozn is wider. The applied stress is not localised around the foundation, as is the case in the unreinforced test. This explains why the pore pressure at PPT 2 is lower and the pore pressure at PPT 3 is higher, for the tests conducted with reinforcement present

7.5 Summary

Results from the five centrifuge test conducted were compared. Deformation behaviour is distinctly different between unreinforced and reinforced tests. Vertical movement in the unreinforced test occurs directly beneath the platform, with little lateral disturbance to the clay horizon beyond the platform edge. The deformation bulge that develops when reinforcement is included is associated to the width of the reinforcement. Deformation is enhanced with the inclusion of an additional layer of reinforcement. The enhancement of deformation comes at the profit of increasing the load bearing capacity with the addition of reinforcement layers, and furthermore with an extended reinforcement

width. Pore pressures show a clear yielding of the clay when no reinforcement is present, but no evidence is seen for yielding in pore pressure responses when two layers of reinforcement are included. Pore pressure responses indicate a spread and transfer of the applied load to the clay horizon when reinforcement is added.

CHAPTER 8 CONCLUSION

8.1 Introduction

Basal reinforcement, where high tensile strength geogrids are employed beneath structures, is becoming an increasingly accepted construction technique along the eastern coast of southern Africa. The presence of compressible, soft, thin and shallow clay horizons, usually associated with complex estuarine or lagoonal deposits, are a major consideration when using basal reinforcement as a founding technique. The study involved the investigation of the deformation behaviour of a clay horizon under a wide loaded platform using five centrifuge tests. These tests compared the behaviour of the clay horizon between unreinforced and various reinforced conditions. This chapter presents an overview of the research, the main findings and concludes the dissertation by satisfying the aim of the study, which was to qualitatively define the behaviour of compressible, soft, thin, shallow clay horizons, under a reinforced sand foundation, loaded by a wide platform.

8.2 Research overview

Physical modelling in geotechnics is an important tool to the profession as it allows simulation and subsequent observation of an actual event at model scale. Centrifuge modelling itself holds an even more significant role in physical modelling due to the ability to replicate *in situ* stresses. This is important because soil behaviour is dependant on stress level. In order to create the correct stress environment, the model is subject to high acceleration levels within the centrifuge.

Basal reinforcement, where a reinforced sand foundation is constructed, is a relatively new technique in southern Africa. It has found application in the extensive estuarine and lagoonal deposits which characterise the ground profile in the harbours along the eastern coast of southern Africa. It has been well documented that the majority of problems associated with founding in these areas, are the presence of soft, compressible, shallow clay horizons, which occur within these unconsolidated deposits. The presence of a geotechnical centrifuge facility at the University of Pretoria allowed the replication of basal reinforcement being utilised when a foundation footprint overlies such a scenario. A centrifuge model was constructed and tested, to qualitatively examine the behaviour of these compressible clay horizons without geogrid reinforcement and with various geogrid reinforcement configurations. The width of the reinforcement and the number of layers of reinforcement were varied for the reinforced tests.

8.3 Findings

A distinctive difference between the unreinforced and the reinforced scenarios, was evident from the centrifuge tests conducted. The majority of the strain which took place in the unreinforced test coincided with the edge of the platform load, and deformation was localised around the platform. The sand directly beneath the platform overlying the clay horizon, acted as a deeper rigid platform, as

distinct shear zones developed adjacent to the platform edges. During vertical displacements of the platform the clay fails and squeezes out laterally. Most of the deformation in the clay horizon further away from the platform is therefore due to this movement of clay from underneath the load.

When reinforcement is added, the deformation behaviour of the clay horizon changes. The lateral extent of the deformation zone in the clay horizon coincides with the width of the geogrid reinforcement in the upper sand horizon. The width of this zone of deformation as well as the offset to the maximum height of the deformation bulge from the edge of the load, do not correlate to an applied stress level or to a specific vertical displacement. Instead, these deformation factors are controlled by the width of the geogrid reinforcement present.

When no reinforcement is present the zone of deformation is narrower, with the offset of the maximum height of the deformation bulge occurring closer to the applied platform load. When reinforcement with a short width is utilised the width of the influence zone is increased, thereby increasing the width of the lateral deformation in the clay horizon as well moving the offset of the maximum height of deformation further away from the edge of the applied load. A geogrid with an extended width furthermore increases the lateral extent of the zone of deformation, and the maximum height of the deformation bulge moves even further away from the applied load.

The maximum height of the deformation bulge, which develops adjacent to the loaded platform, correlates directly with the applied stress level achieved. A similar maximum height of the deformation bulge, which develops under vertical displacement, is expected at similar applied stress levels.

The applied stress achieved is controlled by the presence and configuration of reinforcement. A large applied stress level can be achieved at small vertical displacements when reinforcement is added with an extended width, whilst the same applied stress level can only be achieved at high vertical displacements when no geogrid reinforcement is present.

The pore pressure response is fully mobilised under testing by 5 mm vertical displacement. All pore pressure responses are most likely due to the lateral movement of the clay under load. Large changes in pore pressures occur directly beneath the platform foundation, when no reinforcement is included.

Pore pressures responses are also influenced by the reinforcement configuration. This is highlighted when comparing the response in pore pressures at similar applied stress levels. The pore pressures located at the edge of the platform are lower when geogrid reinforcement with an extended width is utilised, compared with higher pore pressures at the edge of the platform when no reinforcement is used. Pore pressures outside the footprint of the loaded platform are higher when geogrids with extended widths are used, but lower when no reinforcement is present. This comparison is observed, but less clear for the case when geogrid reinforcement with a short width is used. This finding indicates that there is a spread and transfer of the applied load into the adjacent sand when geogrid reinforcement is present.

Yielding of the clay directly underneath the platform footprint clearly occurs when no reinforcement is present, whereby the pore pressures remain constant under an increasing applied load. However, no evidence is seen for this yielding in pore pressure responses when two layers of reinforcement are included and the pore pressure and applied load relationship is linear. This suggests that increasing the number of layers of reinforcement will further increase the stiffness of the reinforced sand. This places the clay directly beneath the platform footprint under a smaller applied stress, as the applied load from the platform is transferred laterally through the reinforcement into the adjacent sand.

Adding reinforcement allows the sand to withstand tension. This allows the load to be transferred into the material adjacent to the loaded foundation, thereby spreading the load, enabling a larger applied load to be achieved. Reinforcement appears to spread and transfer the deformations into adjacent soil so that more material resists the imposed load. This is reflected in the load-displacement behaviour for the respective tests and further validated by the behaviour of the pore pressure within the clay horizon.

The load-displacement behaviour is initially very similar and it is only at relatively large displacements where an improvement in the load-bearing capacity becomes apparent when geogrid reinforcement is used. In order to utilise the load bearing capacity of the reinforced sand foundation, a certain amount of vertical displacement must occur in order for the reinforced sand foundation to take up its maximum load capacity. In addition to the change in deformation behaviour, the inclusion of reinforcement enhances the load-bearing capacity of the system. This increase in load-bearing capacity is further enhanced with the inclusion of an additional layer of reinforcement, as well as a widening the geogrid, relative to the foundation width. Additional reinforcement increases the stiffness of the sand, while an extended geogrid width allows better interaction over a larger surface area in the sand, thereby securing the geogrid into the adjacent material. By ensuring maximum interaction between the sand and reinforcement, the tensile strength of the geogrid can be utilised.

The increase in deformation of the clay includes an increase in the load-bearing capacity, and as such these factors will compliment each other. With the addition of geogrid reinforcement and moreover the increase in the width of the geogrid, the load-bearing capacity is increased at the cost of an enhanced deformation behaviour under vertical displacements. Increased deformation therefore comes with the profit of an increased load capacity when reinforcement is included.

Comparison of the FE analysis and the centrifuge model results shows evidence that more work needs to be conducted into narrowing the gap in between the numerical model and the physical model. This fell out of the scope of work for this research project, but provides a good basis for further research to adjust the numerical models or highlight possible discrepancies with the centrifuge model. The deformation which occurred in the centrifuge tests and those which were calculated in the numerical analysis, are comparable. They are generally similar in their deformation mechanism. However, no shear zone forms adjacent to the loaded platform for the unreinforced scenario in the numerical model. Also, the deformation bulge is far more extensive in the numerical analyses, extending the entire width of the analyses compared to the centrifuge tests.

The implications from the results of the centrifuge tests indicate that large structures constructed on soft compressible clays founded using basal reinforcement techniques, will need certain amounts of displacements in order for the reinforcement to be effective. This is plausibly why the use of basal reinforcement adopted for large warehouses of product stockpiling has been so successful. These structures can tolerate more settlement (specifically the floor platforms), and as such allows the reinforcement to strengthen the soil foundation, by transferring the load to the adjacent sand when tension in the geogrid is fully mobilised. By ensuring adequate anchorage of the reinforcement beyond the edge of the structural footprint, the tensioned membrane effect can be fully developed in order to improve the load bearing capacity. This can be achieved by extending the width of the reinforcement beyond the width of the structural footprint. In addition, an increased reinforcement width allows deformation to be minimised under the applied load because a higher vertical load capacity can be achieved at smaller vertical displacements of the foundation.

By knowing that the maximum height of deformation is controlled by the width of the reinforcement, it is easier to predict where the maximum amount of deformation will occur. If an additional surcharge load is applied to this region, it may improve the use of the tensile strength of the geogrid by anchoring it more effectively into the adjacent sand material.

The centrifuge results also highlight the need for good knowledge of the ground profile and understanding of the stress-deformation behaviour under load when conducting a numerical analysis in common industry practice.

8.4 Concluding remarks

In conclusion:

i. A centrifuge model was produced to replicate a soft, compressible clay horizon, which was relatively thin and occurring at a shallow depth. A load was applied to the model by a wide platform and the model was tested under unreinforced and reinforced founding conditions.
ii. Reinforcement was adjusted such that the width of reinforcement and the number of layers of reinforcement were varied, over the 4 reinforced tests in the centrifuge model.
iii. The change in deformation behaviour of the clay horizon was qualitatively examined for each test.
iv. The deformation behaviour of the clay horizon changes with the inclusion of reinforcement. With no reinforcement present, the deformation is localised to the portion of clay directly beneath the footprint of the applied platform load. As such, the sand directly beneath the platform acts as a deeper rigid platform.
v. When reinforcement is included a wider portion of clay is deformed. The lateral width of this deformation zone is controlled by the width of the reinforcement, as the applied load is spread. A ‘wide-slab’ effect is evident with an increase in the geogrid width, as the tensioned membrane-effect is mobilised to increase the capacity of the reinforced foundation sand. This results in a wider portion of the clay deforming.

vi. Addition of geogrid reinforcement to the sand foundation under a wide platform load enhances deformation of the clay, but has the advantage of an increased load-bearing capacity of the system.

vii. Furthermore, the addition of multiple layers of reinforcement contributes to this increase in load-bearing capacity. Additionally, increasing the installation width of the reinforcement contributes to an increased vertical load-bearing capacity. However, this resultant increase is only mobilised after a certain amount of vertical displacement. This is likely due to the reinforcement requiring a certain amount of vertical displacement to mobilise tension in order to support the applied load.

The behaviour of a thin compressible clay horizon changes with the inclusion of reinforcement under a wide platform load. The deformation behaviour of the clay is increased by additional layers of reinforcement as well as an increase in the width of the reinforcement. However, the increase in deformation comes at the benefit of an increased vertical load-bearing capacity of the reinforced foundation sand.

ACKNOWLEDGEMENTS

There is always a thrill for tendering gratitude to those individuals who assisted in the completion of this dissertation. Undoubtedly, the most pleasant part of completing such work is the opportunity to thank those who were involved; however the list of expressions of gratefulness is always inadequate and incomplete. This page of acknowledgements cannot begin to satisfy the astute gratitude that I have for those that were involved.

Firstly to my supervisor, Professor Louis Van Rooy; thank you for the support and guidance in making the migration to the Bushveld (and Kalahari). It was one filled with many cups of coffee's, glasses of port and poorly planned Afrikaans lessons. Dankie, Oom! Your leadership and advice on my research, from draft (note; singular) to draughts, deserves a special (but inadequate) mention in these acknowledgements, and I am extremely grateful for what you have contributed to this dissertation as well as my life over the past 2 years. Professor SW Jacobsz, thank you for the use of your 'little toy.' I am quite glad I never got round to giving the centrifuge enclosure a new paint-job with lighter shades of grey's and pink's! I'll leave some clay in the laboratory if you ever decide to change your mind. Your immense commitment, knowledge and understanding are beyond admirable to me. Thank you for putting up with my constant knocking at your office door. Gratitude stated in this text will never be sufficient to explain the mammoth contribution you have had to my professional knowledge. Thanks must be extended to Professor Elsabe Kearsley, Mr Rikus Kock, Mr Johann Scholtz and Mr Jaco Botha from the Department of Civil Engineering, for the immense assistance and advice in the laboratory.

Mark Richter and Lionel Moore from WorleyParsons RSA (formerly, Moore Spence Jones). Thank you for your assistance in providing me with this research, and your constant support throughout the time taken to complete it. Your enthusiasm and belief has lit a fire within me which I hope to carry with me for the rest of your life. Thank you for providing me with such a strong professional foundation. Special mention must be extended to Edoardo Zannoni and Maccaferri for the donation of the geogrids and extensive knowledge and advice throughout the research. I would also like to acknowledge the National Research Foundation for the financial assistance.

To my mother and father, as well as extended family; thank you for your extreme support throughout this research, but mostly thank you for the strong establishment you have provided me. The two of you provided the groundwork long before this research was undertaken. Thank you! To the Villa and beyond; Lynt, Nick, Jason, Joe , John, Gareth and Steve, thank you for aiding my conversion from a hobbit from the Shire to one filled with more fish, Richards and cricket and less 'fush,' 'Ruchards' and 'crucket.' To the rest of my friends who walked with me through this journey, thank you for your indirect support through plenty frosty's, laugh's and good times.

"Pro Aris, Et Focis"

REFERENCES

Abu-Farsakh, M., Qiming, C., Sharma, R., & Zhang, X. (2008). Large-scale model footing tests on geogrid-reinforced foundation and marginal embankment soils. *ASTM Geotechnical Testing Journal*, **31**(5), 413-423.

Arnold, A., Laue, J., Espinosa, T., and Springman, S.M. (2010). Centrifuge modelling of the behaviour of flexible raft foundations on clay and sand. In: Springman, Laue, and Seward. (Eds) *Physical Modelling in Geotechnics*, Taylor and Francis, London, 679-684.

Actidyn Systemes SA. (2011). *Civil Engineering Centrifuge – Model C67-4*; Technical Description. Report no: TD C67-40-0000 Rev. b.

Binquet, J., and Lee, K.L. (1975). Bearing capacity tests on reinforced earth slabs. *Journal of the Geotechnical Engineering Division*, **101** (12), 1241-1255.

British Board of Agrément [BBA]. (2010) Paralink Geocomposites, *Linear Composites' Soil Reinforcement Products, Agrément Certificate 03/4065, Product Sheet 1.*

Chen, Q., (2007). *An experimental study on characteristics and behaviour of reinforced soil foundation*. PhD dissertation, Louisiana State University, Baton Rouge, USA.

Huang, C.C., and Tatsuoka, F. (1990). Bearing capacity tests of reinforced horizontal sandy ground. *Geotextiles and Geomembranes*, Vol 9 (1), 51-81.

Ilyas, T., Leung, C. F., Chow, Y. K., & Budi, S. S. (2004). Centrifuge model study of laterally loaded pile groups in clay. *Journal of Geotechnical and Geoenvironmental Engineering*, **130**(3), 274-283.

Jacobsz, S.W. (2013a). Centrifuge modelling of a soil retaining wall. *Journal of the South African Institution of Civil Engineering*, **55** (1), 85-95.

Jacobsz, S.W. (2013b). Geotech @ Tuks. *Civil Engineering Magazine*, April 2013, 61-66.

Jacobsz, S.W., Kearsley, E.P., and Kock, J.H.L. (2014) The geotechnical centrifuge facility at the University of Pretoria, Physical Modelling in Geotechnics, *To be published*.

Jewell, R.A. (1996). *Soil reinforcement with geotextiles, Volume 123 of CIRIA Special Publications*, American Society of Civil Engineers, University of Michigan.

Khing, K. H., Das, B. M., Puri, V. K., Yen, S. C., and Cook, E. E. (1994). Foundation on strong sand underlain by weak clay with geogrid at the interface. *Geotextiles and Geomembranes*, **13**(3), 199-206.

König, D., Jessberger, H. L., Bolton, M. D., Phillips, R., Bagge, G., & Rienzi, R. (1994). Pore pressure measurement during centrifuge model tests: experience of five laboratories. In *Centrifuge 94: International Conference*, AA Balkema, 101-108.

Kutter, B.L., Abghari, A., and Shinde, S.B. (1988) Modelling of circular foundations on relatively thin clay layers. In: Corte, J.F. (Ed). *Centrifuge '88*, Proceedings of the International Conference on Geotechnical Modelling, Paris.

Le Roux, P. (2012). Soil Suction in Platinum Tailings. Unpublished BEng Project Report. University of Pretoria.

Maccaferri (2011) Macgrid EG Polypropylene Bi-Axial Geogrids, *Technical Data Sheet, ZAF/TDS/MGEG: Eng – Rev. 01, Feb 2011.*

Measurement Specialities. (2012). MS54XX Miniature SMD Pressure Sensor. [Electronic document] Available at www.meas-spec.com/downloads/MS.pdf [Accessed 12 May 2013].

Michalowski, R.L., and Shi, L. (2003) Deformation Patterns of Reinforced Foundation Sand at Failure. *Journal of Geotechnical and Geoenvironmental Engineering*, Vol 129 (6), 439-449.

Miyazaki, K., and Hirokawa, F. (1992). Fundamental study of reinforcement of sand layer in model test. In: Ochiai, H., Hayashi, S., and Otani, J. (Eds.) *Proceedings of the Earth Reinforcement Practice*, , Balkema, Rotterdam, The Netherlands.

Moore, L., Richter, M.V., and Gilli, A. (2012). The use of wire mesh steel geogrids in South Africa. *Proceedings of the 5th European Geosynthetics Congress*, Valencia, Spain.

Nakase, A., Kusakabe, O., and Wong, S.F. (1984). Centrifuge model tests on bearing capacity of clay. *Journal of Geotechnical Engineering*, **110** (12), 1749-1765.

Phillips, R. (1995) Centrifuge modelling: practical considerations, In: Taylor, R.N. (Ed.). *Geotechnical Centrifuge Technology*. Blackie Academic & Professional, London, 19-33.

Rajesh, S., & Viswanadham, B. V. S. (2009). Evaluation of geogrid as a reinforcement layer in clay based engineered barriers. *Applied Clay Science*, **46**(2), 153-165.

Schofield, A. N. (1988). An introduction to centrifuge modelling. In: Craig, James & Schofield (Eds.), *Centrifuge in soil mechanics,* Balkema, Rotterdam.

Sharma, J.S., and Bolton, M.D. (1996). Finite element analysis of centrifuge tests on reinforced embankments on soft clay. *Computers and Geotechnics*, **19** (1), 1-22.

Sharma, J. S., & Bolton, M. D. (2001). Centrifugal and numerical modelling of reinforced embankments on soft clay installed with wick drains. *Geotextiles and Geomembranes*, **19(**1), 23-44.

Sharma, R., Chen, Q., Abu-Farsakh, M., and Yoon, S. (2009). Analytical modelling of geogrid reinforced soil foundation. *Geotextiles and Geomembranes*, **27**, 63-72.

Springman, S., Bolton, M., Sharma, J., & Balachandran, S. (1992). Modelling and instrumentation of a geotextile in the geotechnical centrifuge. In *Proceedings of International Symposium on Earth Reinforcement Practice, Fukuoka, Japan* Vol. 1, 167-172.

Stewart, D. P., & Randolph, M. F. (1991, June). A new site investigation tool for the centrifuge. In *Proceedings of the International Conference Centrifuge,* **91**, 531-533.

Taylor, R.N. (1995) Centrifuges in modelling: principles and scale effects, In: Taylor, R.N. (Ed.). *Geotechnical Centrifuge Technology*. Blackie Academic & Professional, London, 19-33.

Viswanadham, B. V. S., & Jessberger, H. L. (2005). Centrifuge modelling of geosynthetic reinforced clay liners of landfills. *Journal of Geotechnical and Geoenvironmental Engineering*, **131**(5), 564-574.

Viswanadham, B. V. S., & König, D. (2004). Studies on scaling and instrumentation of a geogrid. *Geotextiles and Geomembranes*, **22**(5), 307-328.

Viswanadham, B. V. S., & König, D. (2009). Centrifuge modelling of geotextile-reinforced slopes subjected to differential settlements. *Geotextiles and Geomembranes*, **27**(2), 77-88.

Wayne, M.H., Han, J., Akins, K., (1998). The design of geosynthetic reinforced foundations. In: Proceedings of ASCE's 1998 Annual Convention & Exposition. ASCE Geotechnical Special Publication 76, 1–18.

Zannoni, E., Freeman, T., and Richter, M.V. (2012). Basal reinforcement over soft soil using high strength bonded geogrid at Agriport Maydon Wharf. *Proceedings of the 5th European Geosynthetics Congress*, Valencia, Spain.m